3-D Model Development of Metal Building Systems with Hard Walls

by

Michael J. Langley

A thesis submitted to the Graduate Faculty of
Auburn University
in partial fulfillment of the
requirements for the Degree of
Master of Science in Civil Engineering

Auburn, Alabama
May 7, 2016

Keywords: Earthquake Engineering, Metal Building Systems, Energy Dissipation

Approved by

Justin D. Marshall, P.E., Chair, Associate Professor of Civil Engineering
James S. Davidson, P.E., Professor of Civil Engineering
Mary L. Hughes, Lecturer of Civil Engineering

Abstract

      Metal Buildings with precast concrete or masonry walls (hard walls) have been identified by analytical modeling, shake table tests, and earthquake reconnaissance as being susceptible to collapse. While the steel frames have been shown to be resilient, the potential for wall failure and possible collapse is present. There exists a large stiffness differential between the hard walls and steel frames, which in turn generates high demands on brittle connections. Also, there is very little coordination between the metal building systems (MBS) engineer and the engineer-of-record who is responsible for the connections, which can result in improper connection design. When these connections fail in a non-ductile manner, the continuous load path is lost and the wall can fall away from the structure. In order to enhance the global seismic performance and improve life safety of these structures, a new seismic force resisting system that relies on simple energy dissipating connections between the hard wall and the steel frame needs to be developed.

      The initial step towards accomplishing this goal, and the purpose of this research, is development of a 3-D model of metal building systems with hard walls in SAP2000 that can be used in nonlinear response history analyses. A new modeling procedure had to be developed for capturing the post-buckling behavior of a metal building frame during an earthquake. This modeling procedure included the development of a Lateral Torsional Buckling (LTB) Hinge that approximates the post-buckling behavior. The metal building frame capacities, as well as the demarcation between elastic and inelastic behavior, were determined through finite element

analyses using Abaqus. Post-buckled frame behavior was modeled in SAP2000 using the newly developed LTB Hinge. Dynamic analyses were performed for 2-D planar frame models and 3-D models to assess the cyclic behavior of the LTB hinge. This 3-D model, now including post-buckling behavior, can effectively be used to analyze the global performance of a metal building system with hard walls, as well as quantify connection strength, post-yield deformation, and energy dissipation capacities required to achieve enhanced performance of these systems.

Acknowledgments

It is Dr. Justin Marshall's expertise in earthquake engineering and his reconnaissance work in Haiti and New Zealand that laid the groundwork for the research in this thesis. His research has advanced the efforts to improve the performance of metal building systems in earthquake events. He has inspired me to contribute to the research necessary to achieve better and safer metal building systems.

I greatly appreciate being part of the *Resilient Connections between Hard Walls and Steel Frames in Metal Buildings Project* funded by the National Science Foundation. I have found this work to be both rewarding and challenging and hope that I have made a contribution towards the goals laid out for this project.

It was Dr. Matthew Smith of the United States Army Corps of Engineers who personally made the effort to supply me with the metal building frame designs necessary for my research. It was invaluable to me that he took the interest and the time necessary to prepare the documents I needed.

Jeff Walsh, engineer at American Buildings, provided me with information in regards to the design of metal building systems. His willingness to answer my questions was greatly appreciated.

It has been my pleasure to be a part of the Civil Engineering Department at Auburn University. I am indebted to the professors who have guided me through coursework and research.

I would especially like to mention Dr. Chai Yoo, who provided me with the inspiration and encouragement to continue my studies toward a doctorate.

I greatly appreciate the unending support of my family, and their love and encouragement throughout my life.

Table of Contents

List of Tables

List of Figures

Chapter 1   Introduction

1.1   Defining the Problem

The use of Metal Building Systems (MBS) is in high demand in the construction industry. As of 2014, Metal building systems accounted for over 50% of non-residential low-rise construction in the United States (MBMA 2014). Reasons for the increase in the use of these systems include their cost-efficiency, durability, modularity, and speed of construction. Typically, these systems are one to two story structures and have a wide range of applications including use in commercial, industrial, recreational, religious, and educational structures. Metal Buildings with lightweight cladding have been shown to perform well in past earthquake events. This was demonstrated when the performance of metal buildings was examined by the MBMA after four earthquake events from 1983 through 1994, who found them to be resistant to seismic action (Shoemaker 2006).

It has been a recent trend to include precast concrete or masonry walls (hard walls) in these systems, generally for architectural aesthetics. Metal Buildings with hard walls have been shown in analytical studies, experimental tests, and post-earthquake reconnaissance to exhibit poor seismic performance. Specifically, the reconnaissance in New Zealand after the 2011 Christchurch earthquake showed that significant structural and non-structural damage occurred in metal buildings with non-load bearing concrete cladding or unreinforced masonry cladding (Marshall and Gould 2011). This is particularly alarming considering that the modern building codes for New Zealand and the United States are comparable.

Although the steel frame of metal building systems has been shown to be resilient, the potential for hard wall failure and collapse exists in these structures during seismic events. Any non-ductile connections between these two different structural elements will experience significant force and deformation demands. The stiffness incompatibility between light, flexible steel framing and the heavy, stiff concrete or masonry walls (hard walls) can result in failure of these brittle connections. Additionally, there is often little or no coordination between the MBS engineer and the engineer-of-record who is responsible for the connections between the frame and hard walls. If these connections are improperly designed and not detailed for seismic resistance, it can result in the failure of the connections in a non-ductile manner. When this occurs, the continuous load path is lost and the hard wall can fall away from the structure, both of which occurred in MBS in Haiti and New Zealand (Marshall and Gould 2011). The cost of damage in such failures is measured in lives lost, repair costs, and in business interruption expense.

1.2   Proposed Solution

In order to improve seismic performance of metal building systems with hard walls, it is necessary to develop a new seismic force resisting system with energy dissipating connections. Simple, reliable energy dissipating connections in the form of friction slip devices or yielding fuses will relieve the stiffness incompatibility that exists between stiff hard walls and flexible steel frames. These connections will be geared towards energy dissipation in the longitudinal direction (parallel to the ridgeline) while maintaining strength in the transverse (wall out-of-plane) direction. This research is the first to analyze the earthquake response of metal building systems in the longitudinal direction. Because both in-plane and out-of-plane demands must be known, three-dimensional models are necessary to analyze the demands along the continuous load path.

2

Before the connection designs can be developed, it is critical to understand how the new connections will impact the global seismic behavior of metal building systems with hard walls. To achieve this, 3-D models in SAP2000 need to be developed in order to predict the structural behavior of these systems during an earthquake. Ultimately, these models will be used to quantify the necessary connection strength, deformation demands, and energy dissipation capacities necessary to achieve both life safety and enhanced performance of metal buildings during seismic events.

1.3   Scope of Work

A wide range of metal building frame designs were made available for use from the New Approximate Period Study for Metal Building Systems (Smith 2013d). Out of the 48 typical frame geometries designed with hard walls and high seismic risk, five frames were chosen for this research that would provide a high variety of structural geometries and represent a sample of the metal building systems population. A nonlinear static pushover analysis of each frame was performed in the finite element program Abaqus to determine the frame capacity, as well as to determine the inelastic failure mechanism.

SAP2000 (CSI America 2015) was utilized to develop the 3-D models of the metal building systems for the nonlinear dynamic analyses. The longitudinal seismic lateral force resisting system was designed for each of the five structures. The metal building frame was modeled for both elastic and post-buckling behavior. One of the challenges involved the method for including post-buckling behavior of metal building frames. A new lateral-torsional buckling (LTB) hinge was developed to approximate this post-buckling behavior. 2-D planar frame models were used to generate the custom backbone curve for the hinge. The Abaqus pushover analyses were used to

calibrate the hinge such that the pushover curve from the SAP2000 analysis matched the Abaqus pushover curve as closely as possible. The cyclic behavior of the LTB hinge was examined for the 2-D model using a suite of ground motions.

A case study was performed on one of the 3-D models to assess the modeling procedure developed for metal building systems with hard walls. The 3-D model was subjected to a suite of ground motions to determine the LTB hinge behavior, preliminary connection demands, and global seismic performance. These models will be used in later research tasks to quantify connection strength, deformation demands, and energy dissipation requirements needed to improve global performance.

1.4   Organization of Thesis

Chapter 2 introduces recent developments in metal building systems as they relate to general structural behavior and seismic performance. Chapter 3 presents the 3-D model development using SAP2000; this chapter focuses primarily on elastic components. Chapter 4 discusses the Abaqus pushover analysis procedure and presents each of the five metal building frame capacities. The failure mechanisms are identified. The LTB hinge is developed in SAP2000 using the Abaqus pushover curves. 2-D models of the metal building frame are subjected to a suite of ground motions in order to assess the cyclic behavior of the LTB hinge. Chapter 5 presents a case study of one of the 3-D models to assess the modeling procedure developed. Chapter 6 summarizes the findings of the research. Recommendations and future work involving 3-D modeling of metal building systems are provided.

Chapter 2   Literature Review

2.1   Background

Over the past decade, the metal building system industry has shown a desire to understand and improve the reliability of their systems during earthquakes. After the Northridge Earthquake of 1994, the metal building industry was caught up in the numerous building code changes that affected conventional steel moment frames. Hong (2007) states that the Northridge failures were primarily associated with the brittle fracture of welded joints at beam-to-column moment connections in multi-story steel buildings. According to Hong, the new stringent requirements in the seismic design provisions were adopted for use in metal building frames partly due to lack of research. It has been shown that the metal building frames performed well during the Northridge event as well as previous seismic events (Shoemaker 2006). Because metal building frames are completely different building systems from conventional steel moment frames, and because metal building systems performed well in earthquakes, it was unreasonable to adopt the same seismic requirements for both systems. Some of these changes unfairly impacted the metal building industry, which made it more difficult for this industry to remain competitive as an option for building construction. The Metal Building Manufactures Association (MBMA) represents the interests of this industry and has provided funding for recent research projects for improving metal building systems. The ultimate goal of these research tasks is to develop seismic-force resisting systems tailored specifically for metal building frames.   The systems currently being developed

are the Metal Building Ordinary Moment Frame (MBOMF) for lightweight wall cladding, and the Metal Building Intermediate Moment Frame (MBIMF) for hard wall systems.

Research by Hong and Smith has focused on the seismic performance in the moment frame (transverse) direction. No research has been conducted in the seismic behavior of metal building systems in the longitudinal direction.

2.2   Cyclic Tests on Full-Scale Metal Building Frames

Hong (2007) at the University of California San Diego undertook the task to develop a seismic design procedure for metal building systems. It should be noted that at the beginning of his research, there existed very limited metal building test data, and even less for seismic applications. Experimental and analytical studies on metal building frames were required before a new seismic design procedure could be developed.

Hong performed cyclic tests on a full-scale metal building system. Cyclic behavior of metal building frames had not been investigated prior to this. The current seismic design procedure for metal building frames uses the ordinary moment frame (OMF). Because web-tapered members are often composed of non-compact and slender elements, stability limit states control the capacity rather than the formation of a plastic hinge. Figure 2.1 shows the test setup used by the researchers. The testing focused primarily on the performance of the web-tapered steel frame.
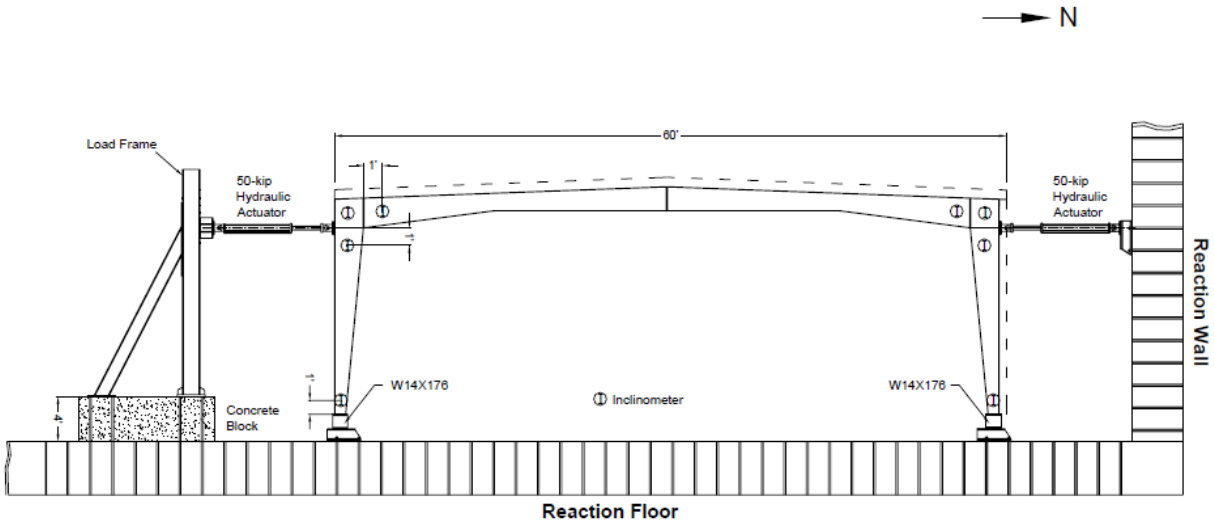
Figure 2.1. Cyclic Testing for Metal Building Frame (Hong 2007)

Several significant findings resulted from the experimental tests. It was shown that the metal building frames exhibited high deformability, but limited ductility. When compared to conventional moment resisting frames, the elastic drift range was significantly larger. The results showed that there was significant strength degradation following lateral buckling. It was also shown that the overstrength of this system was high because non-seismic load combinations controlled the frame design. This inherent reserve strength along with the light-weight characteristic of these systems explained why metal buildings with light-weight cladding performed well in past earthquake events.

Nonlinear finite element analysis models were developed using Abaqus (Simulia 2015) to predict global and local behaviors of the frames. A correlation study was performed to compare the experimental test results with computer analyses. This was done to specifically provide additional insight into the behavior of the metal building frame.

According to Hong's research, predicting the ultimate capacity of metal building frames can be achieved through nonlinear finite element analysis. To accomplish this, the following

procedures were implemented. The Modified-Riks algorithm was used to capture the post-buckling behavior of the frame. Geometric imperfection was introduced into the models using the first buckling mode shape from a linearized eigenvalue buckling analysis. Without this imperfection, the predicted failure mode would be incorrect (flange local buckling instead of lateral-torsional buckling) and the ultimate load would be much higher. A parametric study was conducted to determine the appropriate amplitude of geometric imperfection to apply. The most accurate prediction was obtained when an amplitude of $L_b/1000$ was used, where L_b is the length of the unbraced segment. The correct failure modes from one of the analyses are shown in Figure 2.2.
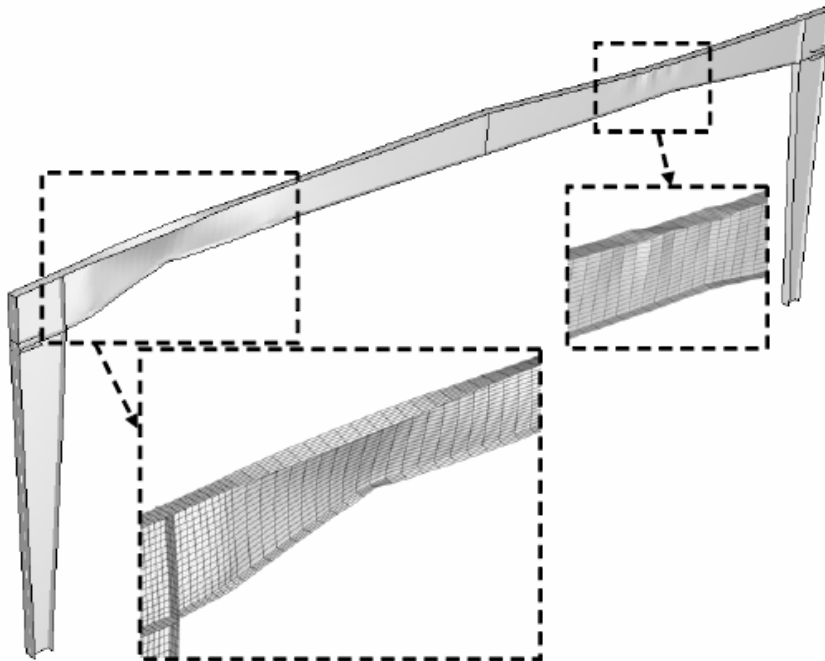
Figure 2.2. LTB Failure and Flange Local Buckling of Metal Building Frame (Hong 2007)

Using the results for the experimental and analytical tests, Hong developed a new drift-based seismic design procedure for metal building frames. This research demonstrated that the

new design procedure worked well for metal building systems with light-weight cladding. However, one important finding from the case study was that metal buildings with heavy sidewalls designed in accordance with current design provisions are vulnerable to collapse under major earthquakes.

2.3   Behavior and Design of General Prismatic and Nonprismatic Members

Further advancements in the design of metal building frames were made by Kim (2010) working at Georgia Tech. The design provisions for web-tapered members were provided in AISC ASD (1989) and LRFD (1999) Specifications, but addressed a small range of practical designs. Kim developed new design procedures for frames containing general prismatic members and web-tapered members. The improvements of the AISC specifications (AISC 2005, 2010a) were incorporated in these new procedures. This research included a comprehensive assessment of beam lateral-torsional buckling behavior and strength using virtual test simulations.

Kim's nonlinear shell finite element analysis procedures for determining the ultimate capacity of nonprismatic frame members was the most comprehensive to date. The results were validated in detail with past experimental tests. Kim recognized that when attempting to capture the real physical behavior of metal building frames, it is imperative to apply appropriate imperfection shapes and residual stresses in order to achieve an accurate strength prediction. Hong's finite element models did not include any residual stresses. The geometric imperfections included were several web-buckling modes from an eigenvalue buckling analysis and a compression flange sweep of $L_b/1000$, where L_b is length of the unbraced segment (Figure 2.3). The compression flange sweep had a greater influence in the LTB capacity than the eigenvalue buckling mode imperfections.
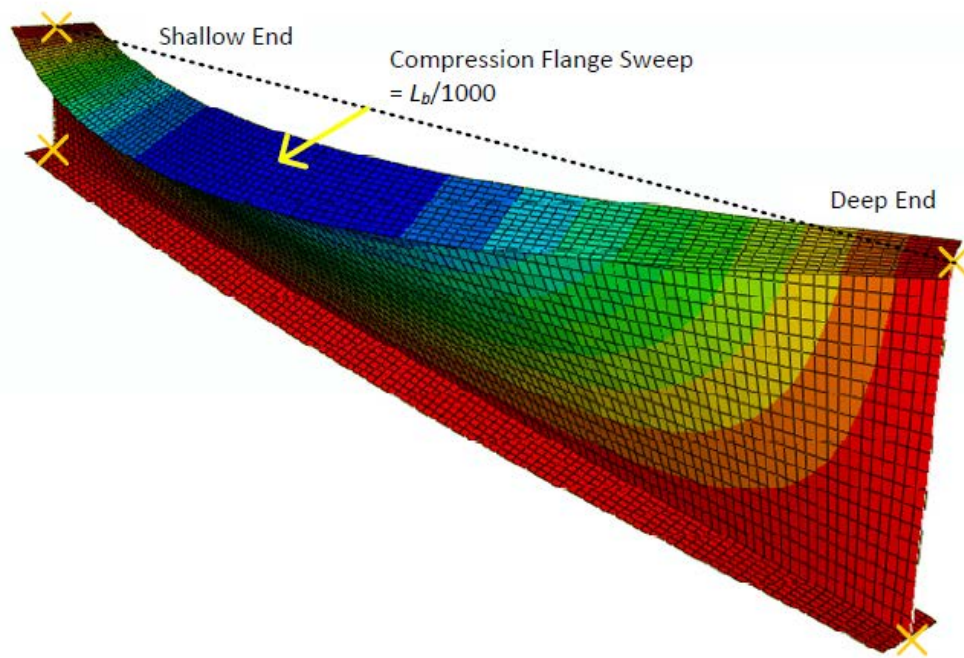
Figure 2.3. Compression Flange Sweep (Kim 2010)

The research in this thesis relied on procedures by Hong and Kim to determine the ultimate capacity and failure mechanism of the metal building frames, which will be discussed in Chapter 4.

2.4 Metal Building Shake Table Tests

Continuing the goal to develop a new seismic force resisting system specific to metal building frames, Smith (2013a and 2013b) first performed full-scale shake table tests to provide experimental data concerning the seismic performance of metal buildings (Figure 2.4).

Figure 2.4. Metal Building with Concrete Walls on Shake Table (Smith 2013b)

The results of the shake table tests revealed several important aspects about the dynamic response of metal buildings during earthquake excitations. One of the test specimens was a metal building system with metal sidewall panels. Another specimen was clad with precast concrete panels. Both specimens exhibited lateral buckling in the rafters near pinch points, as seen in Figure 2.5. The term pinch point refers to a location in the frame where the angle of taper changes from one segment to the other.

(a) LTB   (b) FLB
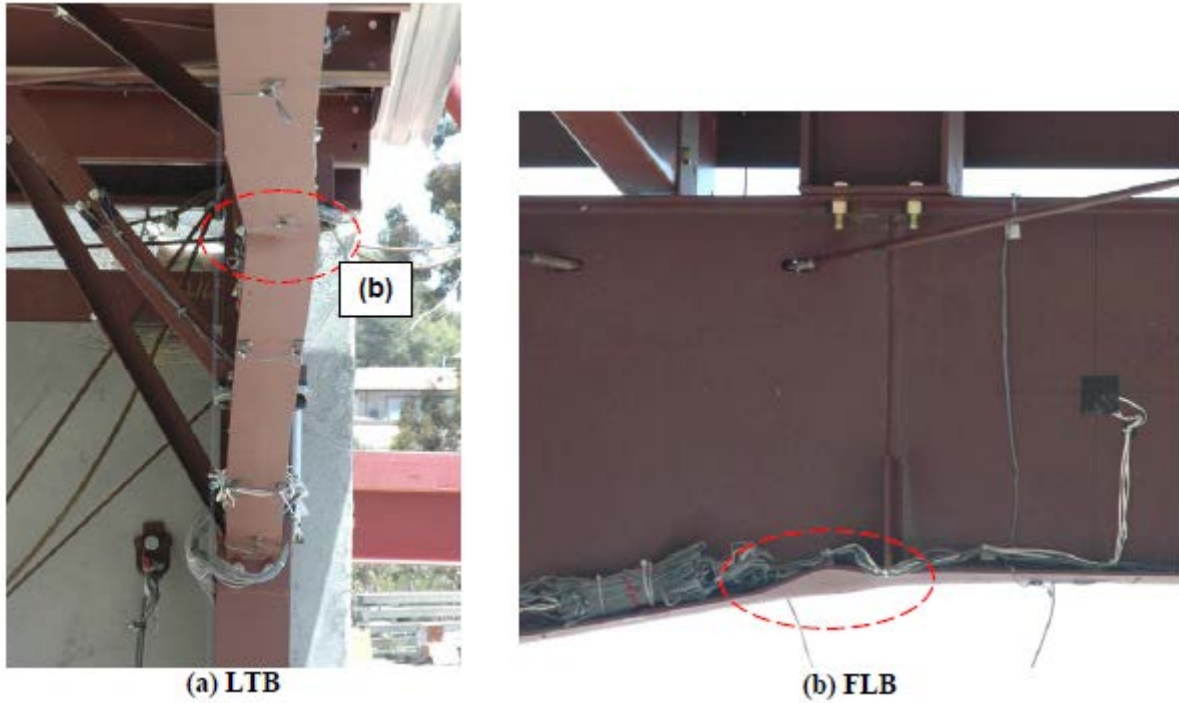
Figure 2.5. Buckling around the Pinch Point (Smith 2013b)

It was discovered that the behavior of the buckled segment was very similar to the behavior of steel Special Concentrically Braced Frames (SCBF). In SCBFs, the buckled segments alternate between buckling and straightening as the loading changes direction (Figure 2.6).

(a) Rightward Loading   (b) Leftward Loading
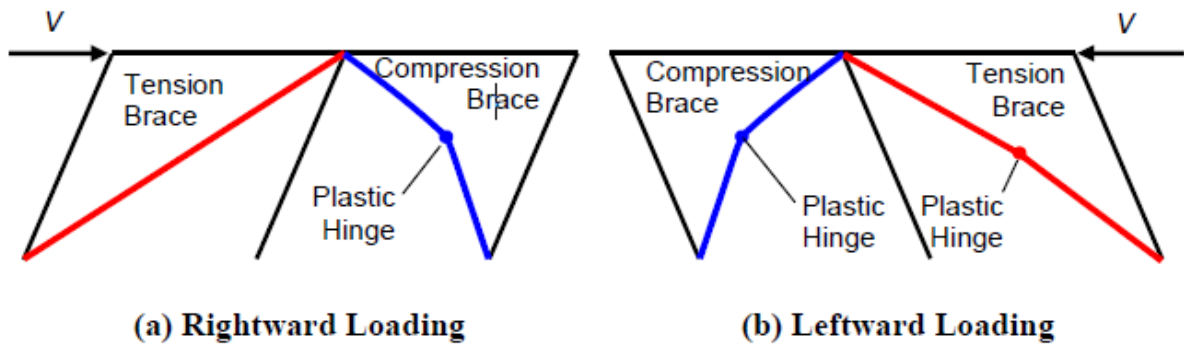
Figure 2.6. SCBF Cyclic Behavior (Smith 2013d)

During the tests, the inner flange of the buckled segment cycled between compression and tension. More than one buckle could not form simultaneously in the frame. None of the test

12

specimens collapsed on the shake table even though they were subjected to very intense accelerations. This can be explained by the fact that only one segment in the frame was buckling at a given time (Figure 2.7). The unbraced segment that undergoes cyclic LTB is referred to as the controlling segment. The post-buckled frame was still statically determinate. The second hinge did not form for two reasons. First, the outer flange is braced more frequently than the inner flange, which increases its resistance to LTB. Second, the post-buckled stiffness reduction requires increasingly large displacements to increase internal force demand in the rafters.

$V_b/2$ $V_b/2$

Inactive CS   Active CS

(a) Earthquake Acting to Right

$V_b/2$ $V_b/2$

Active CS   Inactive CS

(b) Earthquake Acting to Left
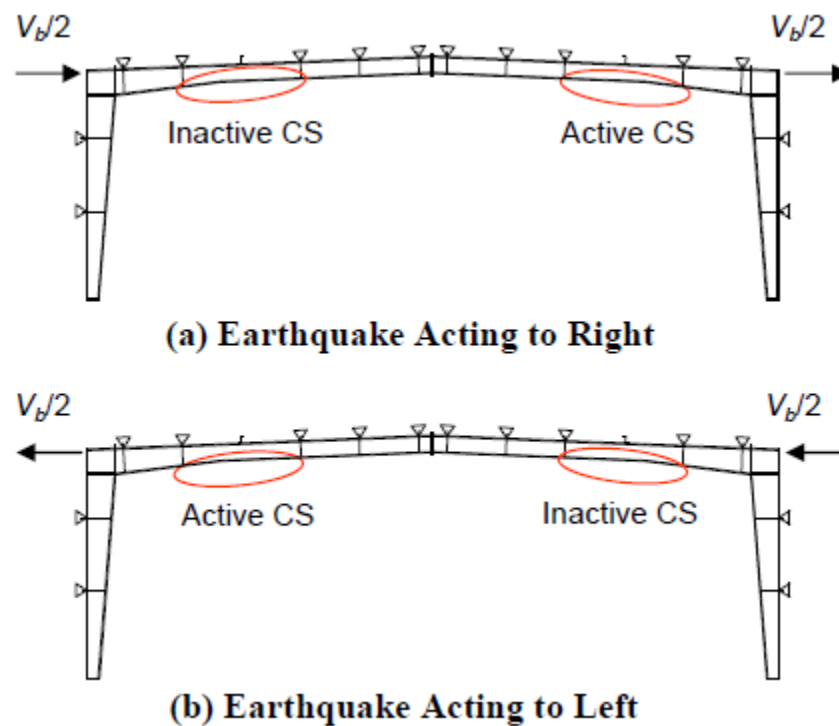
Figure 2.7. Active and Inactive Controlling Segments (Smith 2013d)

The shake table tests agreed with the findings of Hong (2007) regarding the overstrength of metal building frames. For the lightweight specimen, there was a high level of overstrength, suggesting that these types of systems would survive a Design-Based-Earthquake (DBE) or

Maximum Considered Earthquake (MCE) event and remain elastic. The overstrength for the hard-wall metal building system was lower. The hard-wall metal building system did not remain elastic and undamaged at the Design-Based-Earthquake level. Smith's research revealed that the safety factor at design level is less than one for metal buildings with concrete walls. This finding was in agreement with the case study performed by Hong (2007).

It was realized that a lateral-torsional buckling hinge acting as an inelastic mechanism can be used to develop a new seismic force resisting system for metal buildings with hard walls. This was a significant step toward the development of what will become the Metal Building Intermediate Moment Frame (MBIMF). For a new structural system to be approved for inclusion in the building code, a rigorous validation process by means of a FEMA P695 (FEMA 2009) study is required. Component level behavior must be known before any attempt can be made to develop analytical models that simulate the complete behavior of metal building frames during an earthquake.

2.5   Cyclic Lateral Torsional Buckling Tests

In order to provide experimental data for the development of the new seismic force resisting system (SFRS), Smith (2013c) conducted a study to investigate the cyclic lateral-torsional buckling behavior of built-up, web-tapered I-section rafters. As shown in Figure 2.8, the testing setup was comprised of a metal building moment frame subassembly with both a column and rafter segment. A hydraulic actuator loaded the specimens under displacement control. Since the column acted as a moment arm, it was designed to exceed the capacity of all of the rafters and remain elastic. Each rafter was braced in order to achieve the desired buckling mode. A total of ten rafters were cyclically tested.
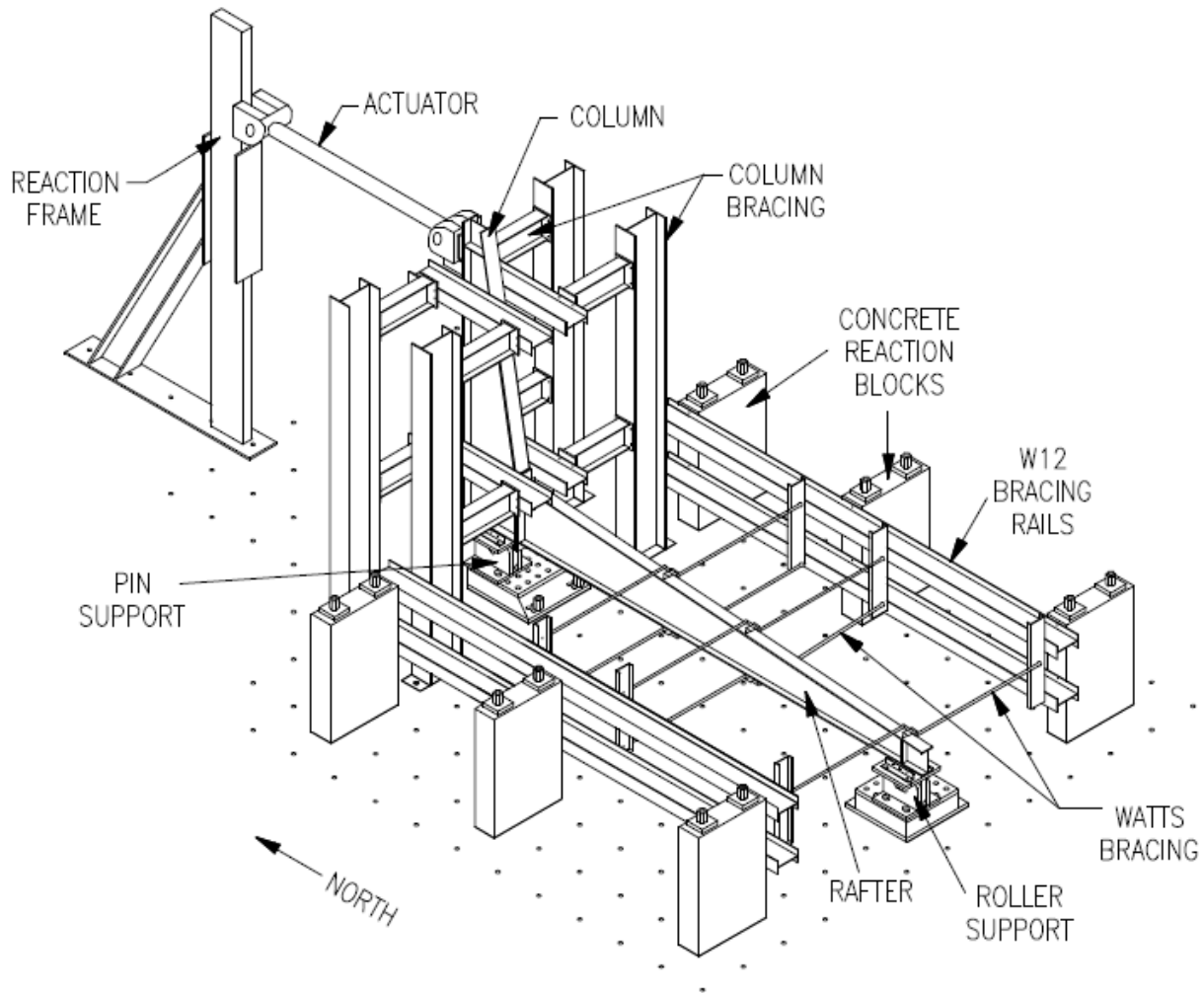
Figure 2.8. Cyclic Test Setup (Smith 2013c)

"Frame Design Using Web-Tapered Members" (Kaehler et al. 2011), herein referred to as Design Guide 25, is the most complete informational guide concerning the analysis and design of web-tapered members. It provides equations for determining member strengths for axial, flexural, and shear limit states. The LTB strength for nonprismatic I-beams is very challenging. An accurate prediction of the LTB capacity is imperative for seismic design, as underestimating the true

15

strength could undersize members around the controlling segment and an undesirable failure could occur.

It was recognized from previous research that adjacent unbraced segments significantly influence the LTB capacity. Smith expanded the LTB equations in Design Guide 25 to include the effects of adjacent unbraced segments as well as plate size changes within the unbraced length, which is not uncommon in metal building practice. The torsional stiffness of an I-beam is much higher when the effects of warping torsion are included, thereby increasing its LTB resistance. When performing an eigenvalue buckling analysis, the elastic lateral torsional buckling load is much more accurate when the analysis model uses a 14 degree of freedom beam-column element which includes a warping degree of freedom. The improved elastic lateral torsional buckling value can be used in the LTB calculations in Design Guide 25.

The results from the cyclic tests provided insight into the critical flexural capacities, load-displacement paths, lateral brace forces, and failure modes. Every rafter specimen developed lateral buckling within the critical segment. The LTB capacities predicted from Design Guide 25 were in agreement with the test results when the effect of the adjacent segments were included. Just as in the shake table tests, the LTB response in the cyclic tests exhibited many characteristics similar to a compression brace of a steel Special Concentrically Brace Frame (SCBF). After LTB, compression flanges formed local buckles at two to three locations within the critical segment. With every positive cycle, the controlling segment buckled in compression at a lower load each time (Figure 2.9). For the negative cycle, the controlling segment flange straightened, while gaining stiffness, until it carried tension. The load-deformation plots showed a significant strength loss after buckling. The rate of strength loss appeared to decrease at an exponential rate with each cycle.
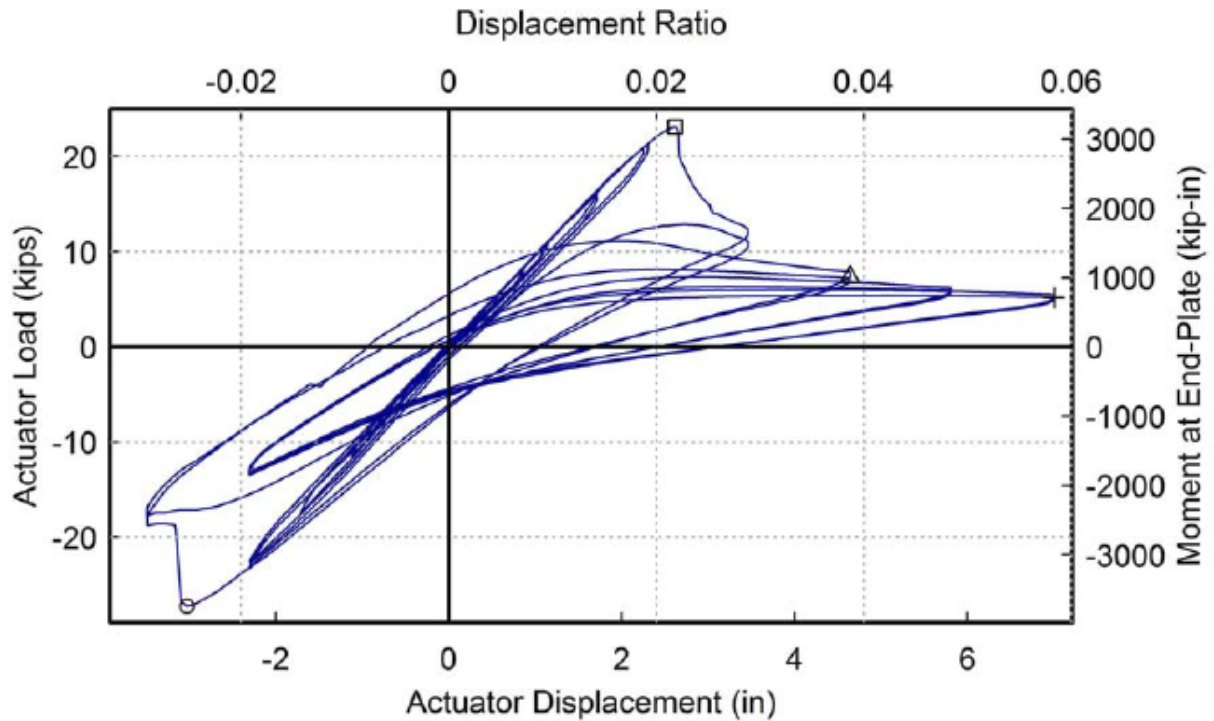
Figure 2.9. Global Response of Rafter undergoing Cyclic LTB (Smith 2013c)

These results help establish the fundamental component frame behavior after the critical segment has buckled. Research for this thesis uses these post-buckling characteristics described above to develop a custom LTB hinge that can be used in nonlinear dynamic analyses.

2.6   Approximate Fundamental Period Study for Metal Building Systems

Metal building engineers use the Equivalent Lateral Force (ELF) Procedure outlined in the *Minimum Design Loads for Buildings and Other Structures: ASCE/SEI 7-10* (ASCE/SEI 2010) for seismic design of metal building frames. One aspect of this procedure involves calculating the fundamental period of vibration, *T*, for initial design. The period equation in ASCE 7-10 uses a sample of multistory steel moment frame buildings. It is obvious that these structures are not comparable to low-rise metal building moment frames. New approximate period equations were

17

needed for metal building systems to improve the significant conservativism that comes with using the ASCE-7 period equations.

In order to develop new period equations, a sample of 192 metal building frames were generated by engineers at Metal Building Software, Inc. These frames were designed under a wide variety of geometric configurations, such as clear span length, eave height, and roof slope. Two levels for seismic hazard, snow load, and wind hazard were selected. Half of the models were designed with metal wall cladding (3psf) and the other half were designed with hard walls (75 psf). Also, half of the models were clear span metal building frames and the rest of the models had interior columns, or modular frames. A story drift of 2% was imposed for metal buildings with hard walls at the DBE level, per ASCE-7.

Smith (2013d) investigated the effect different panel zone models had on the fundamental period and lateral stiffness of metal building frames. Panel zones are composed of a web plate, column cap plate, column outer flange, and horizontal stiffeners. This element transfers moment and shear from the rafter into the column. It is recognized that the panel zone is not a rigid element in metal building frames. The accuracy of analytical models can be improved when this flexibility is taken into consideration. Figure 2.10 displays three panel zone modeling techniques. Any frame with a rigid panel zone model (Figure 2.10.c) overestimates the lateral stiffness of the frame and should be avoided. Metal building engineers often model panel zones using a centroidal extension method. Two elements with the cross-sectional properties of the ends of the columns and rafters are extended into the panel zone and connected at an intersection point (Figure 2.10.b). This model does not capture the true kinematics of a panel zone. A proposed panel zone model (Figure 2.10.a), similar to the "Revised Krawinkler Model" described by Charney and Marshall (2006), uses two

rigid links connected to a rotational spring at the corner of the panel zone. This modeling scheme captures the kinematics of a panel zone accurately.
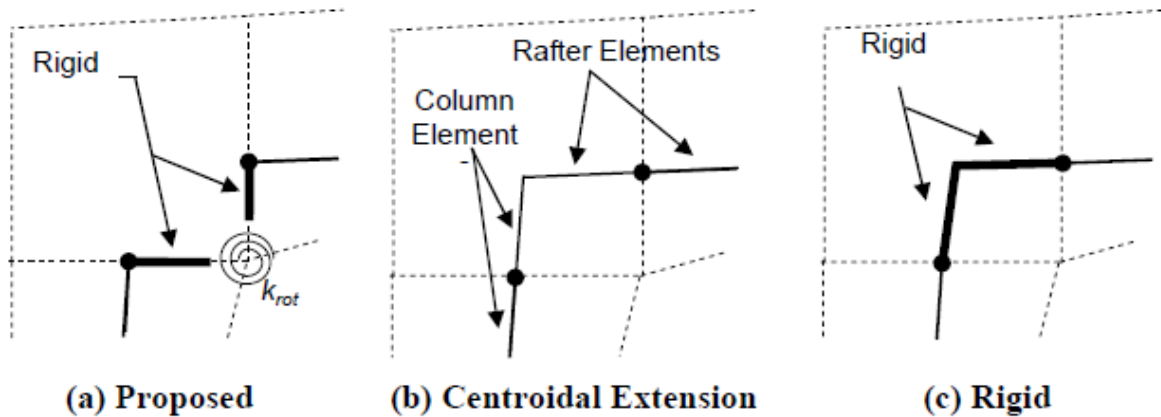
Figure 2.10. Panel Zone Modeling Schemes (Smith 2013d)

Smith calculated the rotational spring stiffness from a shell finite element model using Abaqus (Simulia 2015). Each model was composed of a prismatic column, prismatic rafter and panel zone plates (Figure 2.11). The length of the column and rafter had a length of three times the depth to mitigate stress concentrations from geometric and loading discontinuities. The flanges were discretized into 8 elements and the web into 20 elements. Nominal thicknesses were applied to the plates. Geometric and material nonlinearities were not considered in these models. The relative displacements at nodes A, B, and C were used to calculate the change in angle ABC, θ. The linear rotational spring stiffness was calculated by dividing the applied moment by the angle θ.
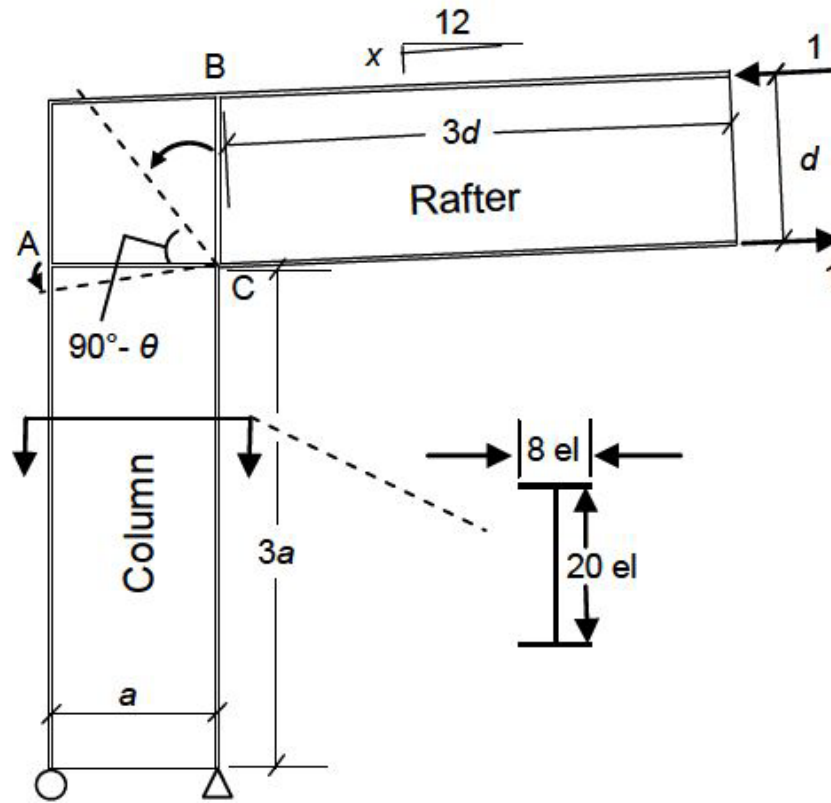
Figure 2.11. Panel Shell Element Model (Smith 2013d)

2.7 Conceptual Development of Metal Building Intermediate Moment Frame

Combining the findings from the cyclic tests by Hong with the shake table tests and the cyclic LTB tests by Smith lead to a conceptual development for the Metal Building Intermediate Moment Frame. The new seismic force resisting system for metal buildings with hard walls relies on LTB as the inelastic hinge. An unbraced length in the rafter, called the Controlling Segment, can be used as the structural fuse that will dissipate energy and protect the frame from excessive forces. The system will remain stable after the formation of one hinge because initially the system was indeterminate to the first degree. If a second hinge is allowed to form, a collapse mechanism will develop. To prevent this, a Capacity Design approach must be used for the frame outside of

the controlling segment.   Smith (2013d) proposed a displacement-based design procedure requiring that the post-buckled frame not exceed any strength limit states at the MCE displacement demands.   The life-safety at MCE intent of the seismic codes is to be satisfied by restricting the collapse mechanism from forming at the MCE, beyond DBE.

2.8   Factors affecting Lateral Stiffness of Metal Building Frames

Bajwa (2010) conducted analytical studies and lateral load tests on a lightweight metal building system to assess the lateral stiffness of frames for wind drift serviceability.   Metal Building Frames are designed assuming an ideal pin condition at the base of the columns.   This assumption is conservative for deflection calculations as the true behavior of the column-to-base connection provides some rotational resistance.   This partial rigidity was found to have a significant effect on the lateral stiffness of the frame.   A variety of modeling configurations for the column-base connection were proposed and analyzed.   Bajwa identified many factors that affect the stiffness of the column-base connection:

-The size and stiffness of the column

-The plan dimensions of the base plate

-The thickness of the base plate

-The arrangement of anchor bolts

-The pretension in the anchor bolts

-The axial stiffness of the anchor bolts (which depends on anchorage details)

-Thickness and material properties of grout

-The axial load present in the column prior to the application of lateral load

-The flexibility of the foundation underlying the anchor bolt

All these effects can be represented in a detailed finite element model of the column-to-base connection. Further research is required to provide closed form solutions for designers to easily use.

Metal building systems are designed assuming a flexible diaphragm assumption. The roof diaphragms in metal buildings are typically light gage sheathing or standing-seam roofs. The results from the experimental tests and analytical studies showed that the roof sheathing had negligible in-plane stiffness because the frames adjacent to the loaded frame deflected only a small percentage of the loaded frame.

2.9   Wall Connection Failures observed after Haiti and New Zealand Earthquakes

Post-earthquake reconnaissance has exposed a significant problem in the performance of metal building systems with hard walls. There exists a stiffness incompatibility between the stiff hard walls and the flexible steel frame. Brittle connections between these two elements can experience large force demands and can fail in a non-ductile manner.

Specifically, the reconnaissance of recent earthquakes in Port-au-Prince, Haiti in 2010 and Christchurch, New Zealand in 2011 highlighted the dangerous effect of poor connections between the steel frames and hard walls in metal building systems (Marshall and Gould 2012).

One prevalent type of failure that occurred with metal building systems in the 2010 Haiti earthquake was the detachment of non-structural masonry. Figure 2.12 shows an out-of-plane failure of a non-structural masonry wall. This wall collapse lead to a roof failure in the adjacent structure. The reconnaissance team found no evidence of wall ties connecting to the steel frame. Because of the absence of wall ties, it is not surprising that the wall failure occurred. The steel frame that carried the gravity and lateral load appeared undamaged (Eberhard et. al. 2010).

Figure 2.12. Infill Masonry Wall Collapse of PEMB in Port-au-Prince (Eberhard et. al.

2010)

The reconnaissance following the 2011 Christchurch earthquake identified that metal buildings systems with precast tilt-up wall panels had connections that were insufficient, causing the wall panels to fall away from the building. As seen in Figure 2.13, a wall segment has fallen away from a metal building system. For wall panels that did not collapse, the connections were so damaged that temporary shoring was required. As mentioned before, the fact that building codes for New Zealand and the United States are similar should be cause for alarm.

Figure 2.13. Loss of panel and temporary shoring of adjacent panel (Marshall and Gould 2012)

2.10 Summary of Literature Review

Identifying the deficiencies of metal building systems in seismic events and improving their performance has been an evolving process. In Hong's (2007) case study, he discovered that metal building systems with hard walls designed according to current standards are vulnerable to collapse. His research also showed that predicting the ultimate capacity of metal building frames can be achieved through nonlinear finite element analysis. Further advancements followed when Kim (2010) developed new procedures for designing frames with nonprismatic members. Her research included a comprehensive assessment of beam lateral-torsional buckling (LTB) capacities through virtual simulations.

Bajwa (2010) performed an analytical study and full-scale experimental testing on a metal building. Common modeling assumptions used for design of metal building frames were analyzed. The flexible diaphragm assumption was shown to be valid for these structures. By including the

partial rigidity of the base-column connection in structural models, the excessive conservatism present in drift calculations can be reduced.

Smith (2013b) identified the cyclic behavior of metal building frames through shake table tests. Cyclic tests were performed to determine the LTB component behavior. A fundamental period study utilized a 2-D frame modeling procedure which included improved panel zone modeling techniques. A conceptual development of the metal building intermediate moment frame (MBIMF) which utilizes LTB as a structural fuse was established.

The findings of these research projects and the performance of hard wall metal buildings have highlighted a problem with the design and construction of these buildings. All research conducted, to this point, has focused on the seismic behavior of the moment frame only (transverse direction). It has been identified though earthquake reconnaissance in Haiti and New Zealand that seismic performance of metal buildings with hard walls in the longitudinal direction is poor. The behavior in the longitudinal direction has not been analytically or experimentally studied. It is the objective of the research presented in this thesis to develop a 3-D computer model that can analyze the seismic performance of metal building frames with hard walls in both the transverse and longitudinal directions.

Chapter 3   Development of the SAP2000 Model

3.1   Selection of Computer Analysis Program

In order to predict the structural behavior and performance of metal building systems with hard walls during seismic events, it was necessary to develop 3-D analytical models for use in nonlinear dynamic analyses. Prior to this research, only 2D models have been used for earthquake analyses. The use of a 3-D model is significant because it is necessary in order to capture the connection demands for both the in-plane and out-of-plane directions.

Three software programs were considered in the development of these 3-D models: SAP2000 Version 17.3.0 (CSI 2015), Perform 3D V5 (CSI 2011), and OpenSEES (Mazzoni et al. 2007). Each has advantages and disadvantages. The solution algorithms that Perform 3D and OpenSEES employ trump SAP2000 in nonlinear dynamic analyses in speed and robustness. Developing a 3-D OpenSEES model would have required an exorbitant amount of time to code. OpenSEES has no graphical user interface, which means finding any errors in the model geometry and section assignments would be very difficult. Also, OpenSEES currently lacks a nonprismatic frame element. For these reasons OpenSEES was eliminated.

Perform 3D is well suited for conventional steel and reinforced concrete structures. However, metal building frames are inherently very different from conventional steel moment frames. Metal building frames do not utilize hot rolled sections. Instead, the column and rafter cross-sections are composed of built-up plate sections that are often web-tapered and singly

symmetric. Perform 3D does not contain nonprismatic frame elements and the I-beam shapes can only be doubly-symmetric. For this reason, Perform 3D was eliminated.

SAP2000 has a very user-friendly graphical interface which makes spotting errors much easier than a program with purely code-based input. It also has nonprismatic frame elements that can be made up of any custom cross-section. Nonprismatic elements eliminate the need to use a series of prismatic elements. This, in turn, reduces the number of degrees of freedom in the model, and can greatly increase the speed of analyses.

Unfortunately, all three programs lacked a beam-column element that includes the warping degree of freedom. Warping plays a crucial role in the torsional behavior of non-circular cross-sections. Without the warping degree of freedom, the St. Venant torsion is the only component used for calculating the torsional stiffness of all the frame elements. All torsional stiffness in the frames will be underestimated. Because of this, any chance of simulating LTB with kinematic accuracy is nearly impossible. Therefore, a clever use of a custom flexural hinge is necessary to approximate post-buckling behavior of metal building frames, which can be accomplished in SAP2000. Ultimately, after all these considerations, SAP2000 was used in the development of the 3-D models of metal building systems with hard walls for nonlinear dynamic earthquake analyses. The rest of this chapter will discuss the development of the SAP2000 model (Figure 3.1).
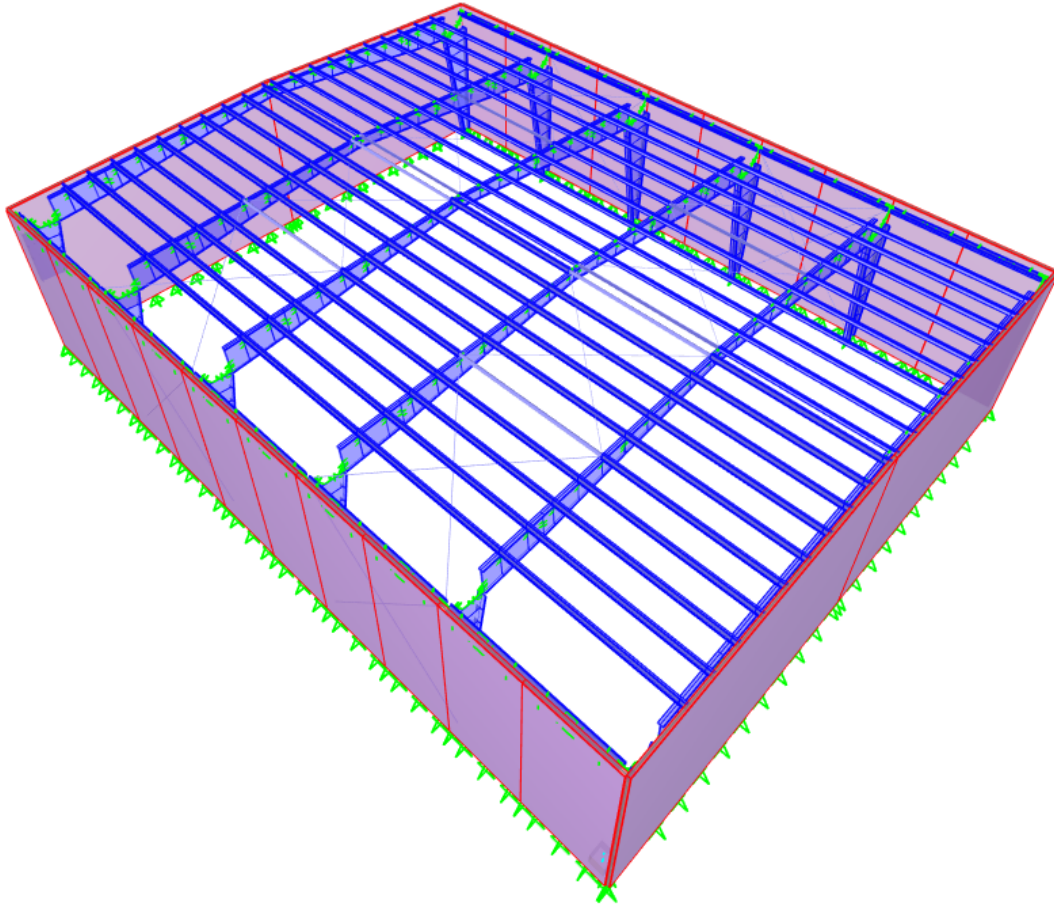
Figure 3.1. Extruded View of SAP2000 Model

3.2   Metal Building Frame Selection

As mentioned in the literature review, 192 metal building frame designs were available from the Approximate Fundamental Period Study for Metal Building Frames (Smith 2013d). The objective was to select frames that would produce a sample with high variety in both building geometry and load conditions. Five frames were selected that, when combined, represent a wide spectrum of the metal building system population. The geometry and design parameters of each

frame are listed in Table 3.1. For consistency, the frame numbers for this research will utilize the

same model numbers as in the Approximate Fundamental Period Study (Smith 2013d).

Table 3.1. Metal Building Design Sample Parameters

Model Number	Building Type	Eave Height (ft)	Length (ft)	Snow Load (psf)	Wind Speed (ASCE 7-05 mph)
16	Clear Span Symmetrical Gable	30	40	0	120
41	Clear Span Symmetrical Gable	30	100	0	85
42	Clear Span Monoslope	30	160	42	85
85	Clear Span Symmetrical Gable	15	40	0	120
138	Modular Symmetrical Gable	30	120	0	85

The selection process only considered frames designed with a high seismic risk. All the

frames used in this research have a roof slope of 0.5:12, as it was believed that any variation in the

slope would not impact connection demands. In Metal Building Systems, both clear span frames

and modular frames are used. Clear span frames are used when the enclosed space requires that

there be no interior obstructions, such as a sports facility. Modular frames can be used for storage

facilities where an open space is not an issue. Four clear span building frames and one modular

building frame were selected to represent these two building uses. One frame, Model 42, included

a high snow load for buildings built in Alaska. This will help determine if a higher roof mass

affects the connection demands. Model 42 has a monoslope roof as opposed to a symmetrical

gable roof. This results in one side wall being taller than the other one. This model was included

29

to see if the geometry of the system would cause differences in the connection demands in the walls on opposing sides of the building due to the differing flexibilities.

All previous seismic metal building research has been geared towards the development of new seismic force resisting systems specifically for metal building frames. It is unknown what the wall weight height limitations for the future metal building ordinary moment frame (MBOMF) and metal building intermediate moment frame (MBIMF) will be, as that research is currently ongoing. For this particular research, it was decided to maintain the wall weight height limitations required for an OMF in Seismic Design Category D, as in accordance with ASCE 7. In the future, these modeling procedures can be used to determine the connection demands on metal building frames with wall heights of 45, and possibly 60, feet.

3.3 Metal Building Frame Modeling Procedure

Metal building moment frames have characteristics that are very different from conventional steel moment frames. Conventional moment frames are constructed using prismatic hot-rolled I shaped members. Metal building frames are constructed of built-up I shapes that have been optimized to reduce material weight (Newman 2004). Web-tapered sections are used to increase the flexural capacities where the moment demand is greater. The highest moment demand is located at the top of the columns and at the ends of the rafters.

3.3.1 Nonprismatic Element

For this research, the frame components will utilize the nonprismatic beam-column element that is proprietary to SAP2000. Another option would have been to use a series of prismatic elements. But, in order to reduce the total number of degrees of freedom while

maintaining accuracy, the nonprismatic beam-column element was used in modeling the columns and rafters of the frames. Smith (2013d) has already shown that the nonprismatic beam-column element in SAP2000 provides sufficiently accurate results when the column or rafter segment is discretized into four elements. Figure 3.2 shows a single frame for Model 85.
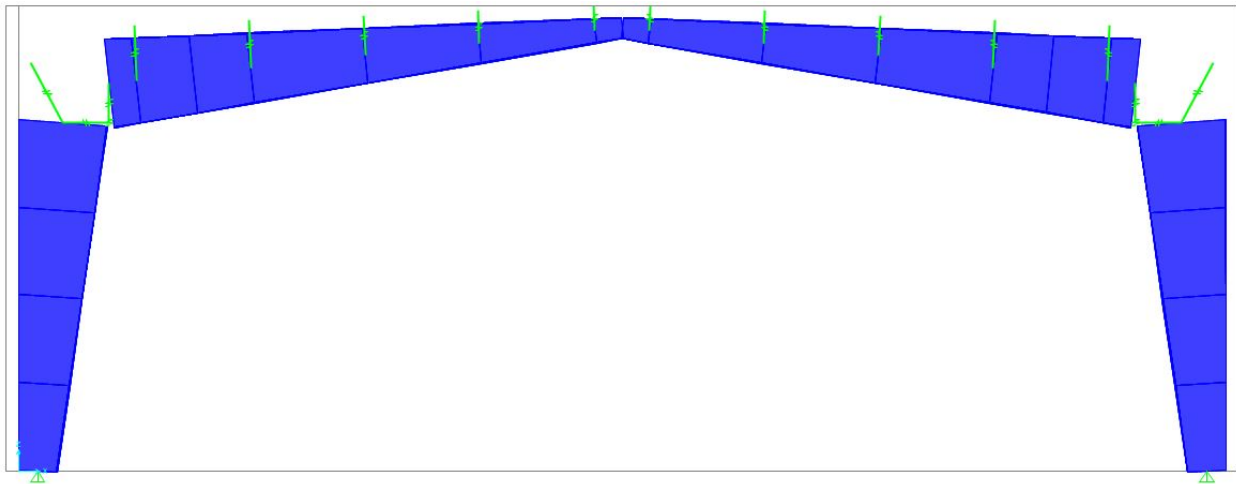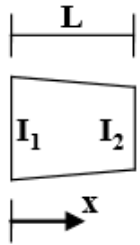
Figure 3.2. Extruded View of Discretization of Frame 85 into Nonprismatic Elements

To build the nonprismatic element, the two end cross-sections were generated. SAP2000 allows the user to set the variation in flexural stiffness for major axis bending and minor axis bending. The formula used in the moment variation for the nonprismatic element is shown in Figure 3.3. For linear web-tapered members, the variation in the major axis moment of inertia is predominantly a parabolic function (Equation 1). The axial, shear, torsional, mass, and weight properties all vary linearly over each segment (CSI 2015). The variation in the major axis was set to parabolic and for minor axis, a linear variation was set.

31

$$I(x) = \left[\left(I_1^{1/n} \right) \left(1 - \frac{x}{L} \right) + \left(I_2^{1/n} \right) \left(\frac{x}{L} \right) \right]^n$$

where,
n = 1 for linear variation,
n = 2 for parabolic variation, and
n = 3 for cubic variation,

Figure 3.3. SAP2000 Nonprismatic Moment of Inertia Variation (CSI 2015)

One fundamental characteristic of singly symmetric cross-sections that are web-tapered is that the centroidal axis is curved (Figure 3.4).   When an axial load is present, this out-of-straightness results in a second order P-δ effect in that segment. For this research, the nodal locations were computed as the centroidal locations. Thus, curvature in the centroidal axis is accounted for in all models.

Top flange: PL ½ × 8
Bottom flange: PL ¼ × 8
Web: ¼ In.
Length: 134 In.
Taper angle: 15°
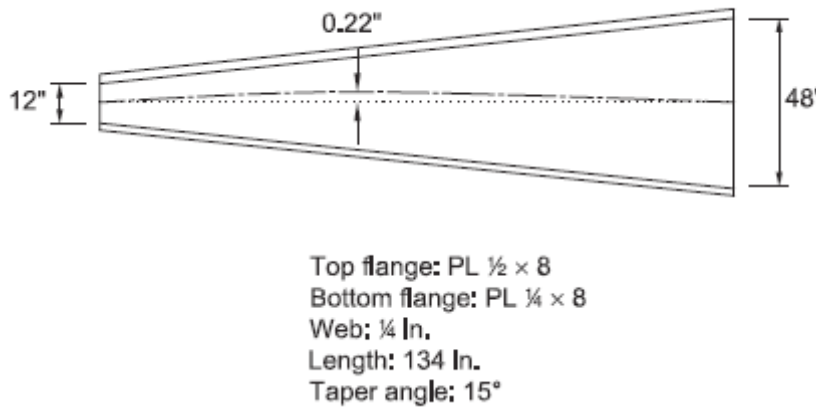
Figure 3.4. Curved Centroidal Axis of Singly Symmetric Tapered Member (Kaehler et al.

2011)

At the location of segment transitions, the use of different flange sizes is common. When this occurs, there exists a discontinuity in the theoretical centroidal axes (Figure 3.5). In some instances, this separation can be as high as a several inches (Kaehler et al. 2011). The SAP2000

frames in this research use a rigid link to connect the two nodes whenever this situation is encountered (Figure 3.6).
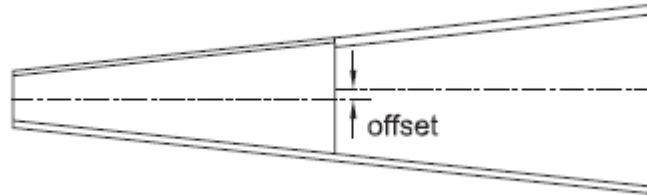
Figure 3.5. Centroidal axis offset at a plate change (Kaehler et al. 2011)
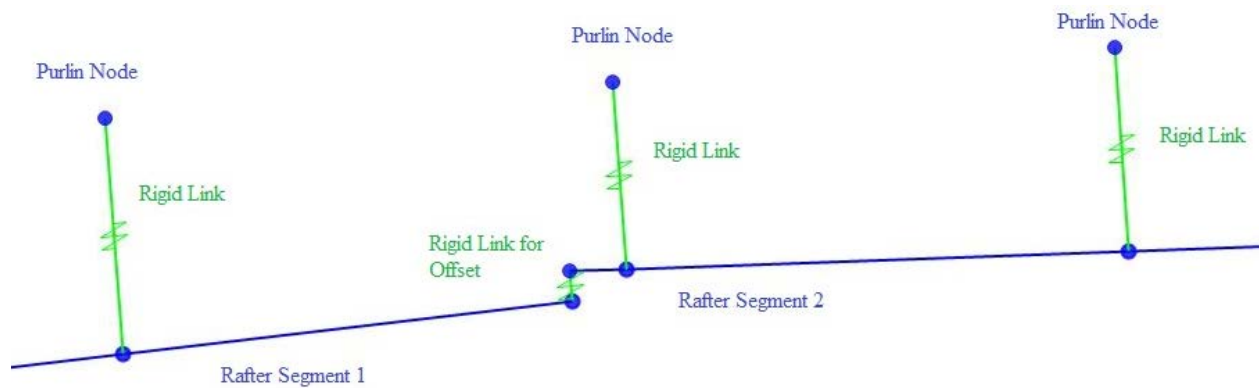
Figure 3.6. Rigid Link connecting two nodes with Different Centroidal Locations

3.3.2   Secondary Framing Systems

The metal building moment frame is the primary lateral resisting system in the frame direction. Purlins are used as a secondary system to transfer the loading from the roof, along the purlin, into the primary frame. The purlins are generally cold-formed steel Z-shaped members that run continuously in the longitudinal direction of the building. For this research, a standard Z-section was used in all the models with a material assignment of a cold-formed steel. The nodal locations were set to the true location of the purlin in relation to the primary frame. A rigid link was used to connect the purlin node to the moment frame node (Figure 3.7).

33
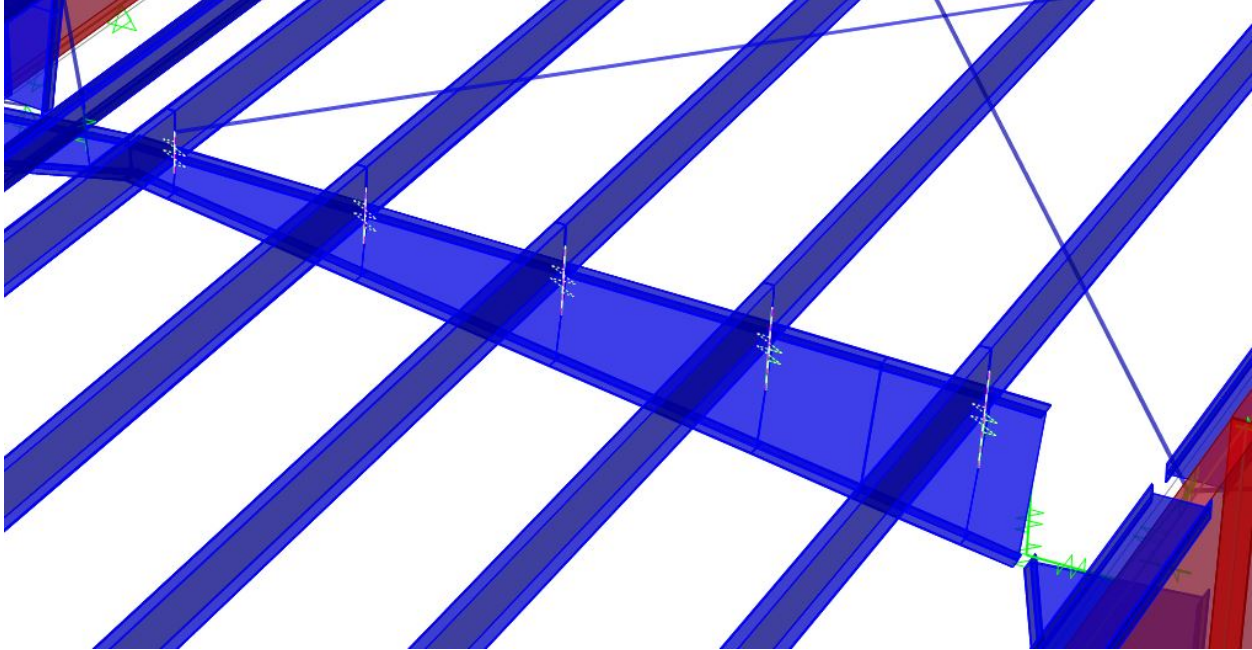
Figure 3.7. Rigid Links connecting Metal Building Frame nodes to Purlin Nodes

For this research, the diaphragm was not explicitly modeled. Bajwa at Virginia Tech experimental and analytically showed that the moment frames in metal building systems act independently from one another. "The roof sheeting appears to provide negligible in-plane shear stiffness" (Bajwa 2010). This is true for any system that has a flexible diaphragm. The research conducted at Virginia Tech only investigated the flexible diaphragm assumptions for a metal building system with light weight metal cladding.

Because the roof diaphragm is not explicitly modeled in SAP2000, careful consideration had to be made in the members connecting the primary frames. The purlins were modeled as a frame element spanning between each moment frame line. There was no shell element to brace and restrain motion in the purlin along the length. It is apparent that the mass distribution of the roof diaphragm could not be lumped along the length of the purlin, as this would generate superfluous modes of vibration in the purlins. Therefore, the mass of the roof is lumped at the

nodes on the frame line based on the tributary area (Figure 3.8). The mass was assigned in all three spatial directions because horizontal ground excitation can induce vertical vibrations in the rafter segments. Twenty percent of the snow load was included in the mass calculations only if the total snow load was 20 psf per ASCE 7-10.
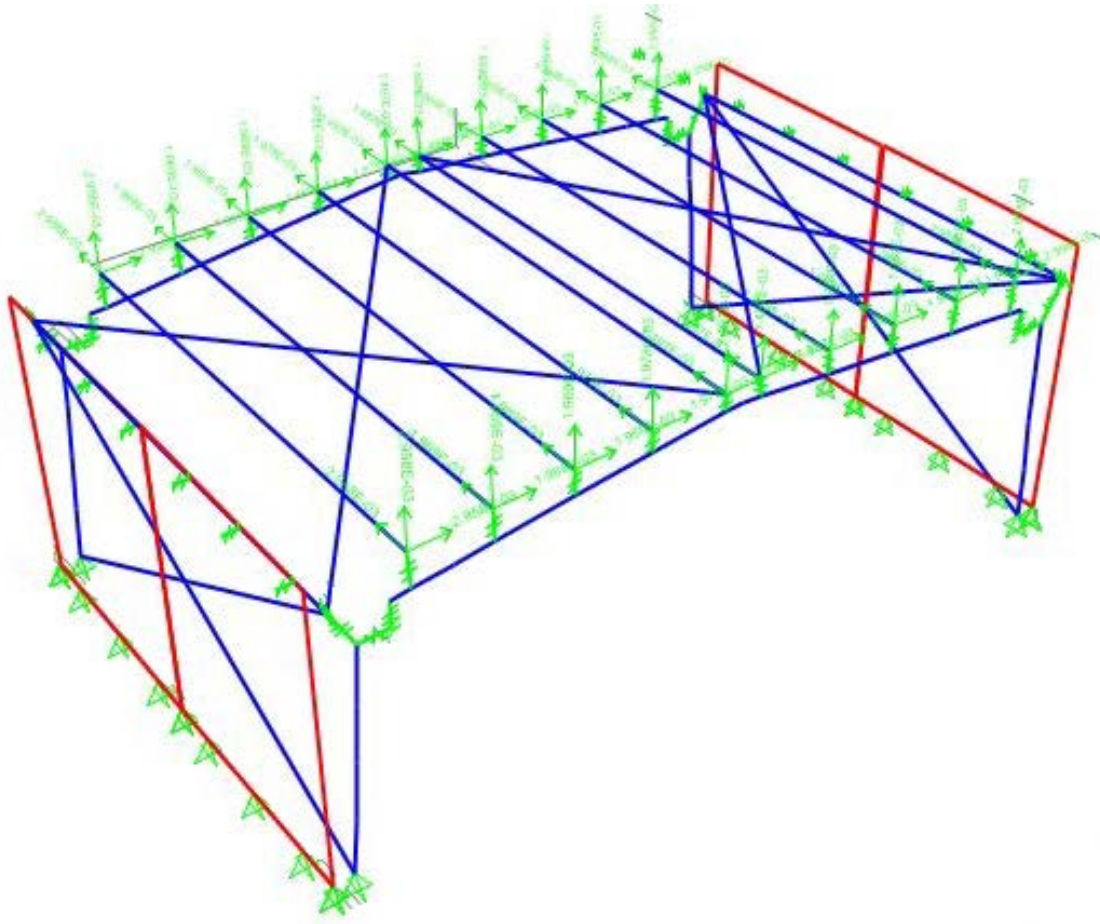
Figure 3.8. Partial SAP2000 Model showing nodal mass at Purlin Nodes

The superimposed dead load, collateral load, live load, and snow load were also applied at the purlin nodes along the primary frame based on tributary area. The self-weight and self-mass of the nonprismatic elements were calculated and included in the models using SAP2000's automatic features. The self-weight and self-mass property modifiers for the purlins was set to zero as the superimposed dead load already included the weight of the purlins.

3.3.3   Panel Zone Modeling

It has been recognized that the panel zone is not a rigid element in metal building systems. There exist several methods for modeling panel zones that have been used in the metal building industry and other that have been proposed in recent research.   This research uses the same modeling technique presented by Smith (2013d). His proposed panel zone modeling was superior to the others due to its kinematic accuracy. Figure 3.9 shows the panel zone region as it was modeled in SAP2000. A rigid link was extended to the location of the spandrel beam near the backside of the panel zone.
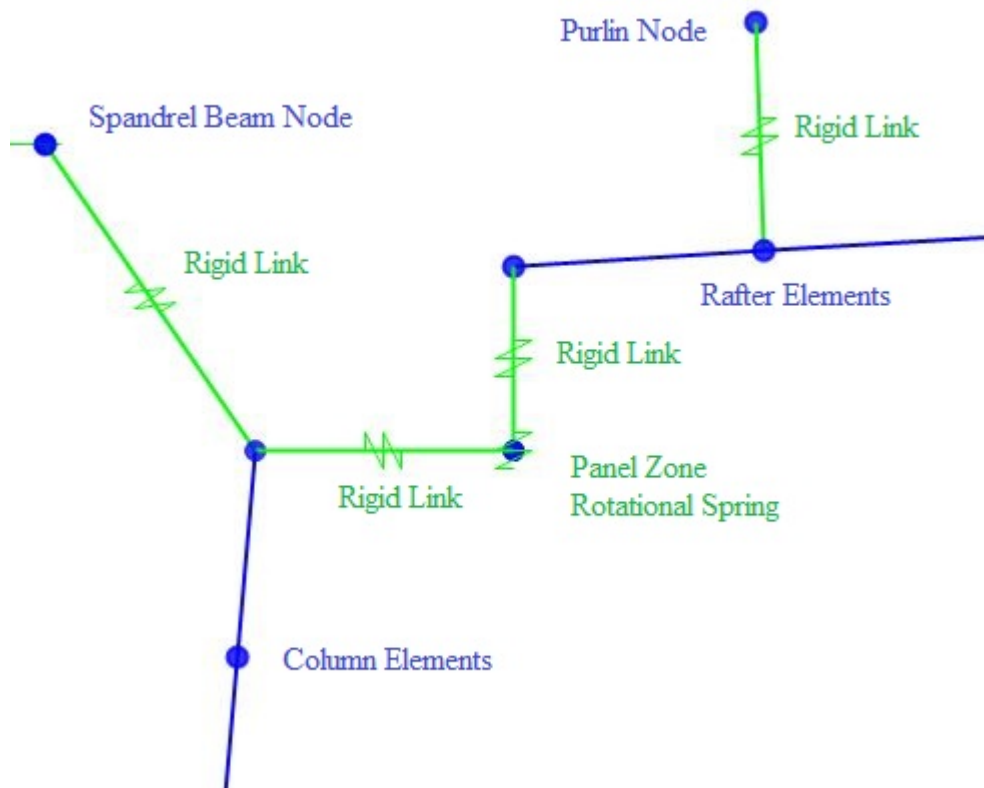
Figure 3.9. Panel Zone Modeling Scheme

The rotational spring stiffness was derived using the same procedure in Abaqus (Simulia 2015) described by Smith. The spring stiffness values calculated in each model are displayed in

the table below. Because Frame 42 was has a monoslope roof, the panel zones for the right side and the left side were different.

Table 3.2. Rotational Stiffness for Panel Zone Spring

Model Number	Rotational Stiffness (kip-inches/radian)
16	2790000
41	6120000
42 Left	4464000
42 Right	6197000
85	1060000
138	4700000

The panel zone modeling scheme was originally developed for use in a 2-D planar frame analysis. For this research, it was assumed that the panel zone flexibility in the out-of-plane direction would not be considered. With this rigidity, the torsional rotation at the top of the column well be equal to the minor axis bending rotation in the rafter. Torsional rotation in the rafter will equal the column minor axis rotation.

3.3.4   Column-to-Base Connections

As mentioned in the literature review regarding Bajwa's research, the true column-base connection is partially rigid. The connection rotational stiffness can be determined through a detailed finite element model of the column-to-base connection. For a static analysis, all the factors identified by Bajwa that affect the rotational stiffness remain constant. A discrete rotational stiffness can be extracted for such static load situations. However, due to the change in axial load in the column during a dynamic analysis, the rotational stiffness of the connection changes during the analysis. It is unlikely that a discrete rotational spring model, or any of the simplified model

configurations that were proposed by Bajwa, could be used to capture the changing rotational stiffness due to the changing axial load that exists during a dynamic earthquake analysis. A refined finite element model of the connection would handle this complex behavior, but it was decided not to include it in the SAP2000 models as it would have significantly increased the complexity of the model. Therefore, the columns in this research utilized an ideal pin condition.

3.4   Hard Wall Modeling

In the development of the SAP2000 models, two hard wall types were considered. The first was precast tilt-up wall panels and the other was a continuous masonry wall. The wall elements were modeled using a thin shell element with an assigned thickness equal to the nominal wall thickness. One important aspect in the finite element analysis is determining the mesh density needed for the results to converge. The shell elements in these models make up the vast majority of the total degrees of freedom in the model. A fine mesh density would increase the time required for a dynamic analysis. Also, one of the performance goals of the new seismic force resisting system is to move the inelastic behavior away from the wall elements and into the resilient connections. A convergence test was performed to find the minimum mesh density required. This study used a maximum element size of 36 in. x 36 in for the wall elements (Figure 3.10).
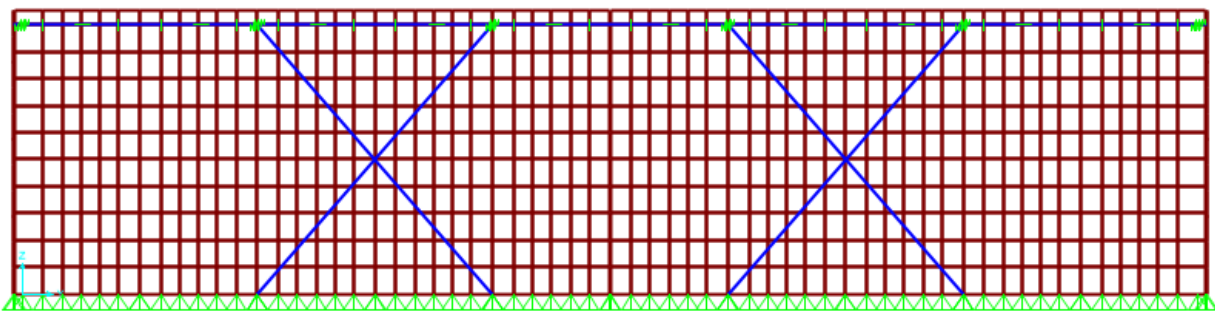
Figure 3.10. Mesh Refinement of Tilt-up Wall Panels

The design of precast tilt-up wall panels are often controlled by the stripping process, transportation, and construction load. The thickness of the panel is sized so that during the removal of the panel from the mold, the wall segment does not crack. Because the seismic loads are not expected to exceed the cracking moment of the tilt-up wall panel, the wall elements were modeled using an elastic concrete material with 4000 psi concrete. For the nonlinear dynamic analyses, it is assumed that the panels will remain uncracked during the earthquake. Precast tilt-up wall panels that are built at a fabrication plant and have to be transported to a work site, must be dimensioned in a manner that is transportable. The distance between frame lines is 25 feet in all the models. For the sidewalls, two discrete tilt-up panels are used in each bay. These panels are not connected to each other and a gap of 0.5 inch separates them. The segmented wall panels are modeled so that they will not interact with each other in any way during the dynamic analysis. The continuous masonry wall will be used as a comparison between the behaviors of the different wall systems. On important difference between the two wall types is the interaction that exists at the corner intersection. As shown in Figure 3.11, the wall panels were modeled with no connection at the intersection. The masonry walls are modeled with the walls connected at the intersection. Any new resilient connection configuration will have to address the displacement variations that exist between the two wall types at the corners of the buildings.
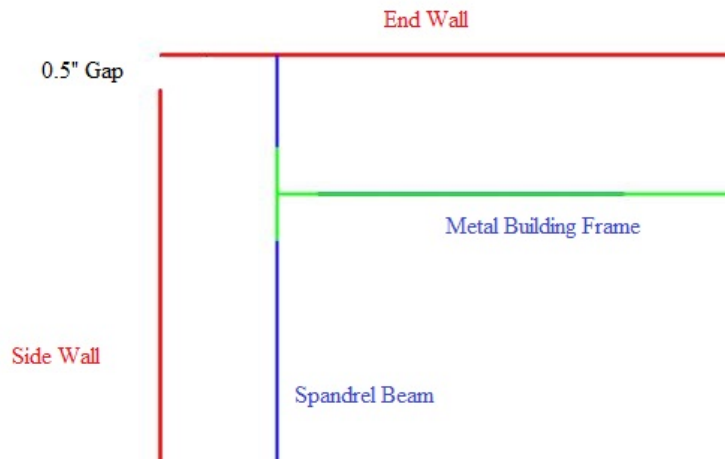
Figure 3.11. Precast Walls structurally separated at Corner of Building

The masonry walls were designed assuming a wall weight of 75 psf. To meet this requirement, the wall consists of 8" CMU blocks that are fully grouted. The assumed specific weight of the concrete is 115 pcf and the specific weight of the grout is 140 pcf. The controlling load case for the masonry wall for the 15 and 30-foot walls was the out-of-plane seismic load case. The 15-foot wall flexural and axial capacities well exceeded the demand required, so the wall only required minimum seismic reinforcement. The 30-foot wall required 2 No. 6 bars spaced every 24 inches. For modeling the masonry wall, the same mesh density as the tilt-up wall panels was used. The compressive strength for the masonry was 1500 psi and modulus of elasticity of 1350 ksi. For the preliminary analyses, it will be assumed that the wall damage will be minimal, so the shell elements will use the elastic material properties.

For both wall system types, openings in the end wall segments were not explicitly modeled. To account for openings, the end wall shell element mass and weight properties were reduced by 20%.

3.5   Longitudinal Bracing and Diaphragm Bracing

For metal building systems, it is typical for the lateral force resisting system in the longitudinal direction of the building to be composed of diagonal tension-only rod braces. Table 3.3 displays the longitudinal dimension of each metal building frame, as well as the number of bays that contain the bracing system. It is not common to place rod bracing in adjacent bays due to constructability issues.

Table 3.3. Longitudinal Geometry of Metal Building Sample

Model Number	Transverse Dimension (ft)	Longitudinal Dimension (ft)	Number of Bays	No. of Bays with Rod Bracing
16	40	75	3	1
41	100	125	5	2
42	160	175	7	3
85	40	75	3	1
138	120	125	5	3

The sidewall bracing for this research was designed as an ordinary concentrically braced frame (AISC 2010b). The equivalent lateral force method was used to size the bracing. Due to the large mass of the end walls, the seismic load combinations controlled the design. The roof diaphragm bracing was designed using overstrength factor, Ω, to ensure the braces remain elastic for the full strength of the energy dissipating fuse elements. The 3-D SAP2000 models were used to perform the structural analysis of the bracing system. This is a departure from common practice, as these systems are designed using 2-D models of the longitudinal frame and roof diaphragm. This was done here for convenience since the 3-D models had already been generated.

The location of the braces in the SAP2000 model were carefully considered. Figure 3.12 shows the details of a typical panel zone in a metal building frame. The spandrel beam's location was assumed to be 18 inches below the eave height. Due to the proximity of the braces near the

spandrel beam, the rod brace connection points for the side wall and roof diaphragm were made at the node where the panel zone intersects the spandrel beam (Figure 3.13). Every brace was modeled using one frame element with a circular cross-section. The compression limit was set to zero as the slenderness ratio of each rod brace is very high. Self-weight and mass property modifiers were set to zero for the braces to simplify the nonlinear dynamic analyses.
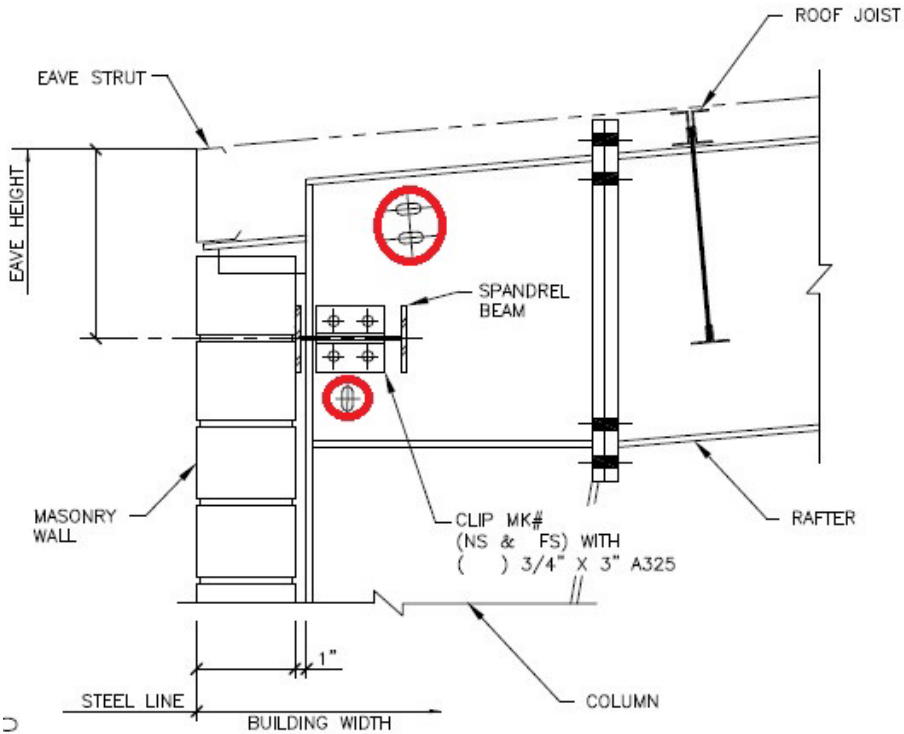
Figure 3.12. Panel Zone Detail (Nucor 2015)
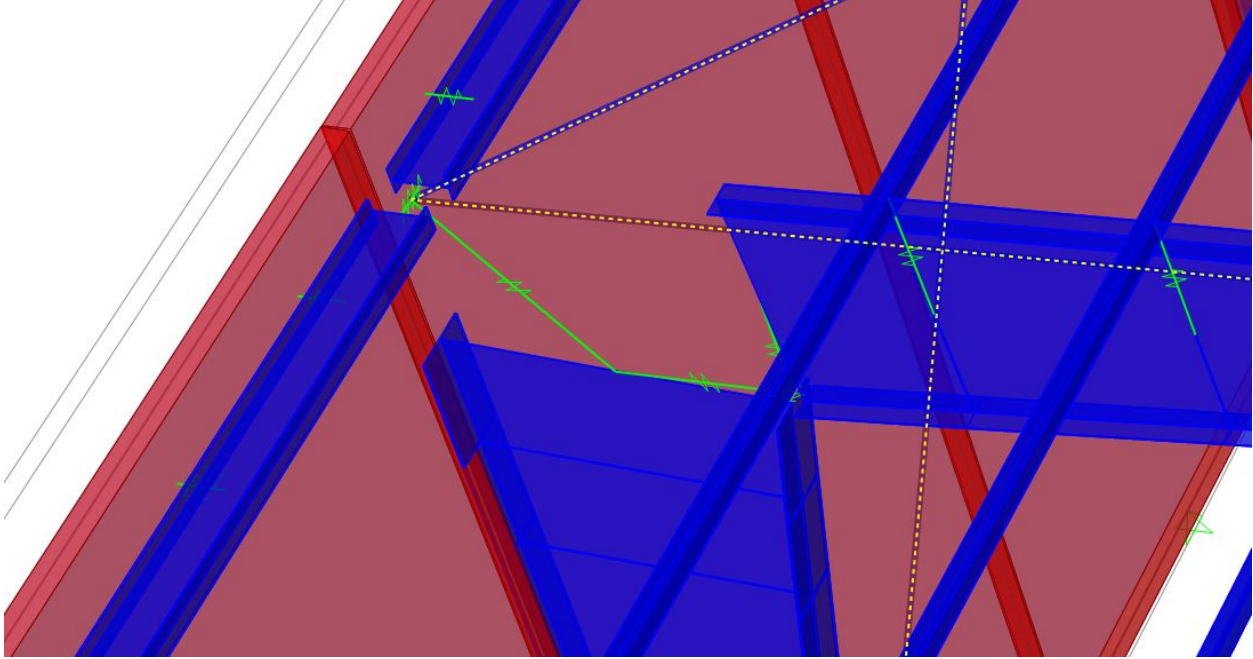
Figure 3.13. Side Wall Bracing Configuration

The roof diaphragm bracing was located at purlin nodes. An effort was made to maintain an aspect ratio close to 1:1 for the x-bracing. The purlins act as struts in the roof diaphragm. If a purlin was found to have inadequate axial capacity, an adequate pipe strut was used to replace the purlin (Figure 3.14).
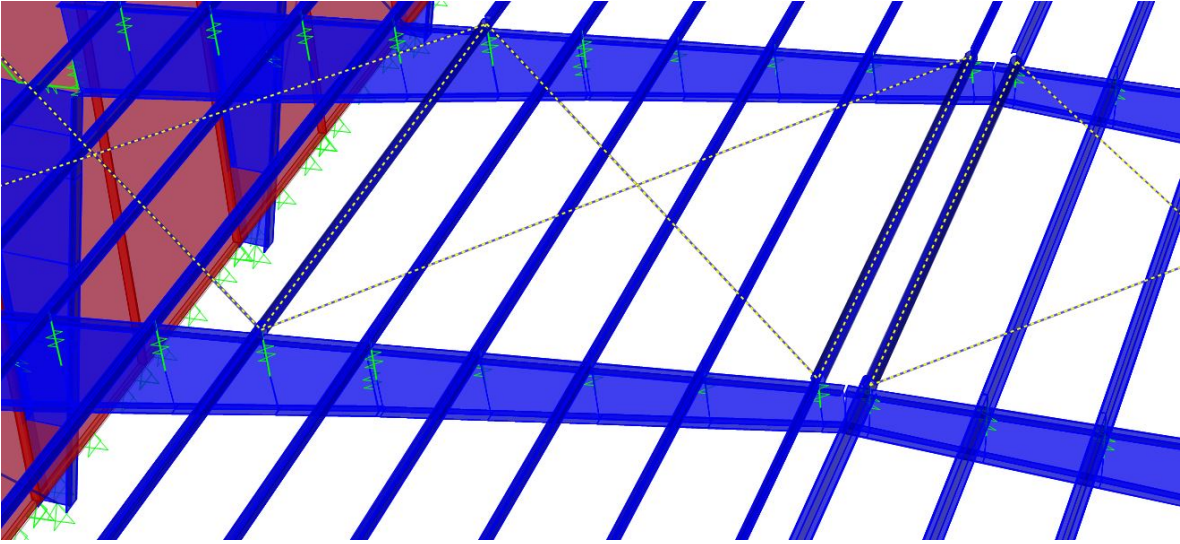
Figure 3.14. Roof Bracing and Pipe Struts in Diaphragm

To model the nonlinear brace behavior, a tension only axial hinge was utilized. The backbone curve assigned to the rod braces was based on the FEMA hinge definitions for a brace in tension (FEMA 2000). Figure 3.15 displays the parameters for the backbone curve. It is assumed that the brace can reach an ultimate capacity of 1.27 times the yield stress.
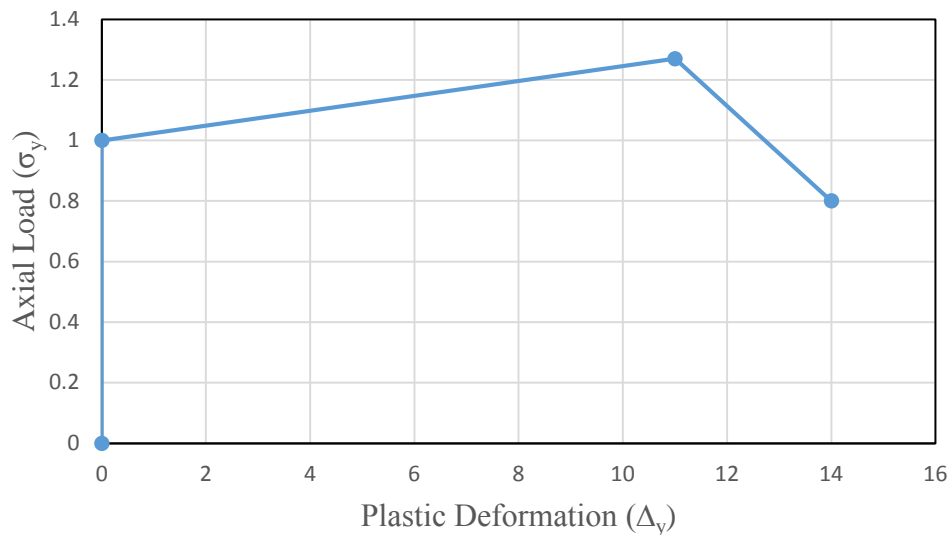
Figure 3.15. Axial Hinge Backbone Curve

3.6   Connection Configurations

The location of the new resilient connections must be constructible, practical, and effective. To provide relief for the stiffness incompatibility between the hard wall and metal building frame, two connection configurations were considered in the SAP2000 models. The spandrel beam transfers the out-of-plane seismic load from the walls into the metal building moment frame. The spandrel beams were designed using ASCE 7 (2010) and AISC 360 (2011). The 15 foot wall required a W12x22 and the 30 foot wall required a W12x26.

The first connection configuration places the energy dissipating connection at the interface between the walls and the spandrel beam (Figure 3.16). For Model 85, one friction connection was placed in each tilt-up panel. A future study will optimize the number of energy dissipating connections required. These connections are designed to slip at a prescribed longitudinal load and are the only connections that have a longitudinal resistance (See Figure 3.16 for slip direction). The other two connections provide out-of-plane resistance and no longitudinal resistance. The metal building framing system will be able to move as one unit in the longitudinal direction, allowing multiple energy dissipating connections to participate. This connection configuration requires communication between the hard wall engineer and the engineer-of-record so that connection forces are accounted for. Also, this connection configuration will require changes to the typical spandrel beam bracing. The flange bracing must not be connected to the wall because it will not allow for longitudinal movement. Instead, the flange bracing will need to be tied into a purlin in the roofing system (Figure 3.17). This will be of benefit to the metal building engineers as they will have full control of the bracing design, and the hard wall engineer will not need to be concerned with bracing details.
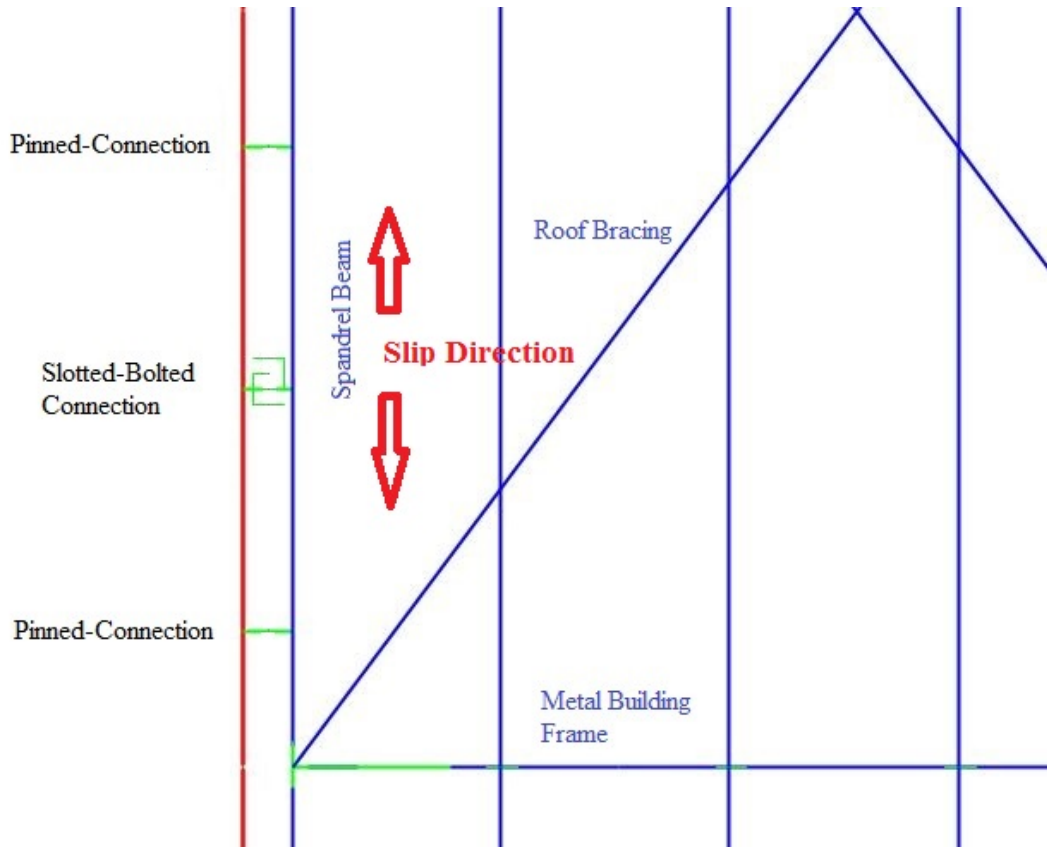
Figure 3.16. Wall-Spandrel Connection Configuration
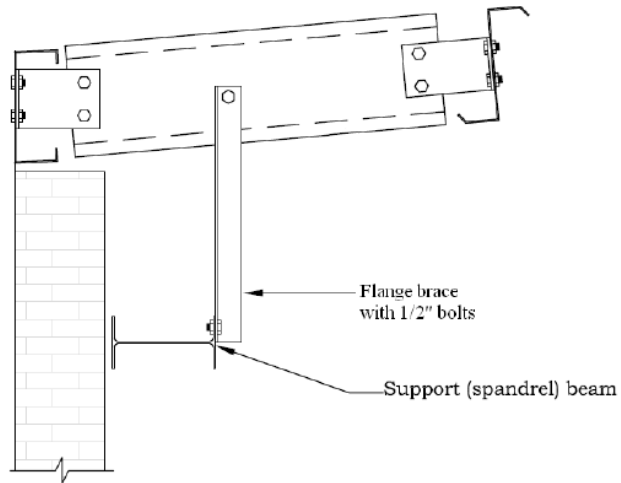
Figure 3.17. Spandrel Beam Bracing Detail (NCI Engineering 2006)

The second connection configuration moves the energy dissipation connections to the interface between the metal building frame and the spandrel beam (Figure 3.18). The connections here will allow the adjacent metal building frame to move longitudinally relative to the spandrel beam. With this configuration, the metal building engineer will have full control over the resilient connection design and details. The typical method of welding the spandrel beam to an embedded plate in the hard wall can still be used. It is predicted that one disadvantage this configuration has is the energy dissipation will be limited to the connections within the bays containing the sidewall and diaphragm bracing. The spandrel beam will not be able to act as an axial collector element to transfer force from the bays with bracing to those without.

Another disadvantage of this connection configuration is that tension-only x-braces would be required in every bay in order to self-center the friction connection. Any means of adding self-centering behavior within the connection increase the complexity of the connection such that it would not be practical. Alternatively, a longitudinal moment frame could provide self-centering behavior to the connections in this configuration. The displacement demands would be larger, as lateral stiffness of a moment frame is less than a braced frame.
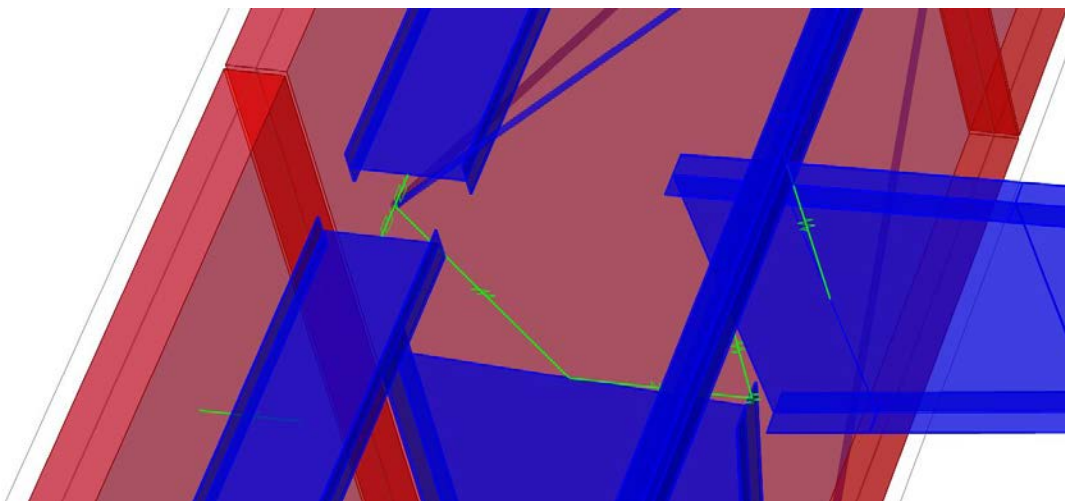
Figure 3.18. Metal Building-Spandrel Connection Configuration

3.7 Connection Parameters

For the case study discussed in Chapter 5, 3-D Model using Frame 85 will use slotted-bolted friction connections between the hard wall and spandrel beam. The resilient friction connection was modeled in SAP2000 using a multi-linear plastic link element. The rotational degrees of freedom of the link element were set as fixed. SAP defines the local axis U1, U2, U3, R1, R2, and R3 respectively as axial deformation, vertical deformation, horizontal deformation, torsional deformation, lateral bending rotation, and vertical bending rotation (Figure 3.19). For the wall-spandrel resilient connection configuration, the link local U3 direction (horizontal displacement) corresponds to the longitudinal direction of the metal building system. The nonlinear properties of an elastic-perfectly plastic behavior were assigned with an initial stiffness of 30 kips/in and a slip force of 3 kips. The axial stiffness (U1) and vertical shear stiffness (U2) was set to remain linear. The axial stiffness assigned was 300 kips/in and the vertical shear stiffness was 30 kips/in. A future 3-D solid finite element analysis study and laboratory testing will be used to calibrate the connection stiffness and nonlinear behavior.

48
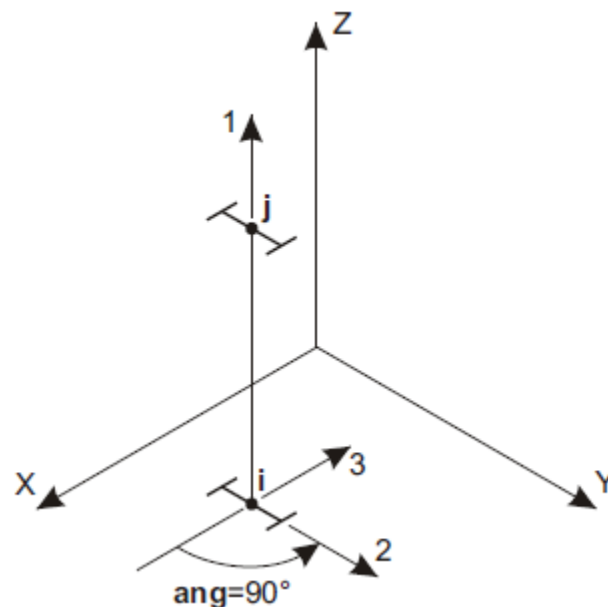
Figure 3.19. Local Axis as defined in SAP2000 (CSI 2015)

It is expected that the friction connections will remain the stiffest components in the longitudinal direction. Seismic load will travel from the roof diaphragm, to the roof bracing, along the spandrel beam, and go to the friction device. The load will initially circumvent tension-only side wall x-braces. It is only after the friction device slips, that load will enter into the x-braces.

3.8   Nonlinear Dynamic Analyses

The earthquake ground motions that were used in the nonlinear dynamic analyses for both the 2-D frame models and 3-D models are listed in Table 3.4. The suite of ground motions were downloaded from the PEER NGA database (PEER 2015). The earthquakes were scaled so that the spectra of the individual ground motions matched the MCE spectra for Riverside, California at three frequencies of importance to the analysis. The earthquake records were selected due to the fact that the shape of the spectra were consistent with the MCE spectrum.

Table 3.4. Earthquake Suite for Nonlinear Dynamic Analyses

	NGA#	Event	Year	Station	Timestep (seconds)	Scale Factor	Duration (seconds)	Frame Direction	Long. Direction
1	57	San Fernando	1971	Castaic Old Ridge Route	0.01	3.1	30	ORR021	ORR291
2	125	Friuli, Italy	1976	Tolmezzo	0.005	3.028	36.345	TMZ270	TMZ000
3	126	Gazli, USSR	1976	Karakyr	0.005	1.073	16.265	GAZ000	GAZ090
4	184	Imperial Valley-06	1979	El Centro Differential Array	0.005	1.456	38.96	EDA360	EDA270
5	725	Superstition Hills	1987	POE	0.01	2.366	22.3	POE270	POE360
6	752	Loma Prieta	1989	Capitola	0.005	1.697	39.955	CAP090	CAP000
7	960	Northridge	1994	Canyon Country - W Lost Canyon	0.01	1.272	19.99	LOS000	LOS270
8	1084	Northridge	1994	Sylmar Converter Station	0.005	0.876	40	SCS142	SCS052
9	1107	Kobe, Japan	1995	Kakogawa	0.01	2.147	40.96	KAK000	KAK090
10	1158	Kocaeli	1999	Duzce	0.005	1.872	27.185	DZC270	DZC180
11	1513	Chi-Chi, Taiwan	1999	TCU079	0.005	1.434	90	TCU079-N	TCU079-E

The inherent damping used in all analyses was represented using Rayleigh Damping (Figure 3.20). Metal building systems have been shown experimentally to have lower inherent damping than conventional moment frames due to fewer connections (Smith 2013d). The damping ratios were set to 2% critical damping at periods that corresponded to the natural period of vibration and 20% of the natural period ($0.2T_n$).
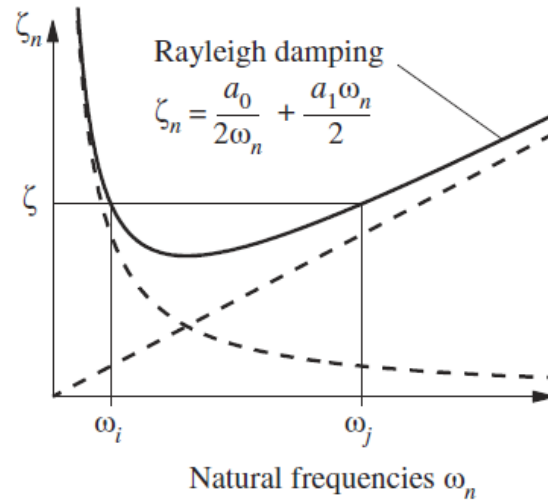
Figure 3.20. Rayleigh Damping (Chopra 2009)

Before each nonlinear dynamic analysis, a nonlinear static analysis with P-delta effects was performed with the dead load, collateral load, and 20% of the full snow load. The nonlinear dynamic analyses started from the last step of that nonlinear static analysis. The time-integration method used was the Hilber-Hughes-Taylor alpha method (Hilber et al. 1977). This method was selected because excess vibrations that have a frequency less than the time step can be damped out. A nonlinear solution is more likely to converge when small amounts of numerical damping are used (CSI 2015). The default alpha value used in the all analyses was -0.05.

3.9   Summary

Chapter 3 detailed the 3-D modeling procedure for metal building systems with hard walls. SAP2000 was selected over Perform 3-D and OpenSEES because it was deemed most practical for this research. The elastic behavior of the metal building frame was modeled using the nonprismatic beam-column element. After considering three panel zone modeling techniques, the modified Krawinkler method was selected to model the panel zone due to its improved kinematic

accuracy. The wall panels were modeled using elastic 4-node shell elements. New slotted-bolted friction connections between the hard walls and steel frame were modeled using a 2-node multi-linear plastic link element. The parameters used in the nonlinear dynamic response history analyses were discussed. This modeling procedure provides the groundwork for quantifying the seismic response of metal building systems with hard walls.

Chapter 4   Frame Capacity Determination and the Development of the Lateral-Torsional Buckling Hinge

4.1   Procedure for Nonlinear Static Pushover Analysis

One very crucial and challenging aspect about modeling the full behavior of metal building frames was how to include inelastic behavior in the SAP2000 model. Because metal building frames are composed of noncompact flanges and slender webs, flexural capacities are controlled by stability limit states such as lateral-torsional buckling (LTB). The formation of a plastic hinge, like those in conventional steel moment frames, simply cannot happen. Therefore the use of a traditional plastic hinge is not appropriate for modeling inelastic behavior of metal building frames. A modeling procedure that captures the post-buckling response of a metal building frame during an earthquake excitation using only frame elements does not currently exist. The use of shell elements has the capability of capturing this post-buckling behavior, but for this research, the exorbitant time required to run numerous nonlinear response history analyses would be prohibitive. This research relies on the fundamental characteristics of LTB to develop a custom frame hinge in SAP2000 that approximates the post-buckling response.

In a conventional steel moment frame, the location of the plastic hinges are well known. For metal building frames, the location of the critical segment is not as straightforward because the nonprismatic frame has been optimized for the capacity to meet the demand along the entire frame. In order to determine the capacity of the metal building frame, nonlinear static pushover analyses were performed in Abaqus.

As stated in the literature review, Hong (2007) developed a finite element analysis procedure for determining the capacity of metal building frames. In order to verify the finite element analysis procedure used in this research, the Hong test frame was recreated in Abaqus and the analysis results were compared with experimental results.

The metal building columns and rafters were modeled using a reduced integration shell element with 4 nodes (SR4). Twenty shell elements were used along the depth of the web, and the flanges were discretized into 12 elements (Figure 4.1).
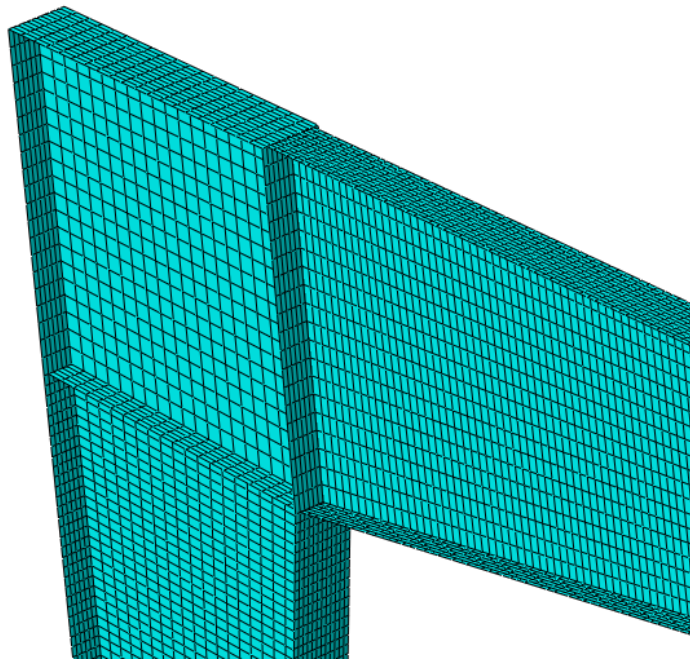
Figure 4.1. Mesh Refinement for Flanges and Webs

The stress-strain diagram used for the steel material is shown in Figure 4.2. The true stress strain curve was used because the SR4 element is formulated for large displacements.
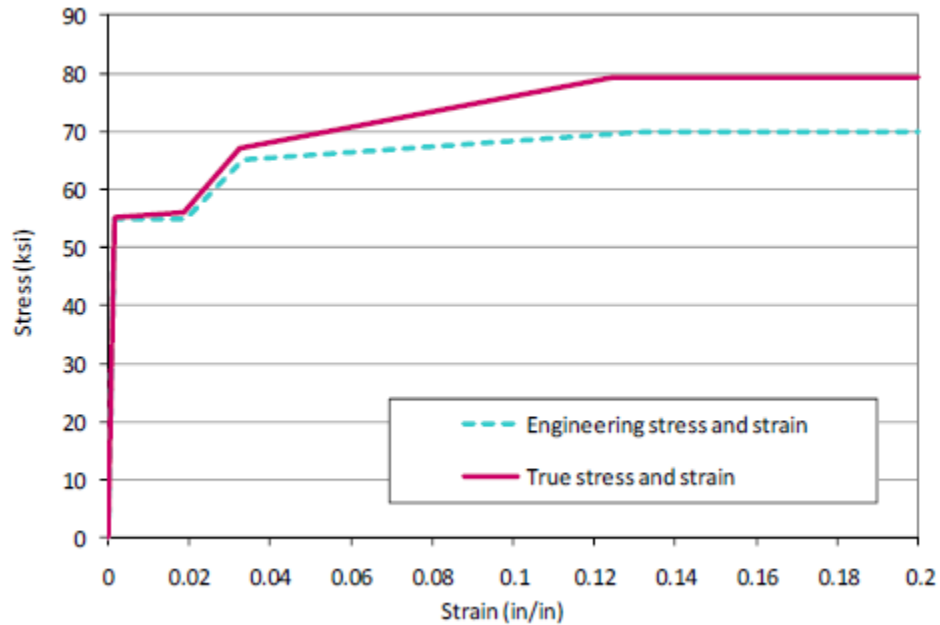
Figure 4.2. Typical Stress-Strain Curve (F_y = 55 ksi) (Kim 2010)

Hong (2007) showed that the inclusion of a rotational spring at the base of the column improved the accuracy of the finite element model. However, the rotational spring stiffness was derived from the experimental results. Because such data does not exist for the frames used in this research, the base of the columns assume an ideal pin condition. The out-of-plane displacement was restrained at locations where a purlin with a flange brace exists. Wherever there was a purlin, the out-of-plane displacement at the centroid of the purlin (four inches above the flange) was restrained. The rafter was constrained to rotate about the centroid of the purlin (Figure 4.3).

Figure 4.3. Constraint Condition for Outer Flange (Smith 2013c)

One of the models was a modular frame in which interior columns were present. The interior columns were not modeled using shell elements. Instead, the interior column was discretized into 10 frame elements. Because the interior column is a leaner column, the base and the connection with the rafter were modeled as pinned connections.

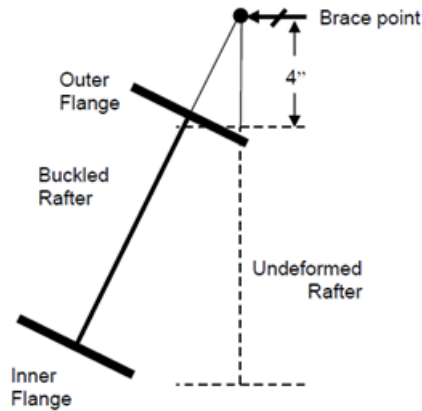To accurately simulate a physical system like a metal building frame, it is imperative to include appropriates imperfections. Without such imperfections the failure mechanism would be incorrect. An eigenvalue buckling analysis was performed using the ELF load, dead load, collateral load, and snow load. The buckling mode shapes exhibited web buckling. The first positive buckling mode shapes were imposed as an initial geometric imperfection with the magnitude set to L/1000, with L being the length of the unbraced segment (Hong 2007).

The inclusion of residual stresses and an additional compression flange sweep was investigated to see if it had a significant impact in the frame's capacity. A residual stress pattern for welded I-shaped members was imposed in the Abaqus model (Figure 4.4). When the web residual compressive stress exceeded the critical plate buckling load of the web, the residual stress values were scaled back to just below the critical buckling stress. To generate this sweep, a

distributed out-of-plane load was applied to the nodes along the compression flange. The maximum displacement of the compression flange sweep was set to a magnitude of L/1000 (Kim 2010).
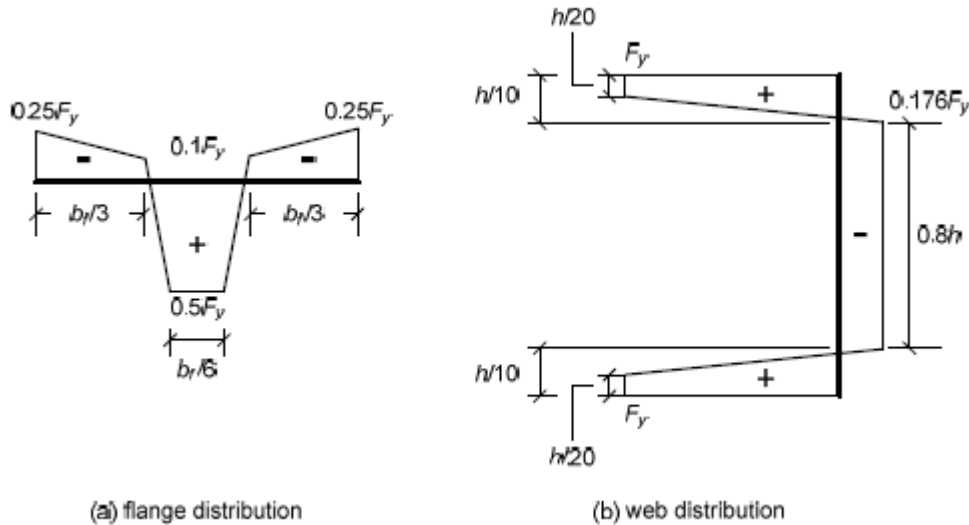
Figure 4.4. Residual Stress Pattern for Flanges and Webs (Kim 2010)

Before the pushover analyses were performed, the dead, collateral, and 20% of the full snow load were applied to the imperfect frame. The pushover analysis was performed using the Modified-Riks Algorithm. The only load pattern that the solution algorithm adjusted was the lateral load.

4.2   Model Verification

Figure 4.5 shows the comparison of the two modeling procedures of the Hong test frame with the experimental results. The first modeling procedure includes the eigenvalue buckling mode imperfection and the second modeling procedure includes the addition of a residual stress pattern and a compression flange sweep. Both modeling procedures underestimate the lateral

stiffness of the frame because a column base was idealized as a pin-connection. The first modeling procedure underestimated the frame's peak capacity by 15% while the second underestimated the strength by 40%. It is likely that the residual stress pattern was too severe. The compression flange sweep imperfection was set to the maximum tolerance allowed for in-field construction. Based on these results, the first modeling procedure was deemed acceptable and was used for all remaining pushover analyses.
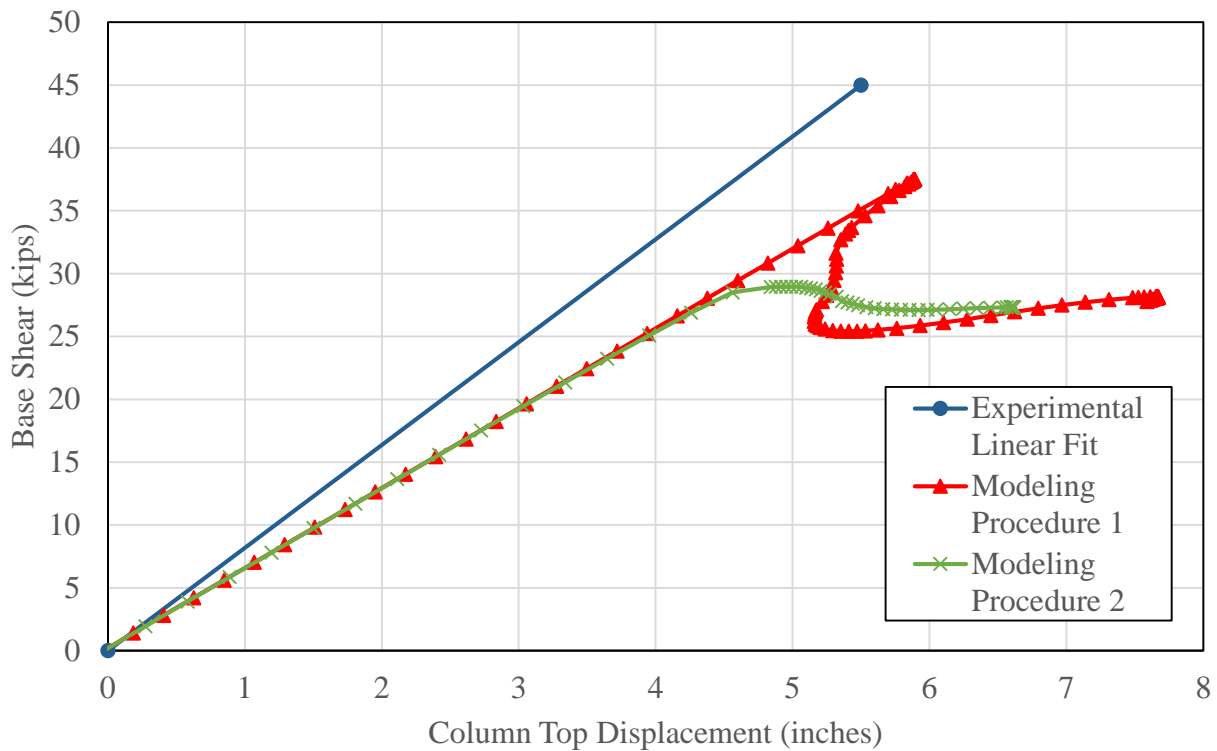

Figure 4.5. Comparison of Finite Element Analysis Modeling Procedures

4.3   Pushover Analysis Results

The pushover analysis results and failure mechanisms for each frame are discussed in the following section.

4.3.1   Frame 16 Pushover Results

This model was a clear span symmetrical gable frame with a span of 40 feet and eave height of 30 feet (Figure 4.6). The post-buckled shape at the end of the analysis is shown in Figure 4.7. The pushover curve for Frame 16 is displayed in Figure 4.8. The elastic behavior ends at roughly 2.8 inches of displacement or 0.8% story drift. When the base shear reached 35 kips, inelastic lateral torsional buckling occurred in segment S4 in the unbraced segment closest to the column. The von Mises stress contours and equivalent plastic strain contours for the buckled segment are shown in Figures 4.9 and 4.10. According to Smith (2013c), LTB of a rafter segment was accompanied by flange local buckling at the middle of the segment and at the flange brace points. This characteristic can be seen in Figure 4.9.   After LTB, the frame lost 23% of its peak strength. At 4.0 inches of displacement or 1.1% story drift, flange local buckling occurs at the top flange in segment S3 in the unbraced segment closest to the column. The von Mises stress contours and equivalent plastic strain contours for this buckled segment are shown in Figures 4.11 and 4.12. At this point in the analysis, the frame has formed a collapse mechanism.
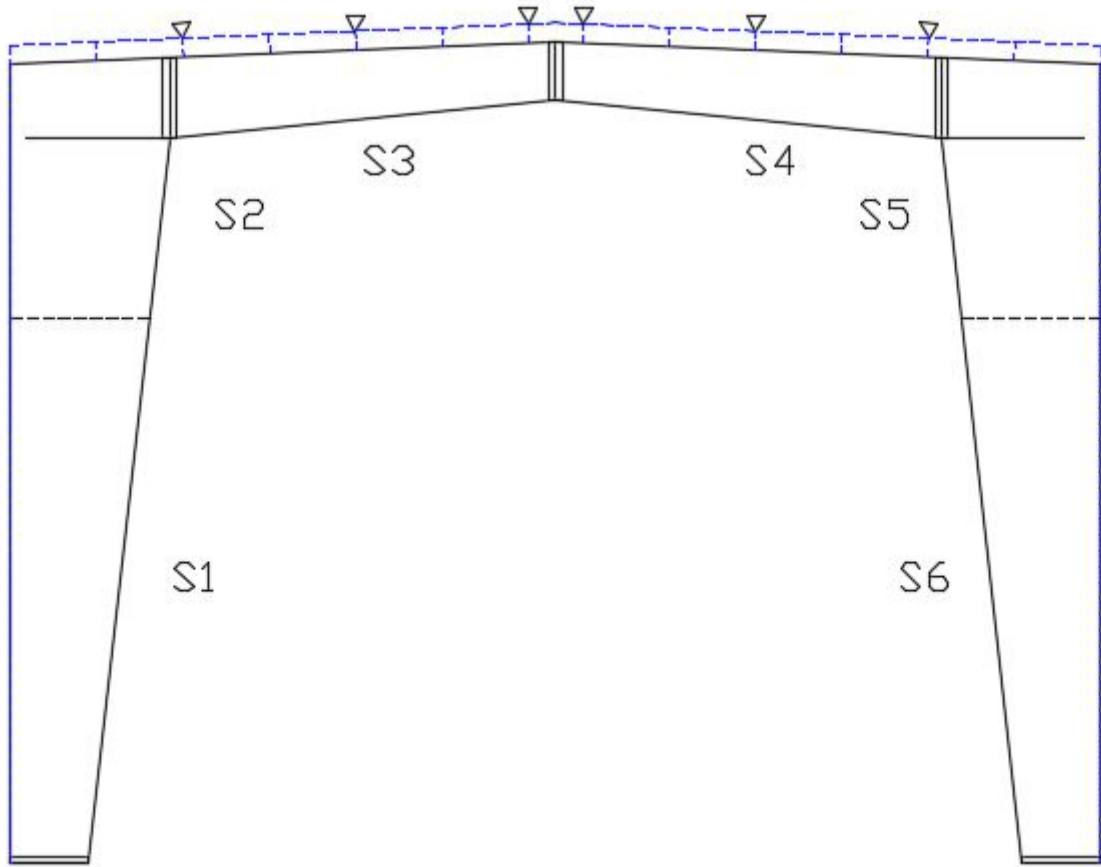
Figure 4.6. Segment Identification for Frame 16

ODB: Frame_16_Push.odb   Abaqus/Standard 6.14-1   Sat Jan 30 16:29:55 Central Standard Time 2016

Step: Push
Increment   126: Arc Length =   2.650

Deformed Var: U   Deformation Scale Factor: +3.000e+00

Figure 4.7. Post-Buckled Frame at the End of Analysis (Deformation Scale Factor = 3)
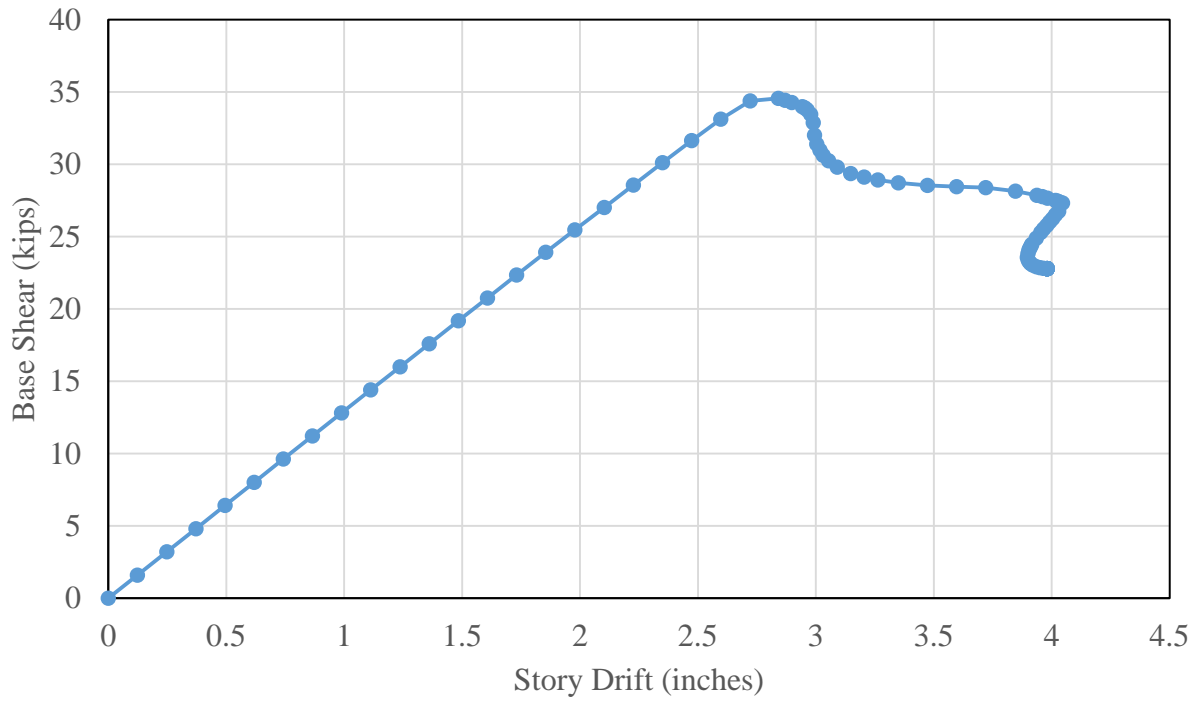
Figure 4.8. Pushover Curve for Frame 16
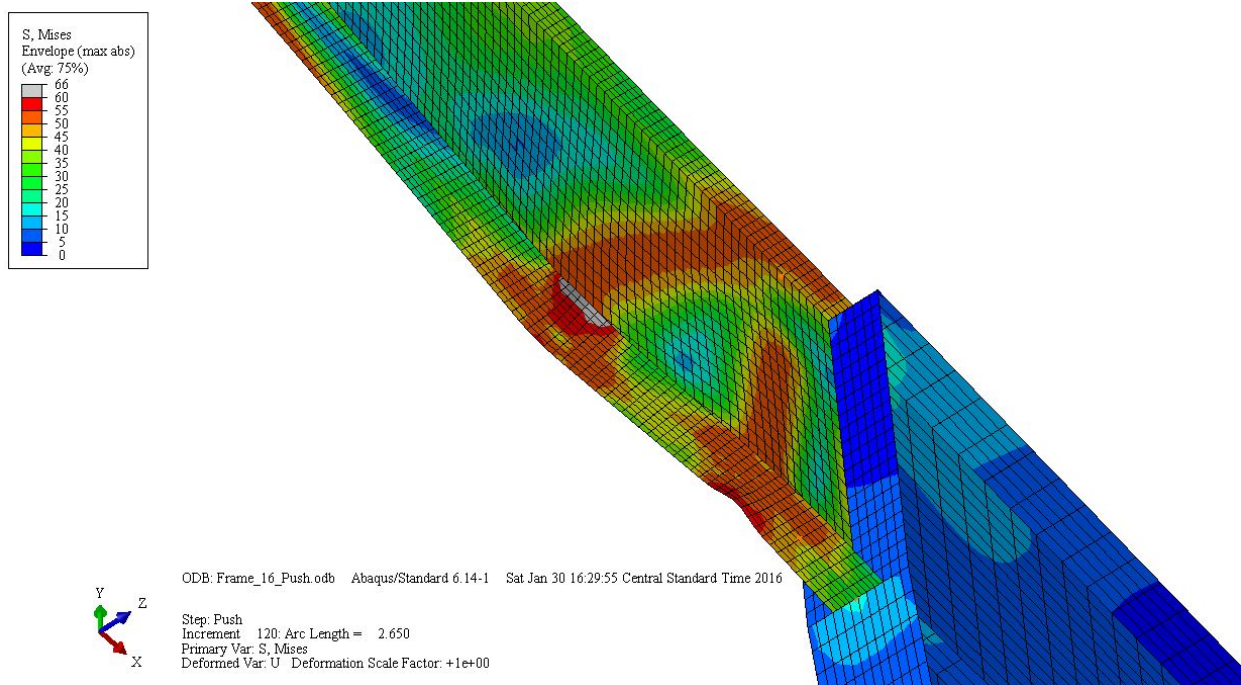
Figure 4.9. Von Mises Stress Contours for LTB Segment in Frame 16

Figure 4.10. Equivalent Plastic Strain Contours for LTB Segment in Frame 16

Figure 4.11. Von Mises Stress Contours for FLB Segment in Frame 16
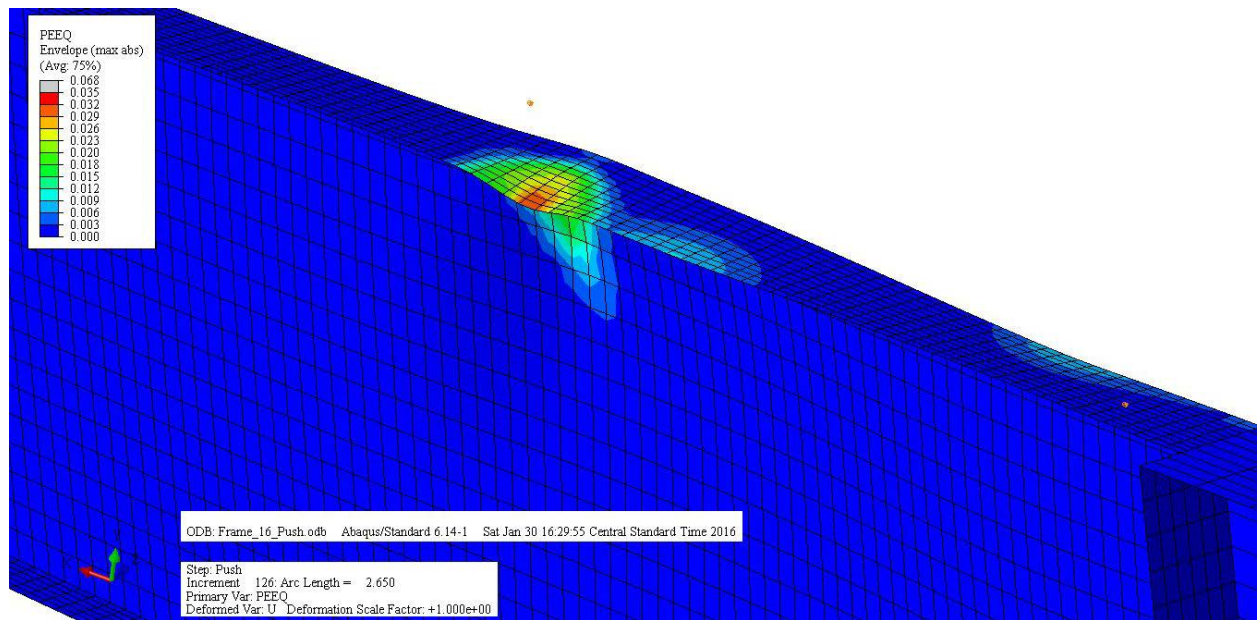
Figure 4.12. Plastic Equivalent Strain Contours for FLB Segment in Frame 16

4.3.2 Frame 41 Pushover Analysis

This model was a clear span symmetrical gable frame with a span of 100 feet and eave height of 30 feet (Figure 4.13). The post-buckled shape at the end of the analysis is shown in Figure 4.14. The pushover curve for Frame 41 is displayed in Figure 4.15. The elastic behavior ends at roughly 5.4 inches of displacement or 1.5% story drift. When the base shear reached 69 kips, inelastic lateral torsional buckling occurred at the pinch point between segments S6 and S7. The von Mises stress contours and equivalent plastic strain contours for the buckled segment are shown in Figures 4.16 and 4.17. Unlike Frame 16, the pushover analysis failed to converge soon after LTB occurred. This frame exhibited the most severe post buckling path of all the frames analyzed.
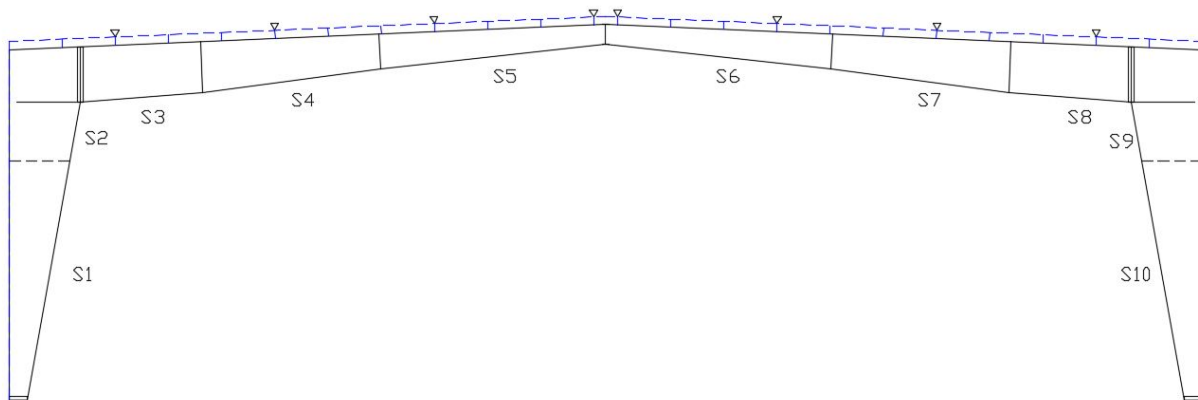
Figure 4.13. Segment Identification for Frame 41

ODB: Frame_41_Push.odb   Abaqus/Standard 6.14-1   Mon Feb 01 09:51:03 Central Standard Time 2016

Step: Push
Increment   111: Arc Length =   3.705

Deformed Var: U   Deformation Scale Factor: +3.000e+00

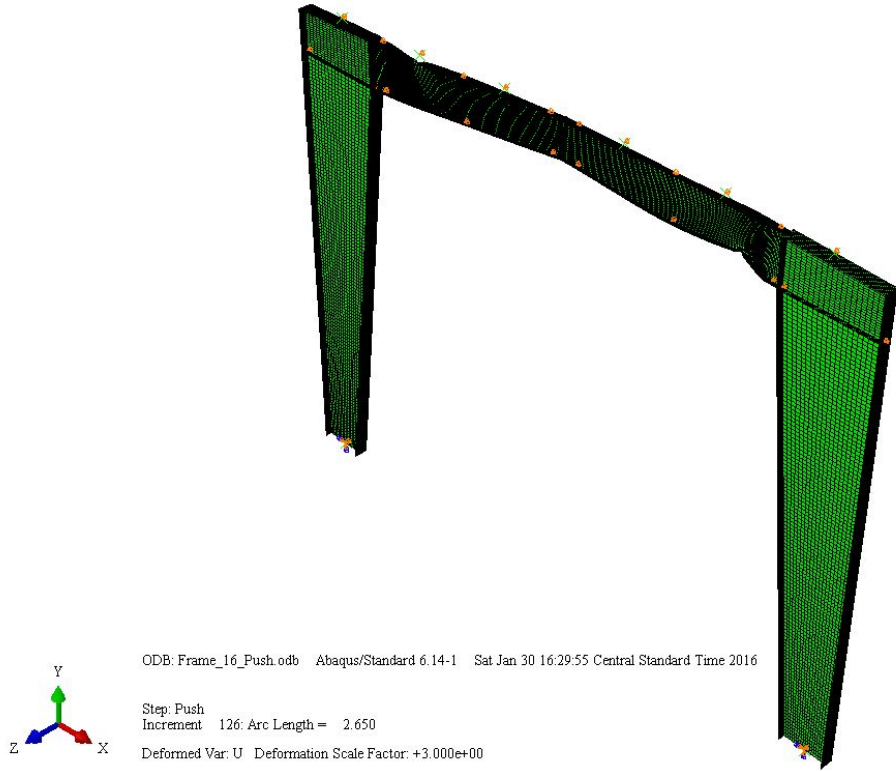**Figure 4.14. Post-Buckled Frame at the End of Analysis (Deformation Scale Factor = 3)**
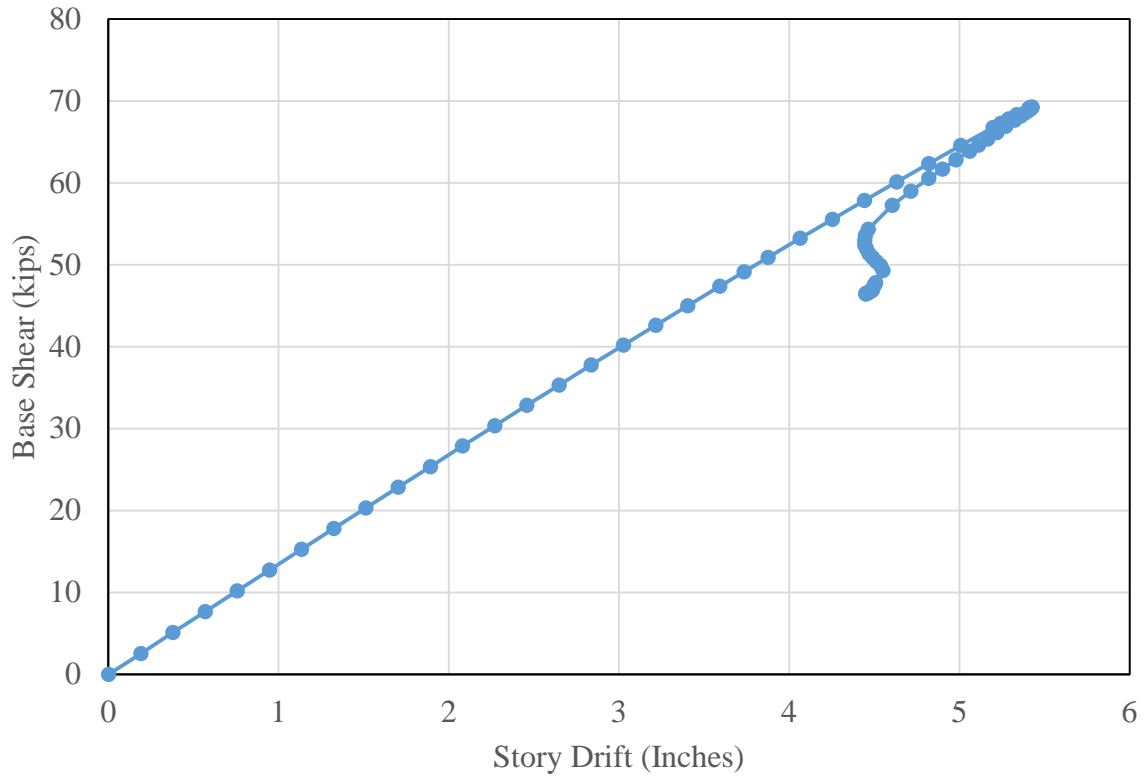
Figure 4.15. Pushover Curve for Frame 41
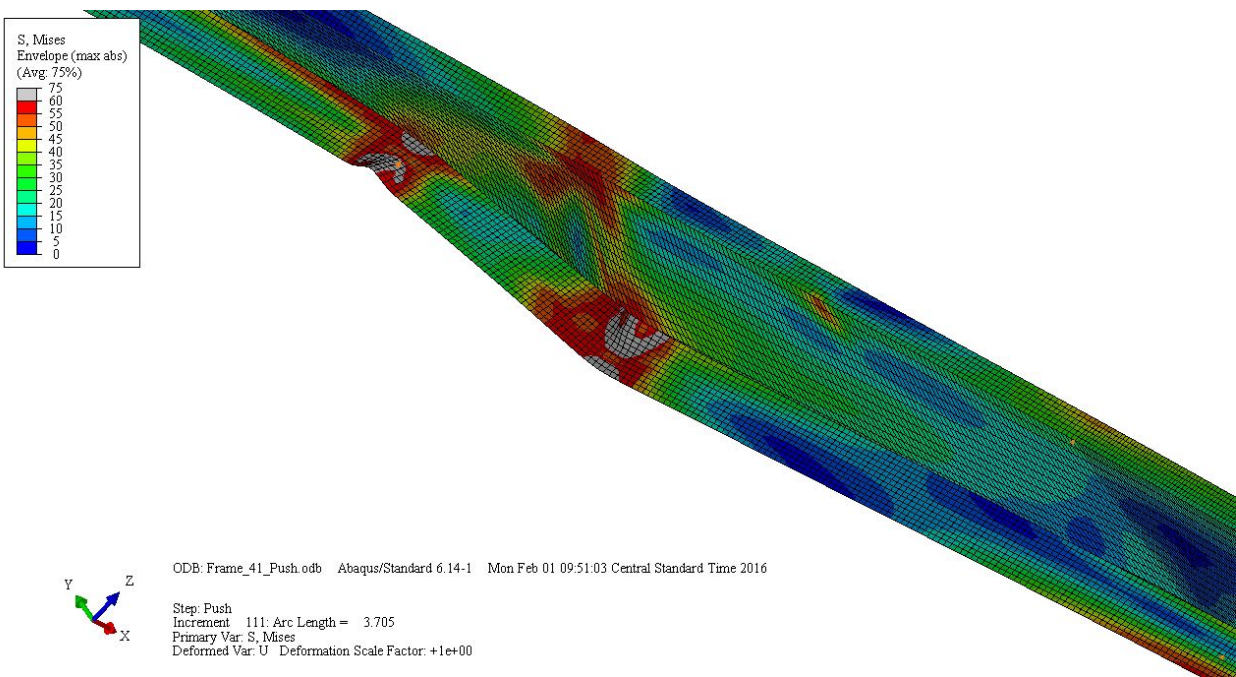
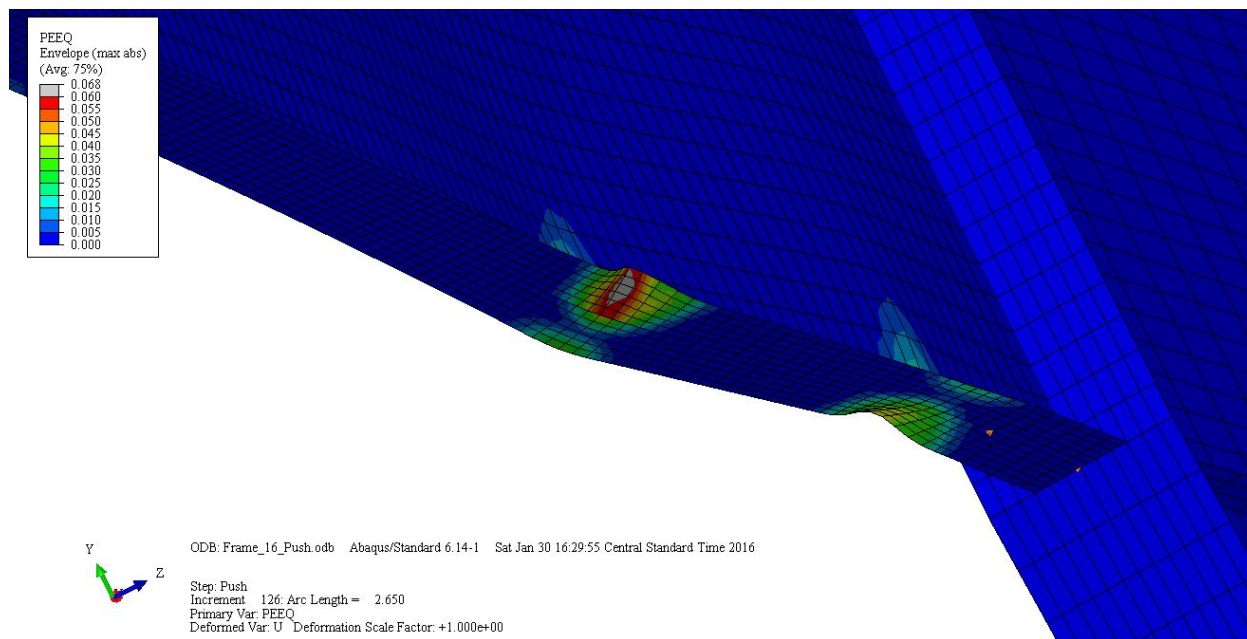**Figure 4.16. Von Mises Stress Contours for LTB Segment for Frame 41**
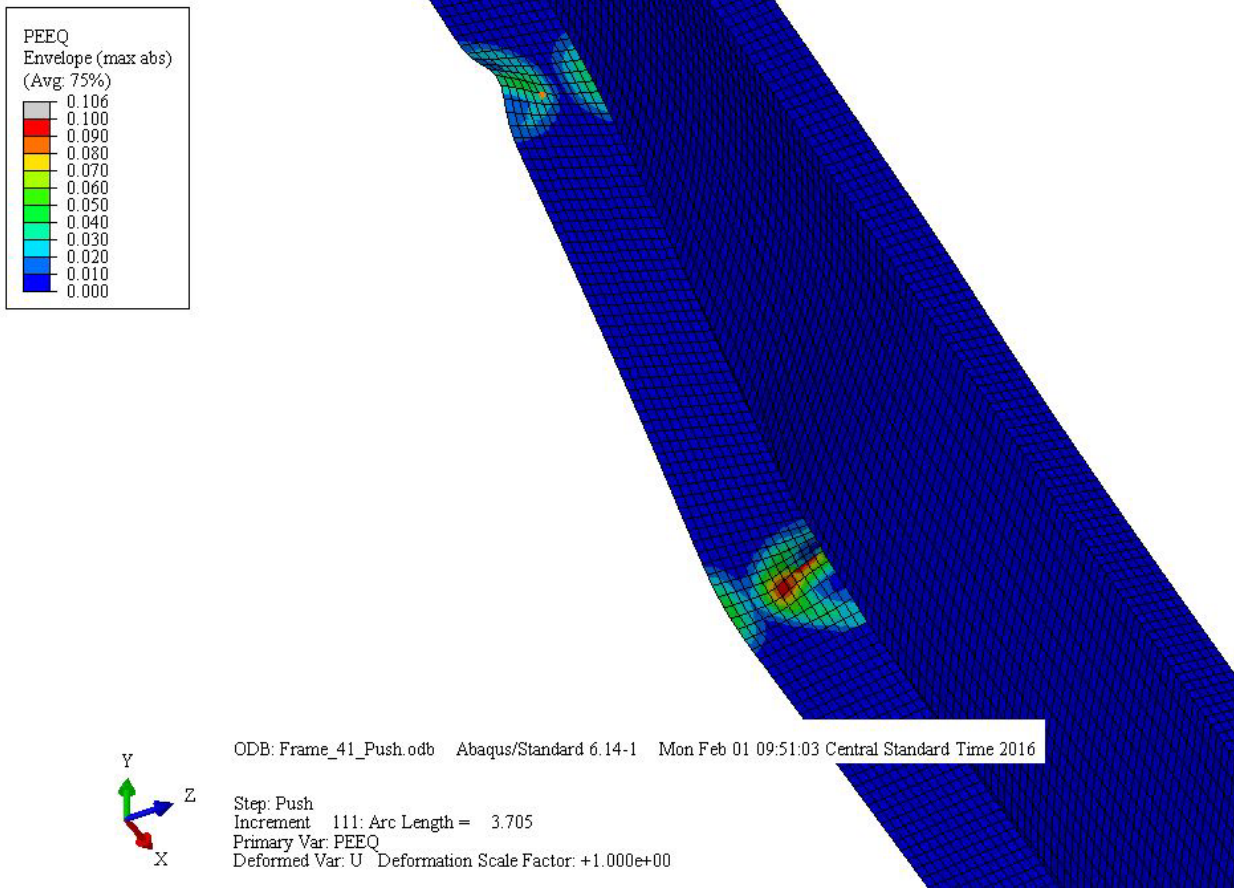
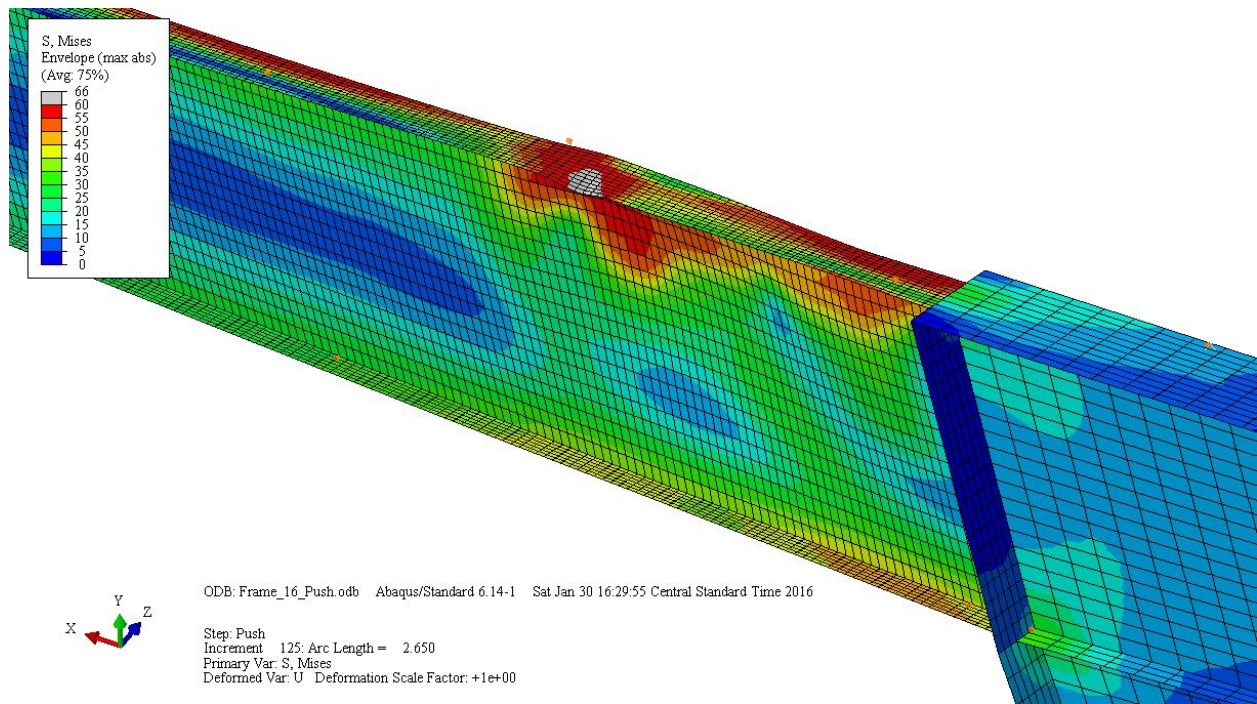**Figure 4.17. Equivalent Plastic Strain Contours for LTB Segment for Frame 41**

4.3.3 Frame 42 (Push East) Pushover Results

The same frame was analyzed with the lateral load application to the right (Figure 4.18).

The post-buckled frame is displayed in Figure 4.19. The pushover curve for this frame is shown

in Figure 4.20. The elastic behavior ends at roughly 8.7 inches of displacement or 2.4% story drift,

which is quite considerable. When the base shear reached 184 kips, LTB occurred at the pinch

point between segments S9 and S10. The von Mises stress contours and equivalent plastic strain

contours for the buckled segment are shown in Figures 4.21 and 4.22. By the end of the analysis,

the frame experienced a strength loss of 23% and a lateral displacement of 10.2 inches.
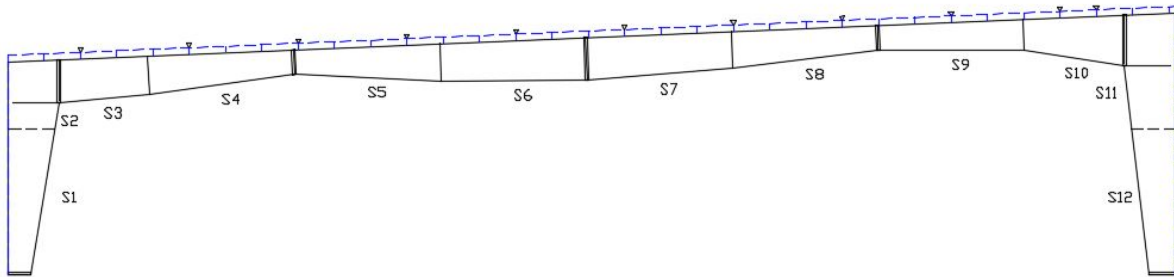
Figure 4.18. Segment Identification for Frame 42

ODB: Frame_42_Push_Right.odb   Abaqus/Standard 6.14-1   Mon Feb 01 11:22:20 Central Standard Time 2016

Step: Push_Right
Increment   74: Arc Length =   7.004
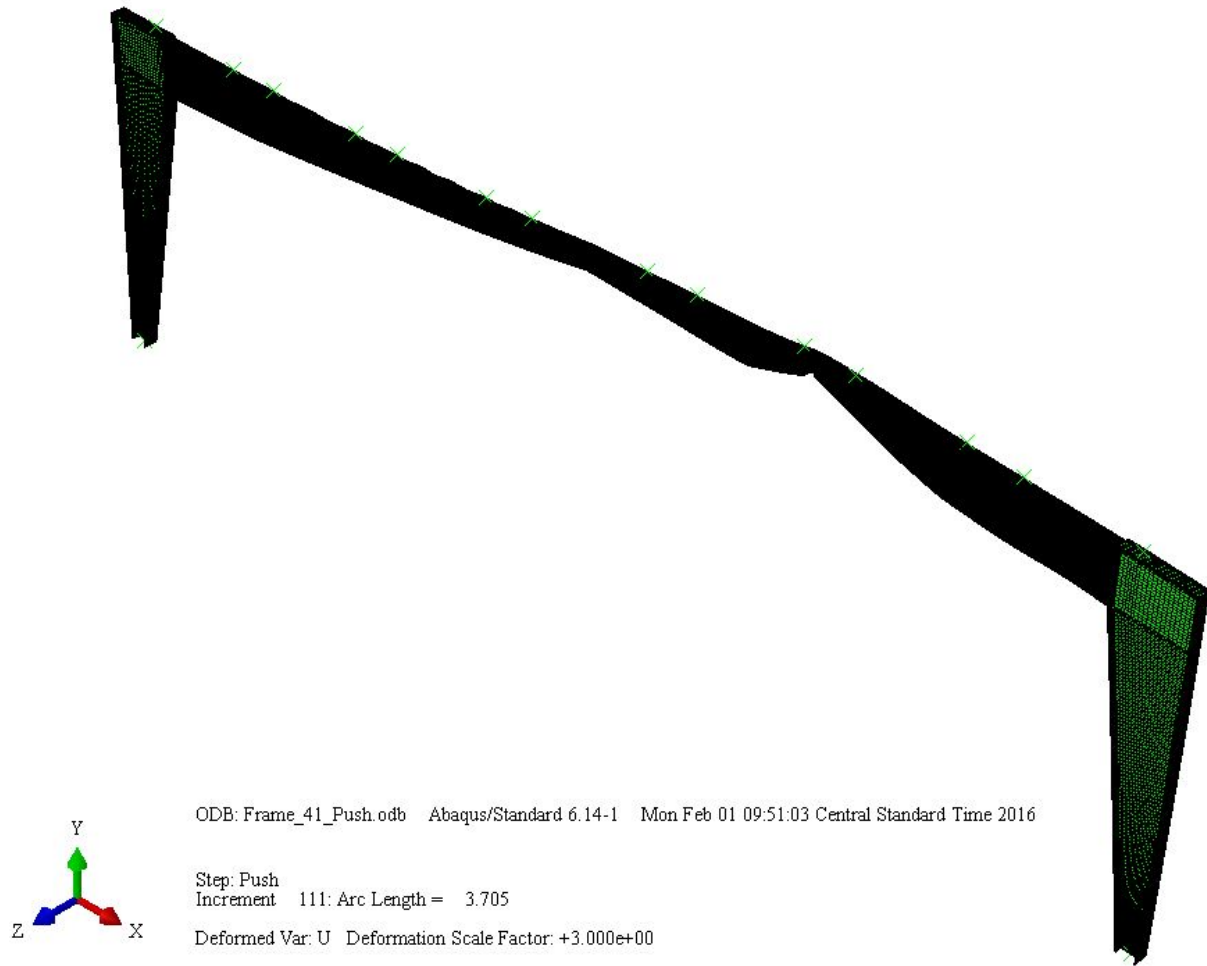
Deformed Var: U   Deformation Scale Factor: +3.000e+00
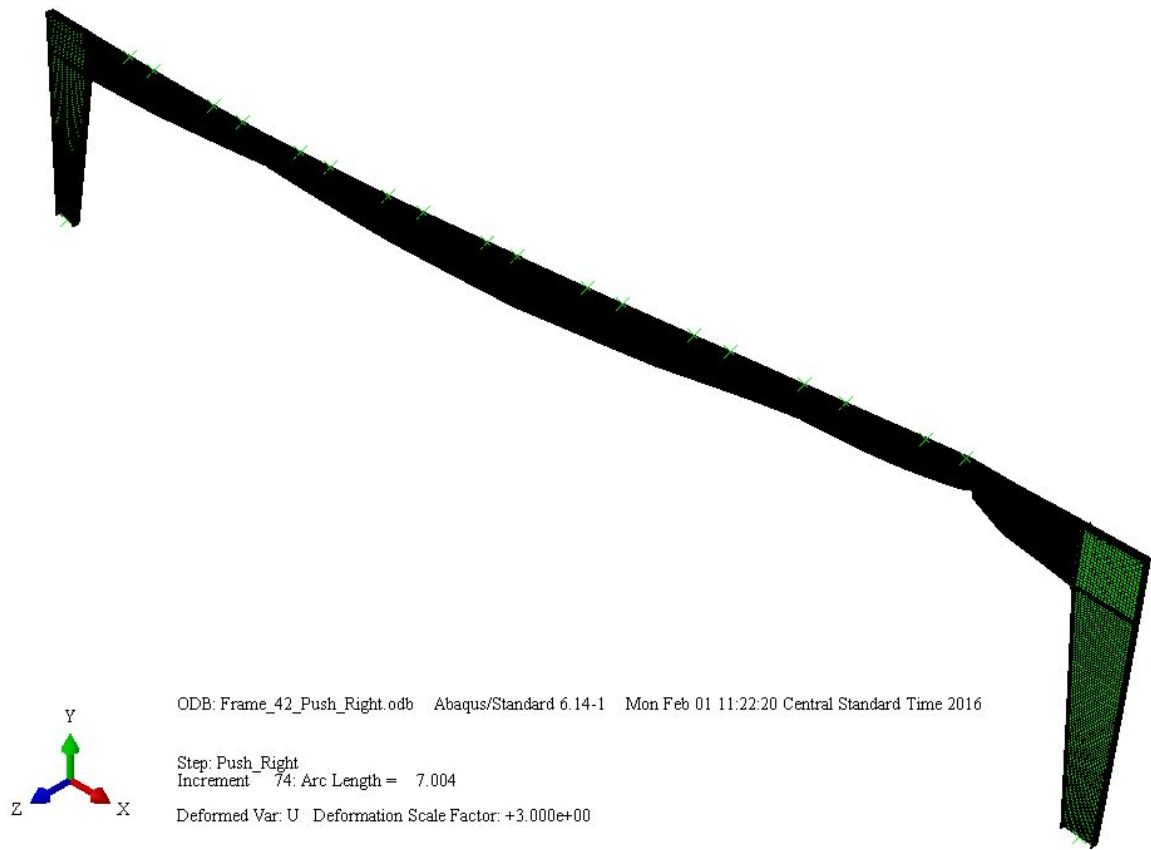
Figure 4.19. Post-Buckled Frame at the End of Analysis (Deformation Scale Factor = 3)
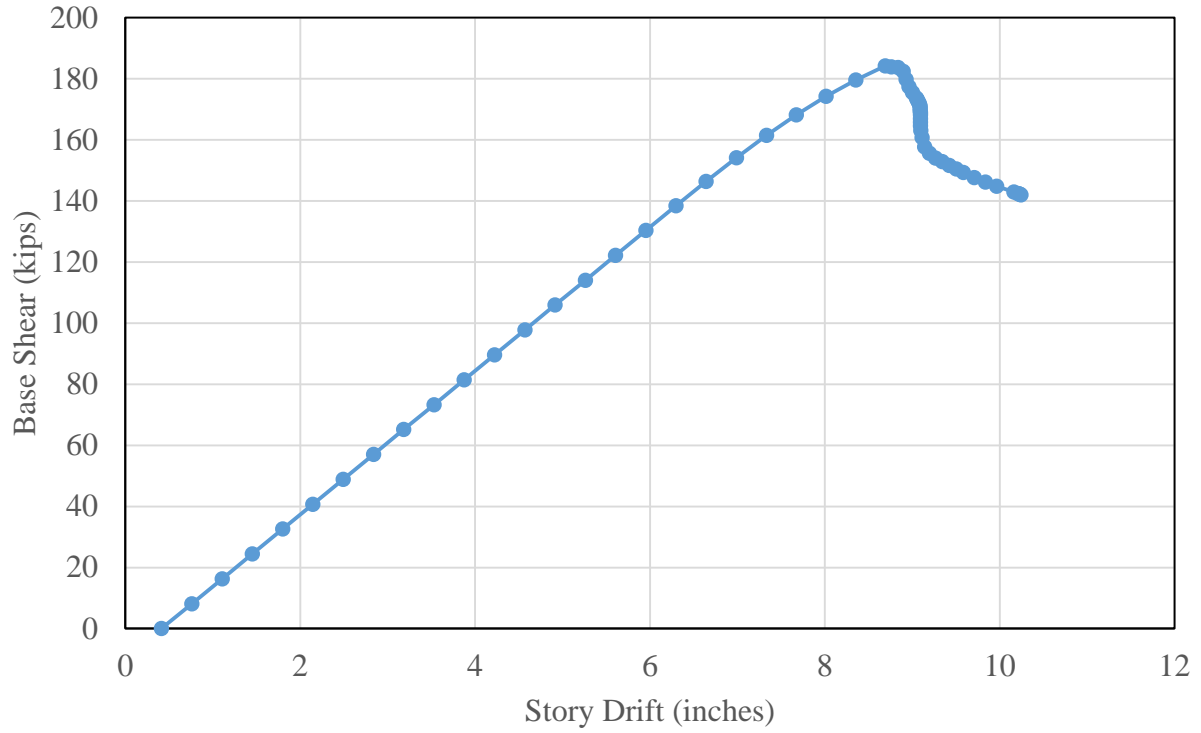
Figure 4.20. Pushover Curve for Frame 42 (East)
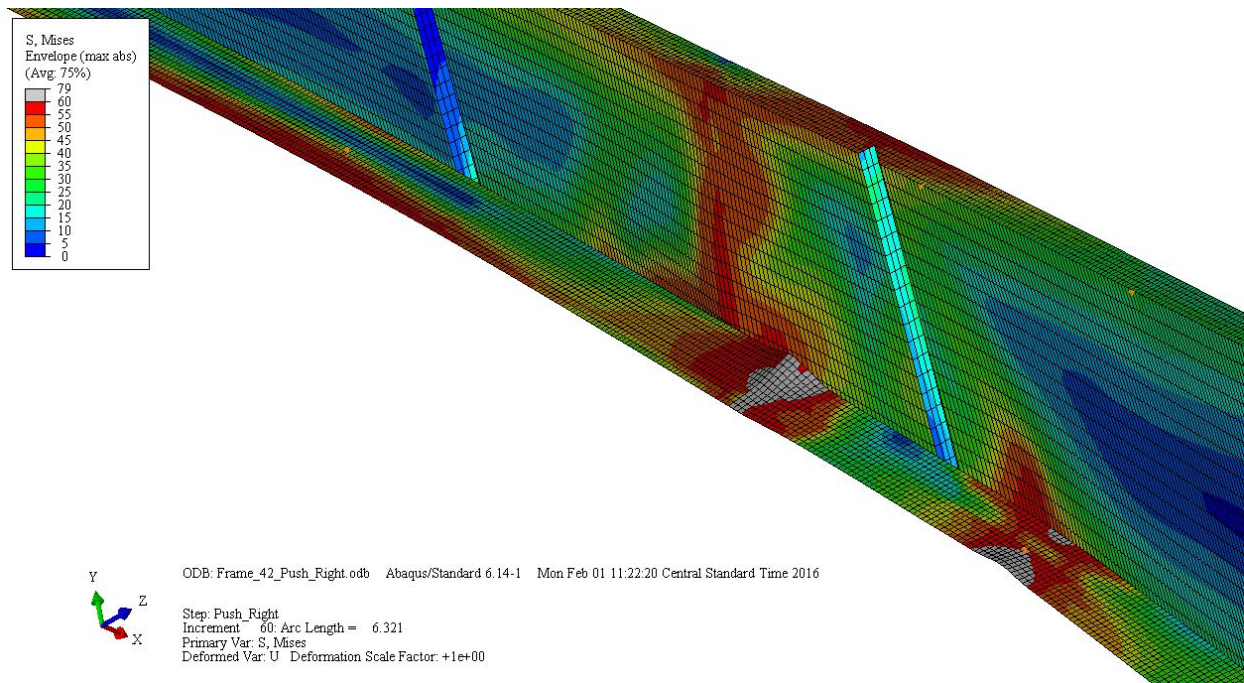
**Figure 4.21. Von Mises Stress Contours for LTB Segment for Frame 42 (East)**

69

PEEQ
Envelope (max abs)
(Avg: 75%)
0.145
0.140
0.128
0.117
0.105
0.093
0.082
0.070
0.058
0.047
0.035
0.023
0.012
0.000

ODB: Frame_42_Push_Right.odb   Abaqus/Standard 6.14-1   Mon Feb 01 11:22:20 Central Standard Time 2016

Step: Push_Right
Increment   61: Arc Length =   6.330
Primary Var: PEEQ
Deformed Var: U   Deformation Scale Factor: +1.000e+00
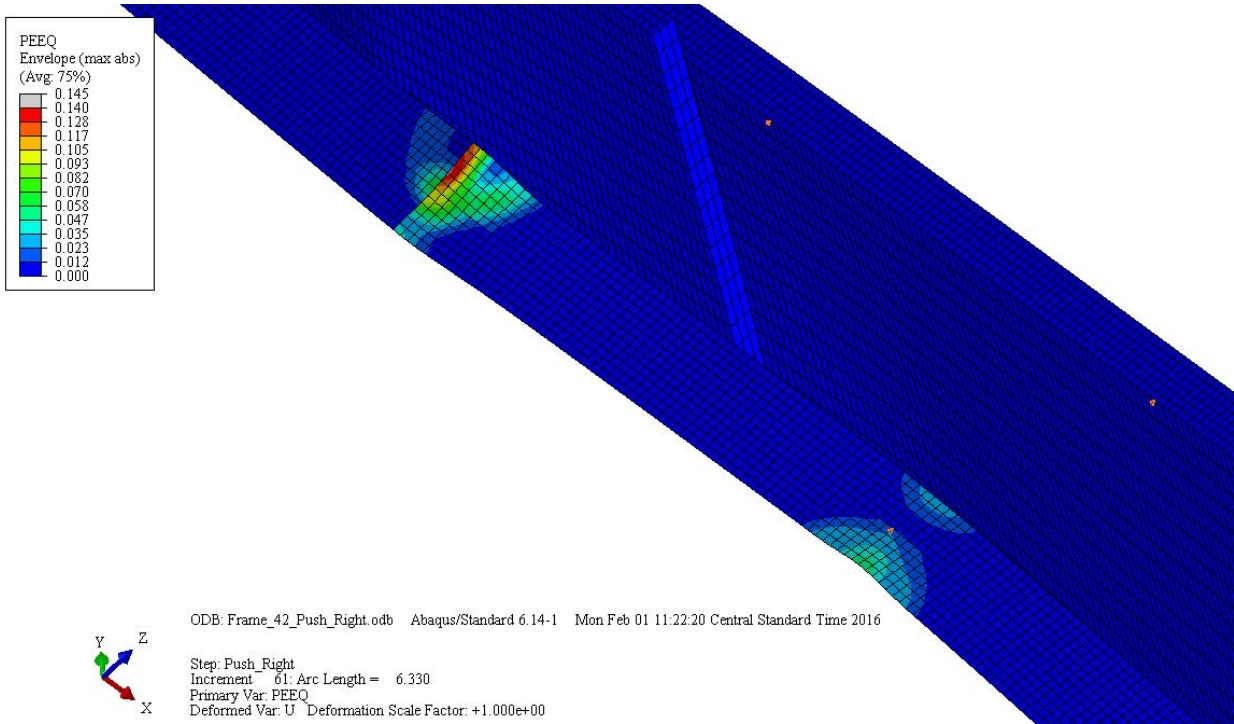
Figure 4.22. Equivalent Plastic Strain Contours for LTB Segment for Frame 42 (East)

4.3.4   Frame 42 (Push West) Pushover Results

This model was a clear span monoslope frame with a span of 160 feet and left eave height of 30 feet (Figure 4.23). Because this is an unsymmetrical frame, two pushover analyses were necessary to determine the failure progression for each direction. The pushover curve for this frame is shown in Figure 4.24. Because the frame is unsymmetrical, the application of the dead, collateral, and snow loads caused the frame to displace to the right. Due to this initial sway, the pushover curve does not begin at a lateral displacement of zero. The elastic behavior ends at roughly 6 inches of displacement or 1.7% story drift. When the base shear reached 147 kips, flange local buckling occurred in segment S5 in the region closest to segment S4. The post-buckled path

70

showed a load reversal followed by a reduced positive frame stiffness. The analysis terminated at a story drift of 7.5 inches.
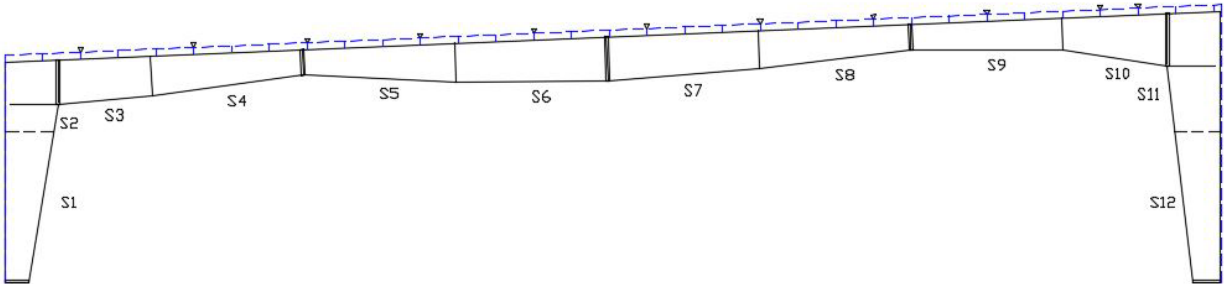
Figure 4.23. Segment Identification for Frame 42
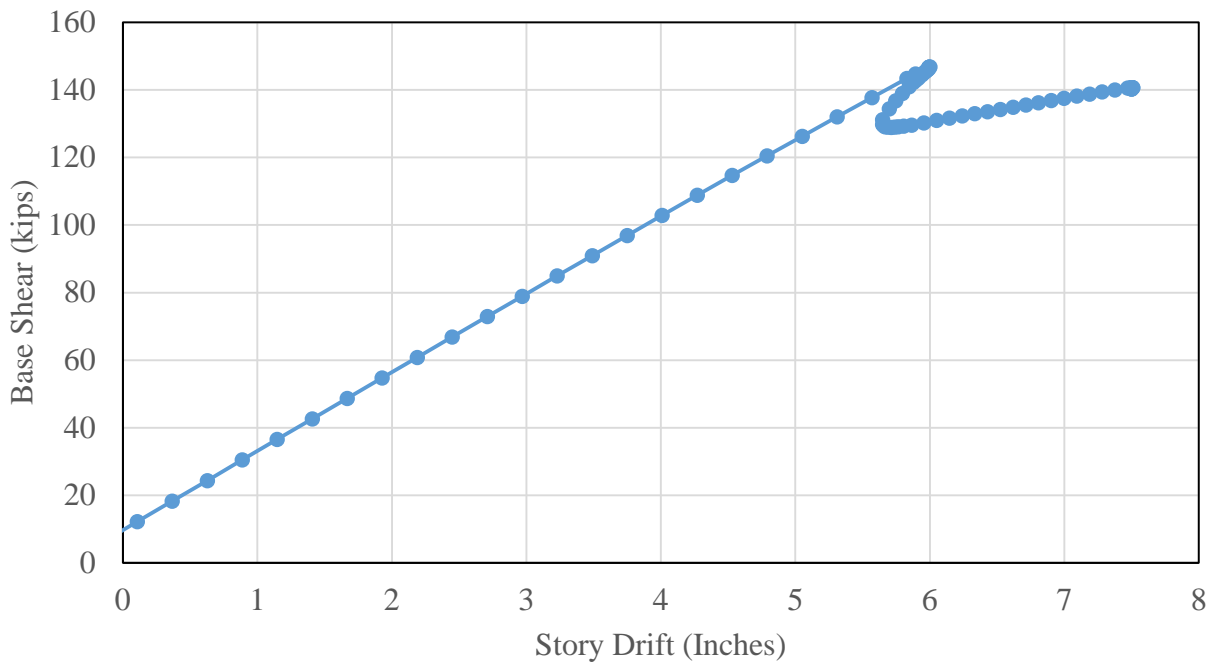
Figure 4.24. Pushover Curve for Frame 42 (West)

71

4.3.5   Frame 85 Pushover Results

This model was a clear span symmetrical gable frame with a span of 40 feet and an eave height of 15 feet (Figure 4.25). An analysis was performed using the flange web thickness for the column that was specified for the design. The first significant inelastic behavior occurred in the column in the form of FLB and LTB. Because the gravity load is supported by the column, any stability failure of the column could compromise the integrity of the entire structure. This was deemed unsuitable for a seismic design. In order to move LTB into the rafter segment, a complete frame redesign that is highly optimized would have been necessary. As this is outside to scope of this research, the column flange thickness was increased from 0.188 inches to 0.25 inches so that LTB first occurred in the rafter segment.
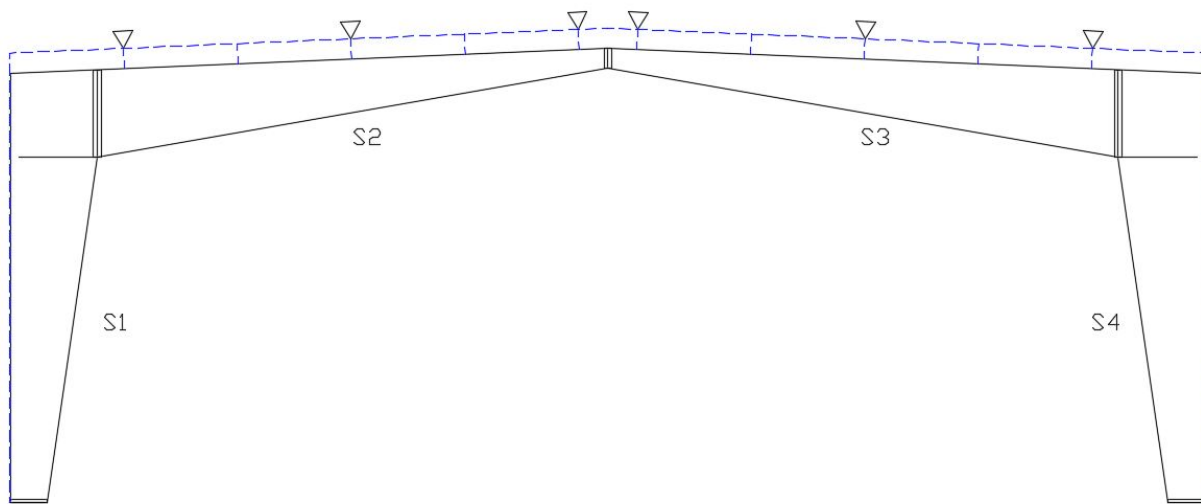
Figure 4.25. Segment Identification for Frame 85

The modified post-buckled frame at the end of the analysis is displayed in Figure 4.26. The pushover curve for this frame is displayed in Figure 4.27. Elastic behavior ends at a lateral displacement of 2.5 inches or 1.4% story drift. When the base shear reached 40 kips, distortional buckling occurred in segment S3 in the unbraced length closest to the column. The von Mises

72

stress contours and equivalent plastic strain contours for the buckled segment are shown in Figures 4.28 and 4.29. This distortion lead to a LTB buckling in the rafter segment. The frame never achieved a positive stiffness following buckling. The second inelastic event was flange local buckling in the top flange near the ridgeline (Figures 4.30 and 4.31). The analysis terminated in a convergence failure at a story drift of 4.8 inches. However, at this point in the analysis, a collapse mechanism in the frame has formed.

ODB: Frame_85_Push.odb   Abaqus/Standard 6.14-1   Tue Feb 23 11:37:09 Central Standard Time 2016

Step: Push
Increment   201: Arc Length =   20.76

Deformed Var: U   Deformation Scale Factor: +3.000e+00

Figure 4.26. Post-Buckled Frame at the End of Analysis (Deformation Scale Factor = 3)
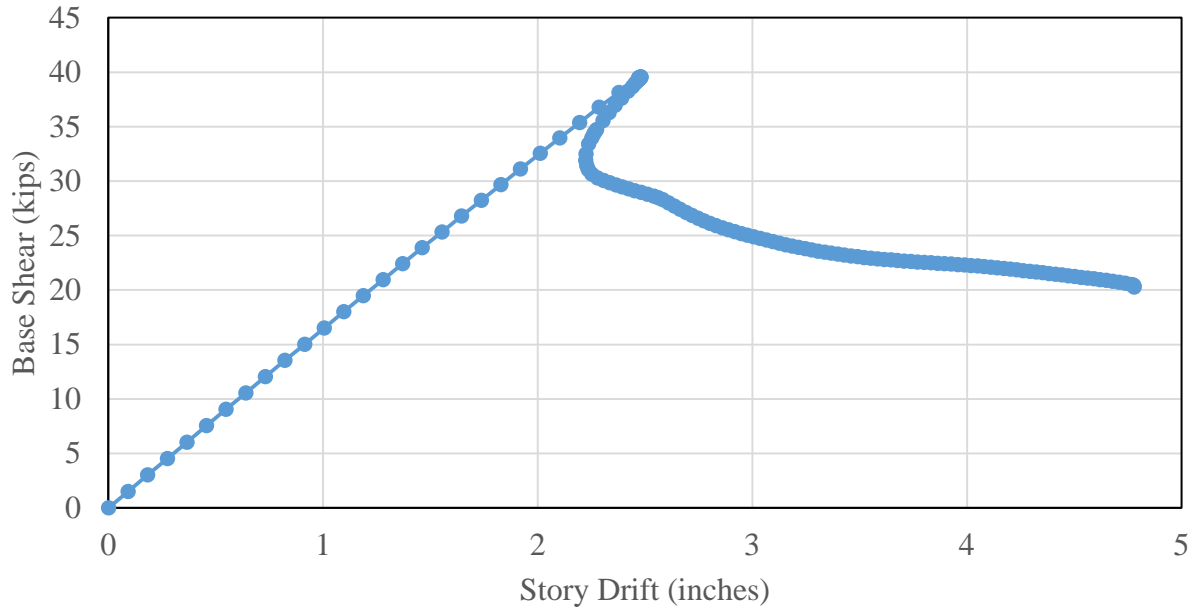
Figure 4.27. Pushover Curve for Frame 85

ODB: Frame_85_Push.odb   Abaqus/Standard 6.14-1   Tue Feb 23 11:37:09 Central Standard Time 2016

Step: Push
Increment   147: Arc Length =   15.47
Primary Var: S, Mises
Deformed Var: U   Deformation Scale Factor: +1e+00
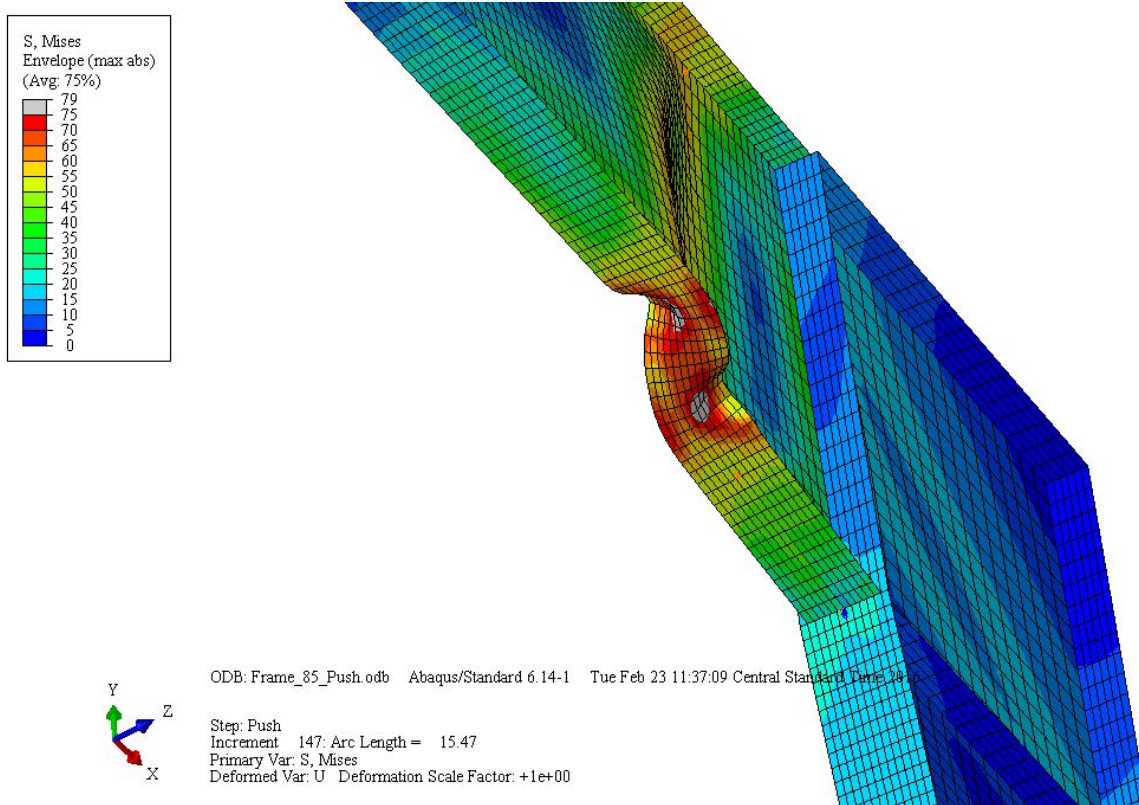
Figure 4.28. Von Mises Stress Contours for Buckled Segment in Frame 85
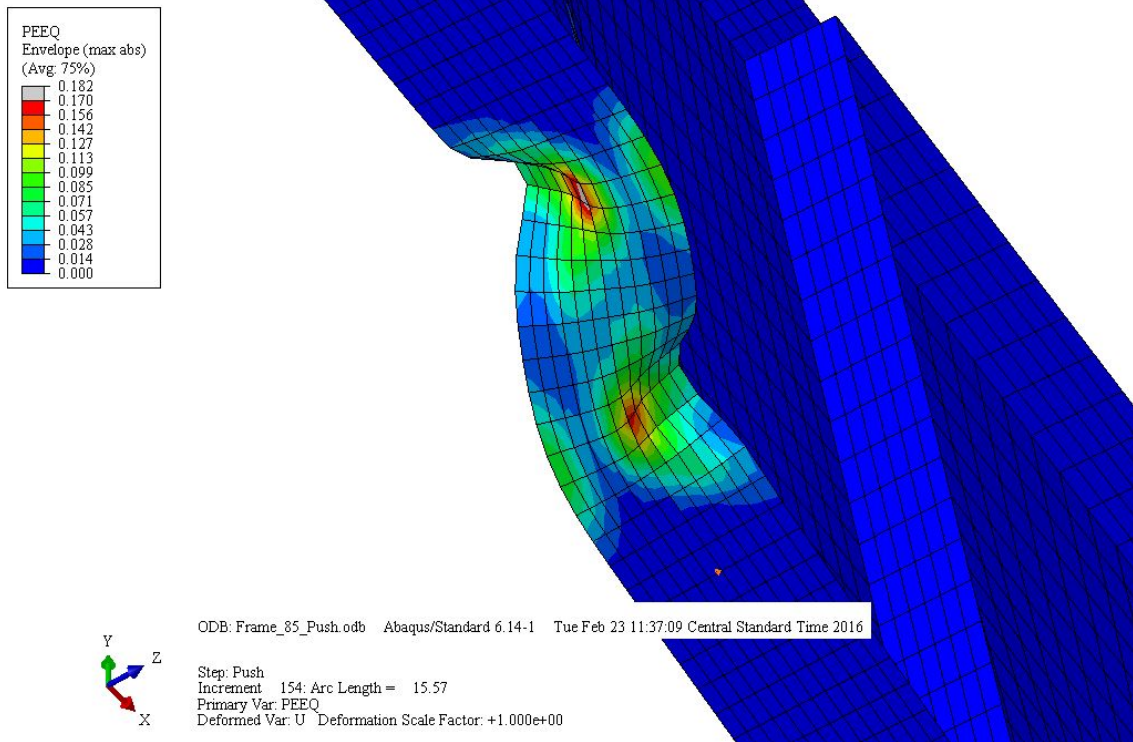
Figure 4.29. Equivalent Plastic Strain Contours for Buckled Segment in Frame 85
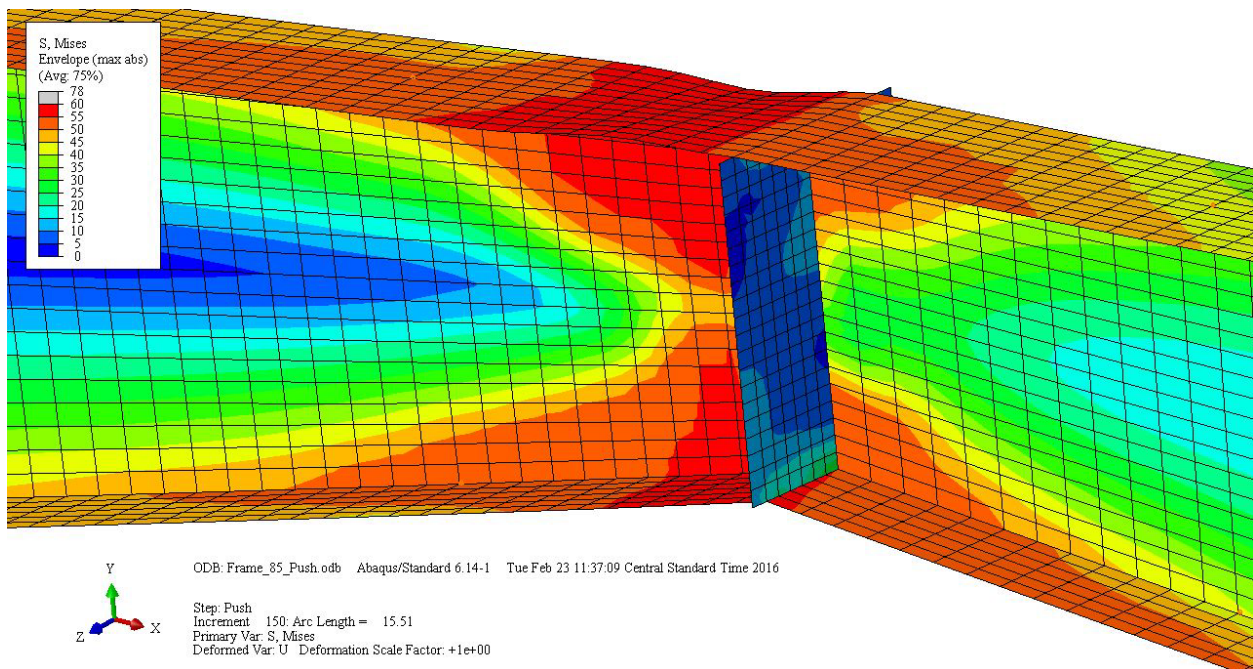
Figure 4.30. Von Mises Stress Contours for FLB in Frame 85
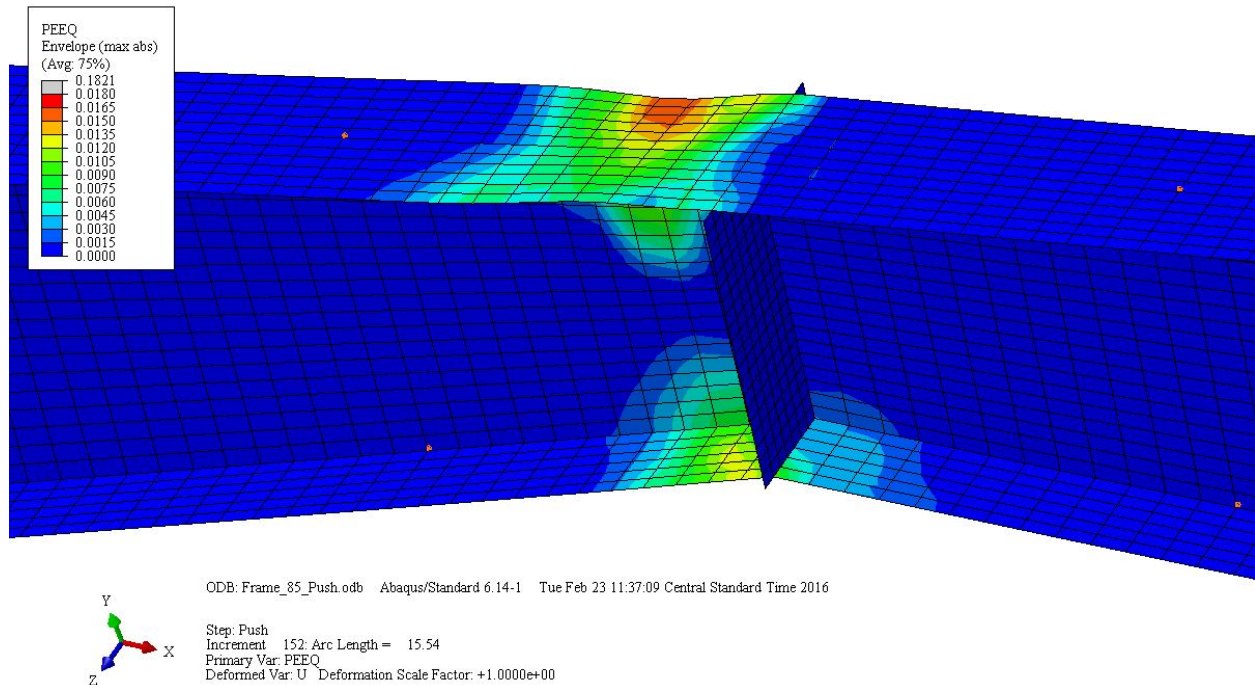
Figure 4.31. Equivalent Plastic Strain Contours for Buckled Segment in Frame 85

4.3.6   Frame 138 Pushover Results

This model was a modular symmetrical gable frame with one interior column. The frame

has a total span of 120 feet and an eave height of 30 feet (Figure 4.32). The post buckled frame is

shown in Figure 4.33. The pushover curve for this frame is displayed in Figure 4.34. The elastic

portion ends at 5 inches of displacement or 2.4% story drift. When the base shear reached 58 kips,

yielding of the column flanges near the base occurred first, followed by lateral torsional buckling

of the column segment. When the frame was designed, the column base was fixed in order to meet

the 2% seismic drift requirement. This consequently caused yielding in the columns flanges to

occur first in the frame, which led to the column stability failure. It was desired to move the LTB

critical segment into the rafter. After several attempts at increasing the plate thicknesses of the

column, it became clear that an entire frame redesign would be necessary to force the critical

segment to be located in the rafter. Since this was outside of the scope of this research, the nonlinear dynamic analyses in SAP2000 will be run assuming the entire frame remains elastic. The maximum story drifts will be investigated to see if this assumption is reasonable.
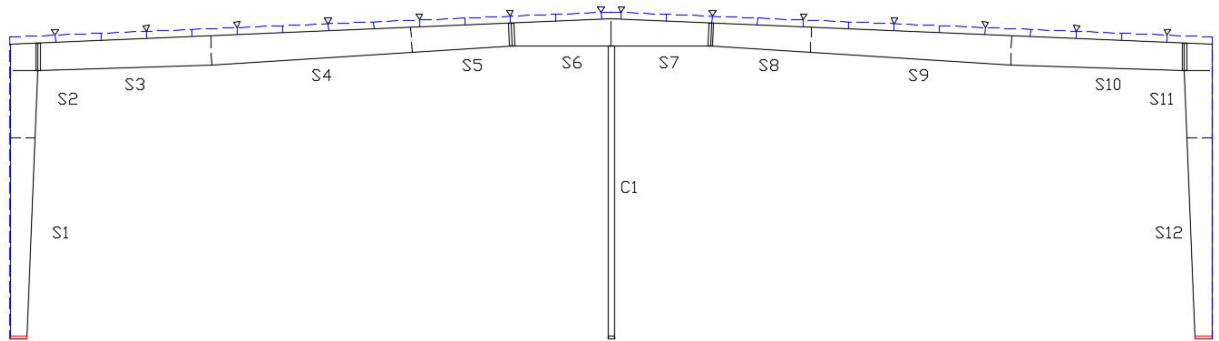
Figure 4.32. Segment Identification for Frame 138

ODB: Frame_138_Push.odb   Abaqus/Standard 6.14-1   Wed Feb 03 21:35:48 Central Standard Time 2016

Step: Pushover
Increment   74: Arc Length =   4.364

Deformed Var: U   Deformation Scale Factor: +1.000e+01
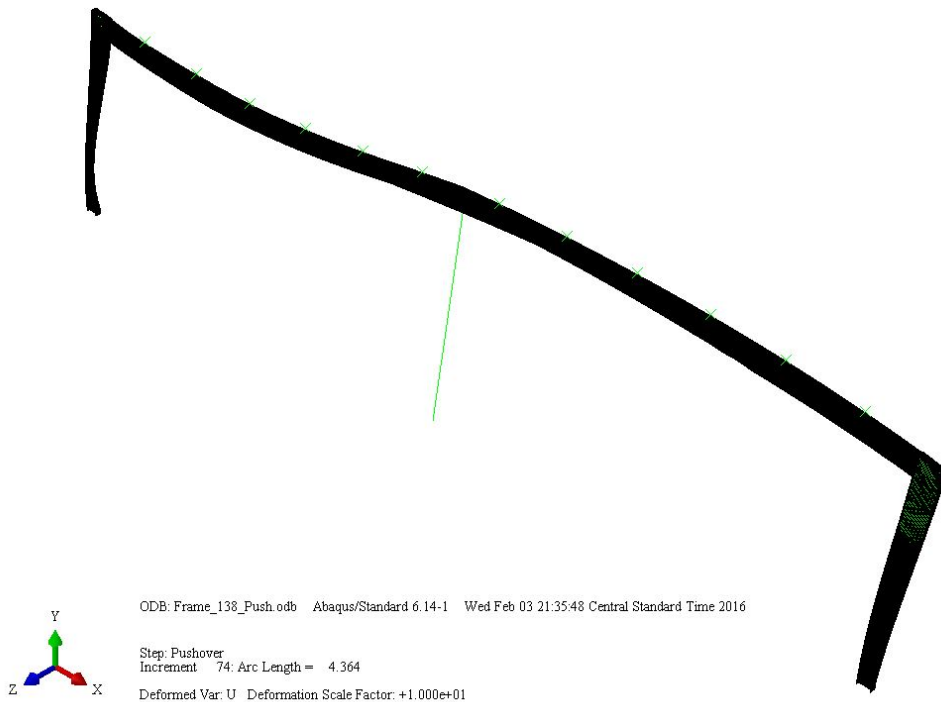
Figure 4.33. Post-Buckled Frame at the End of Analysis (Deformation Scale Factor = 10)
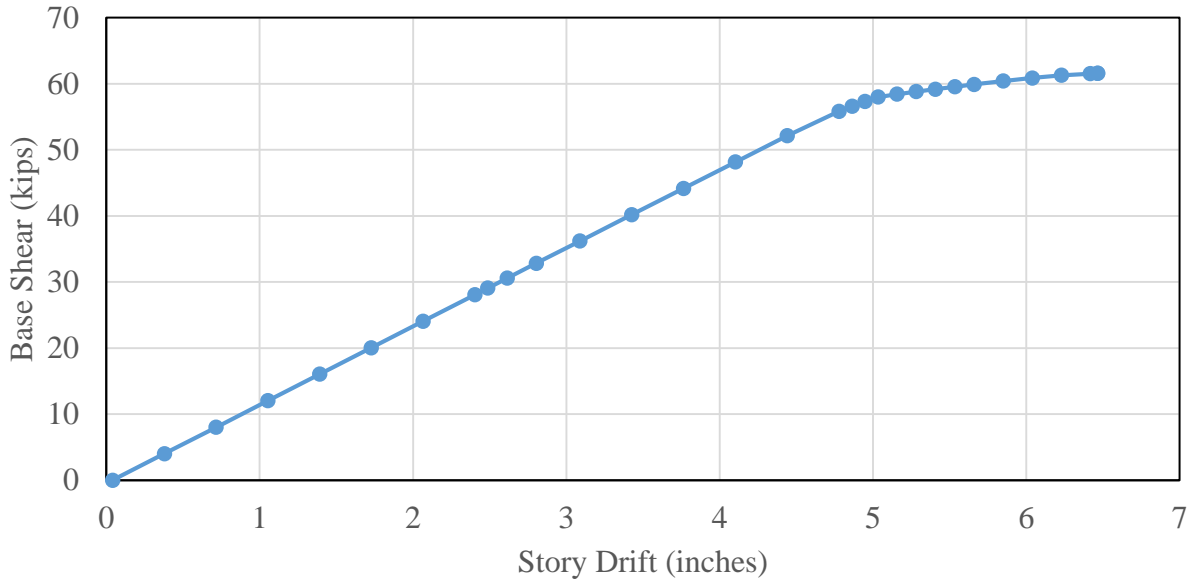
Figure 4.34. Pushover Curve for Frame 138

These analyses show the demarcation between elastic and inelastic frame behavior. The location of the critical segments and the inelastic mechanisms were identified. These pushover analysis results were used to calibrate the SAP2000 custom hinge.

4.4 LTB Hinge in SAP2000

This research approximates the post-buckling behavior of the frame using a custom flexural frame hinge in SAP2000. An analysis that assumes that the frame will remain elastic and undamaged will likely result in unrealistic connection demands. However, with the inclusion of a LTB hinge, frame damage can be accounted for in the analysis, making the results more realistic. As stated earlier, there does not exist a modeling technique using frame elements that captures the behavior following lateral-torsional buckling during earthquake excitations. In SAP2000, the user can define a custom backbone curve for the plastic response. The type of hysteresis behavior can

also be assigned. Through clever manipulation of the available hinge parameters that can be adjusted in SAP2000's interface, post-buckling behavior can be approximated. The proposed hinge was developed to include several critical characteristics of post-buckling.

1. There is a significant reduction in strength following the critical buckling load.

2. There is a significant reduction in global lateral stiffness following buckling.

3. During an unloading cycle following buckling, the buckled compression flange straightens out and can carry tension (Smith 2013d).

One important aspect to note about this flexural hinge is that the true kinematics of LTB will not be captured. The model developed for the critical segment will not be physically buckling out-of-plane and twisting. Rather, the hinge will undergo large plastic rotations about the major axis of bending while remaining in-line with the frame. A similar modeling technique is applied for modeling concentrically braced frames in compression. The out-of-plane buckling of the brace is mimicked through axial deformation alone.

4.4.1 SAP2000 Pushover Procedure

The first step of the LTB hinge is to define a backbone curve such that the pushover curves from the Abaqus models match, as closely as possible, the SAP2000 pushover curve. A single frame line from the 3-D SAP2000 model was isolated to be used for a planar frame analysis (Figure 4.35). The wall elements were changed from shell elements to a series of 6 frame elements with cross-sectional properties based on a tributary width of 25 feet. A rod constraint was used to connect the side wall to the metal building frame. The unbraced length typically spans two to three nonprismatic frame elements in the SAP2000 model. The element closest to the inelastic mechanism of the unbraced length was subdivided into two equal length elements. A major axis

flexural hinge was assigned to one of the newly created subdivided elements. Traditional plastic hinges for wide flange sections assign a frame hinge length of two times the depth of the cross-section. Because the backbone curve is being calibrated, the choice of hinge length is arbitrary. This research assigns a hinge length equal to the entire length of the newly subdivided element for all models (Figure 4.36).
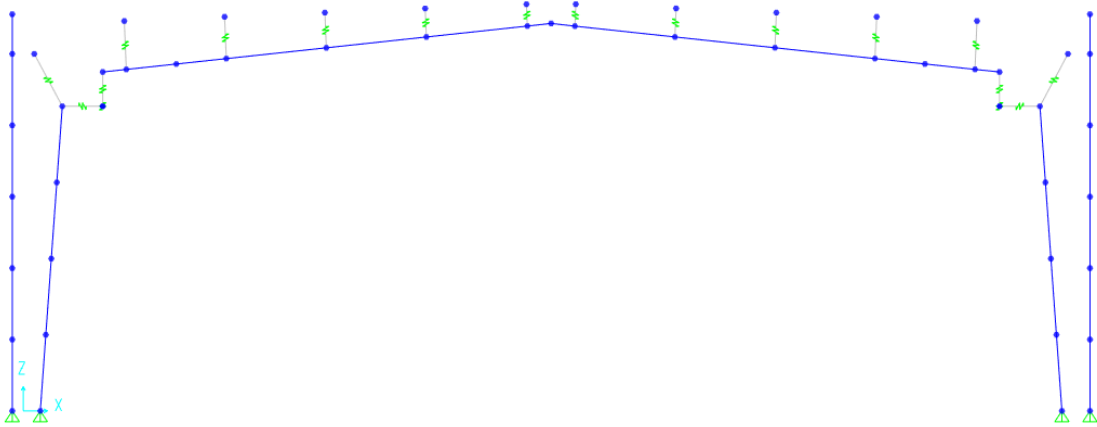

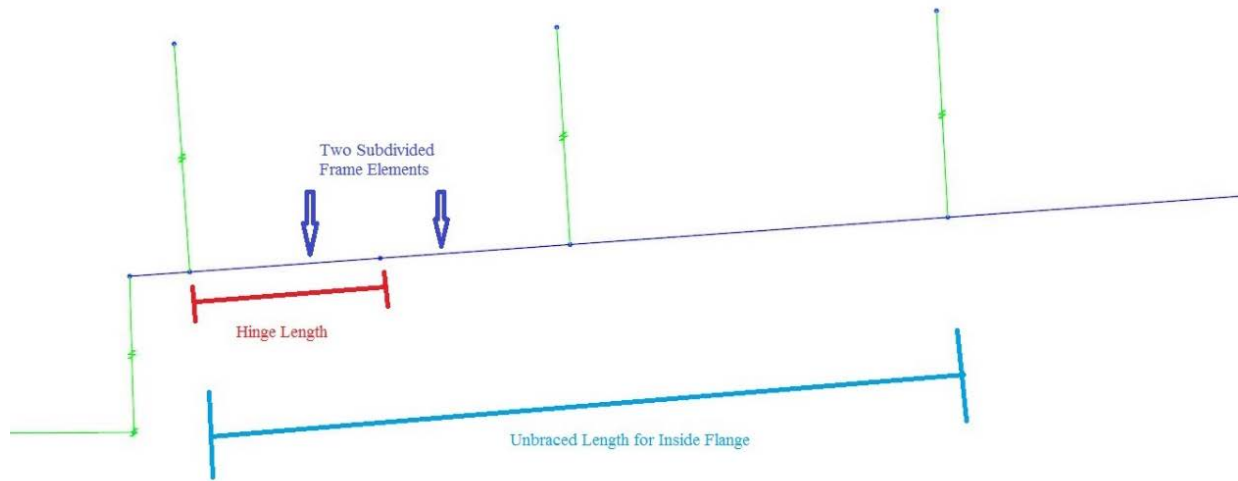**Figure 4.35. Planar Analysis of Frame 85**

Figure 4.36. LTB Hinge Length Definition

A nonlinear static analysis with P-Δ geometric nonlinearity was performed with the applied dead load, collateral load, and snow load. In SAP2000, there are three methods for analyzing hinges that exhibit a sharp drop in load-carrying capacity. They are "Unload the Entire Structure," "Apply Local Redistribution," and "Restart using Secant Stiffness." The pushover analyses for this research used the "Restart using Secant Stiffness" method because it is the most robust of the three.

A trial and error process was performed to calibrate the points of the custom backbone curve for the LTB hinge using the pushover curves from the Abaqus models. For convenience, the moments were scaled using the plastic moment of the cross-section at the hinge location, and the plastic rotations were scaled with the yield curvature. The general shape of the negative moment side of the backbone curve includes either a small yield plateau at the critical LTB load or a slight positive slope up to the critical LTB load, a significant decrease in flexural strength with increasing curvature, and finally a constant residual strength (Refer to Figure 4.37). Because large

81

rotations can be expected due to LTB, the hinge allowed the backbone curve to be extrapolated beyond the last point and never drop load to zero. For the positive moment side of the backbone curve, all but Frame 16 used the plastic moment as the ultimate strength. It is not expected for the positive moment strength to reach this level during the dynamic analyses.

The following figures, 4.37 through 4.44, show the assigned backbone curve for the LTB hinge and the resulting pushover curves from both the Abaqus analysis and SAP2000 analysis. For each of the frames, the pushover curves from the Abaqus analysis reasonably matches with that of the SAP2000 analysis. Based on these results, the SAP2000 model successfully approximates the post-buckling path of the metal building frame.

Frame 16

As stated earlier, Frame 16 experiences LTB first, and then is followed by FLB when the story drift reaches 4 inches. According to Smith's (2013d) recommendations for the development of the future Metal Building Intermediate Moment Frame (MBIMF), the frame should be able to undergo large displacements after LTB of the first segment without forming a second inelastic hinge elsewhere in the frame. When the second hinge activates, a collapse mechanism is formed, and should be avoided. There was no attempt to match the Abaqus pushover curve after a second inelastic event occurred. In lieu of this, the positive moment backbone points maintain a constant value of 0.75 times the plastic moment instead of losing strength. That is why a divergent behavior is visible in the two pushover curves for Frame 16 after 4 inches of displacement.
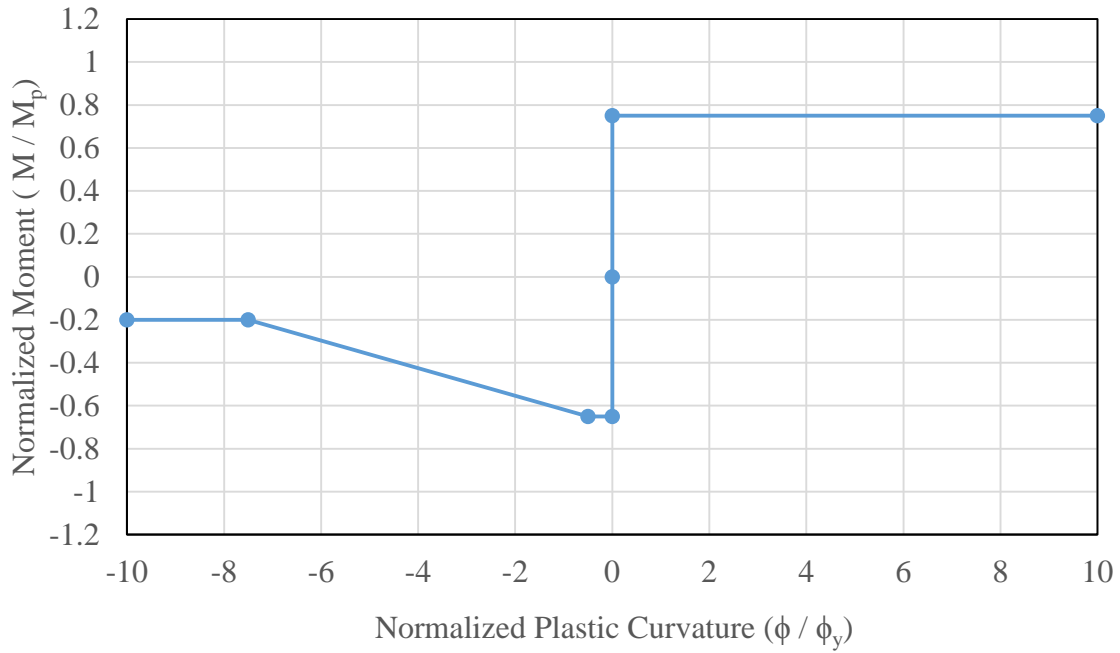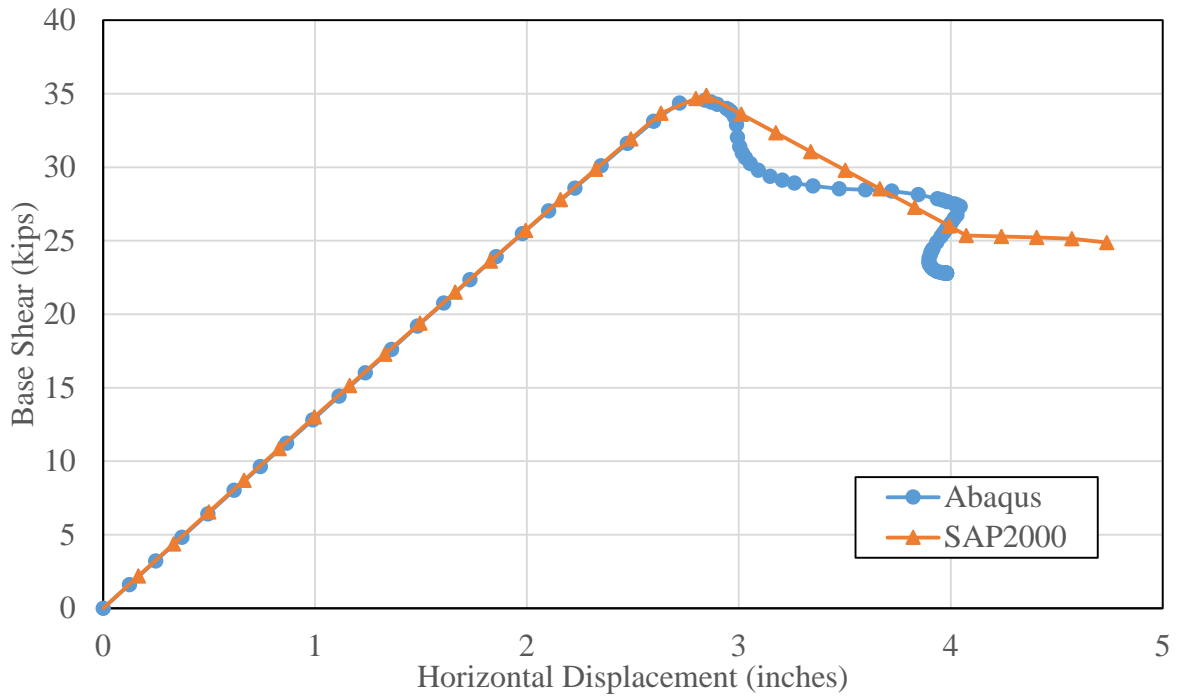
Figure 4.37. Backbone Curve for LTB Hinge in Frame 16

Figure 4.38. Comparison of Pushover Analyses for Frame 16

Frame 41

The post-buckled path for Frame 41 was the most severe of all the frames analyzed. The LTB hinge procedure developed in this research is not applicable for such a severe post-buckling path. All earthquake analyses for this frame will assume the frame remains elastic because this post-buckling path cannot be captured.

Frame 42

The pushover curves for Frame 42 (Figures 4.40 and 4.42) match each other the best of all the frames. These results best illustrate that SAP2000 can be used to model inelastic behavior of metal building frames. Though flange local buckling was the first inelastic mechanism when the frame was pushed to the left, the same procedure developed for the LTB hinge appears to work for flange local buckling as well.
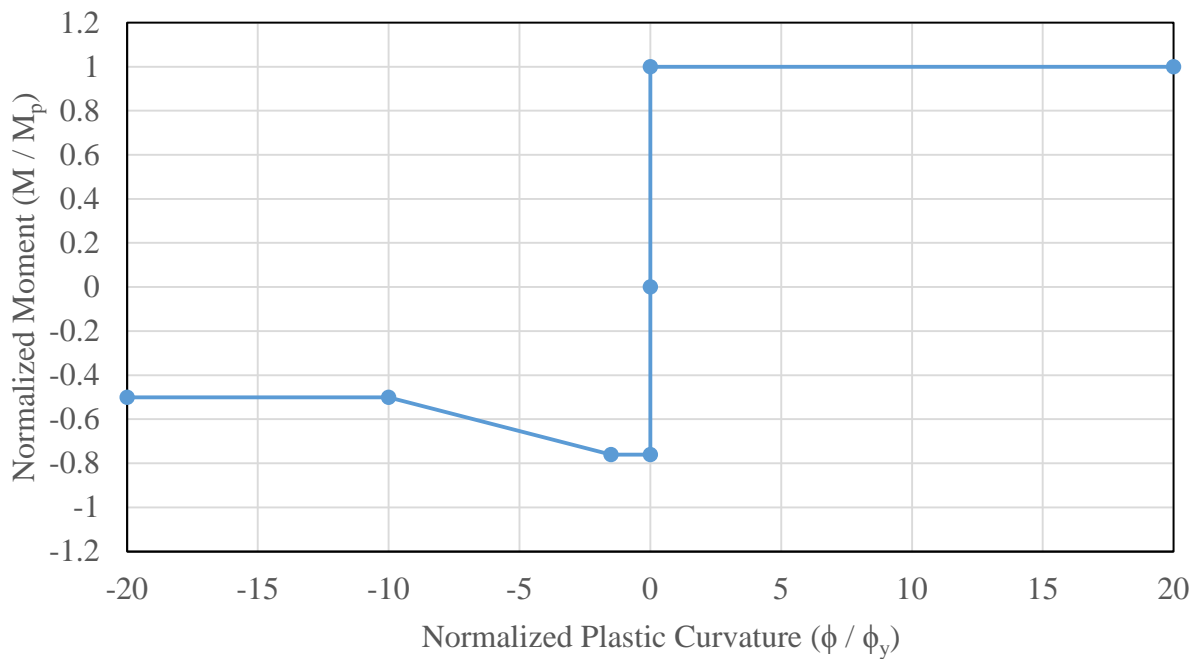

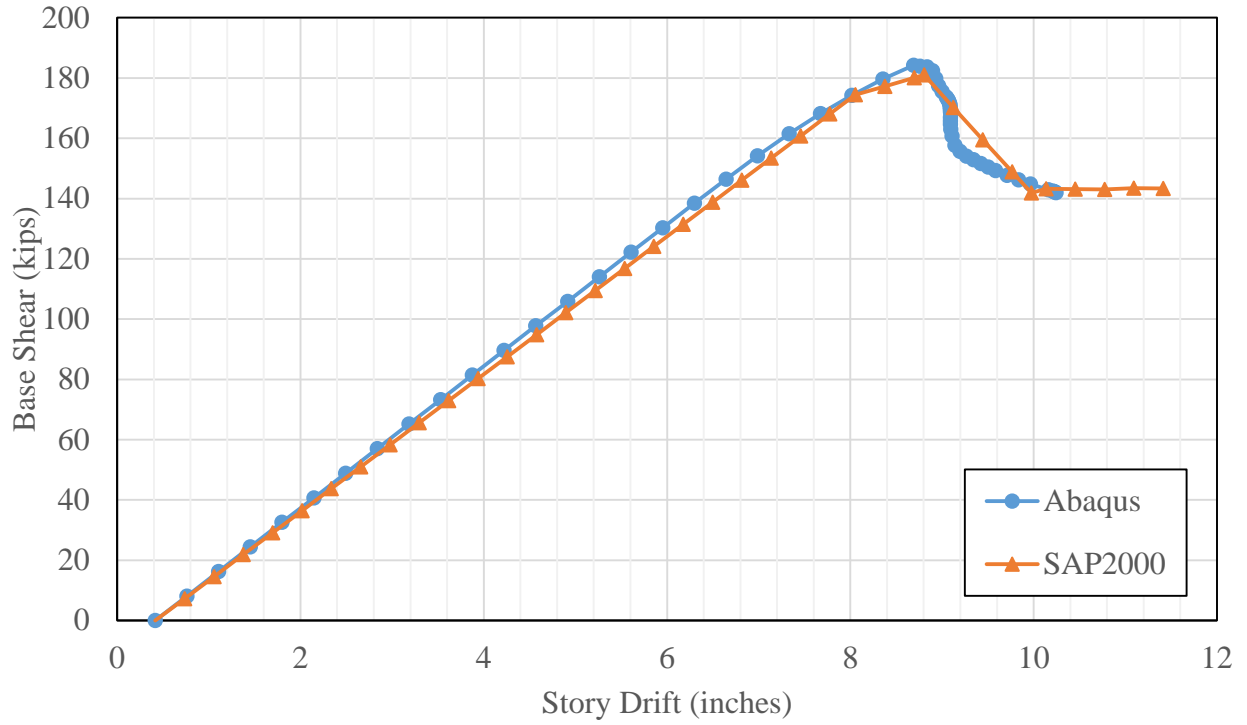**Figure 4.39. Backbone Curve for LTB Hinge in Frame 42**

Figure 4.40. Comparison of Pushover Curves for Frame 42 (Right)
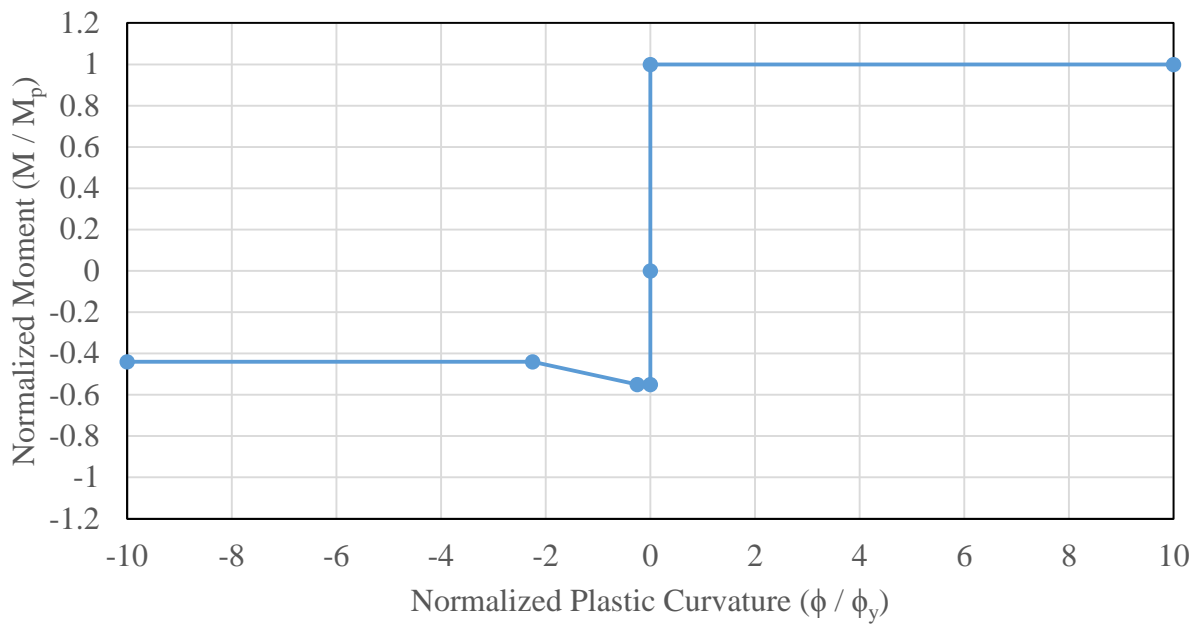
Figure 4.41. Backbone Curve for FLB Hinge in Frame 42
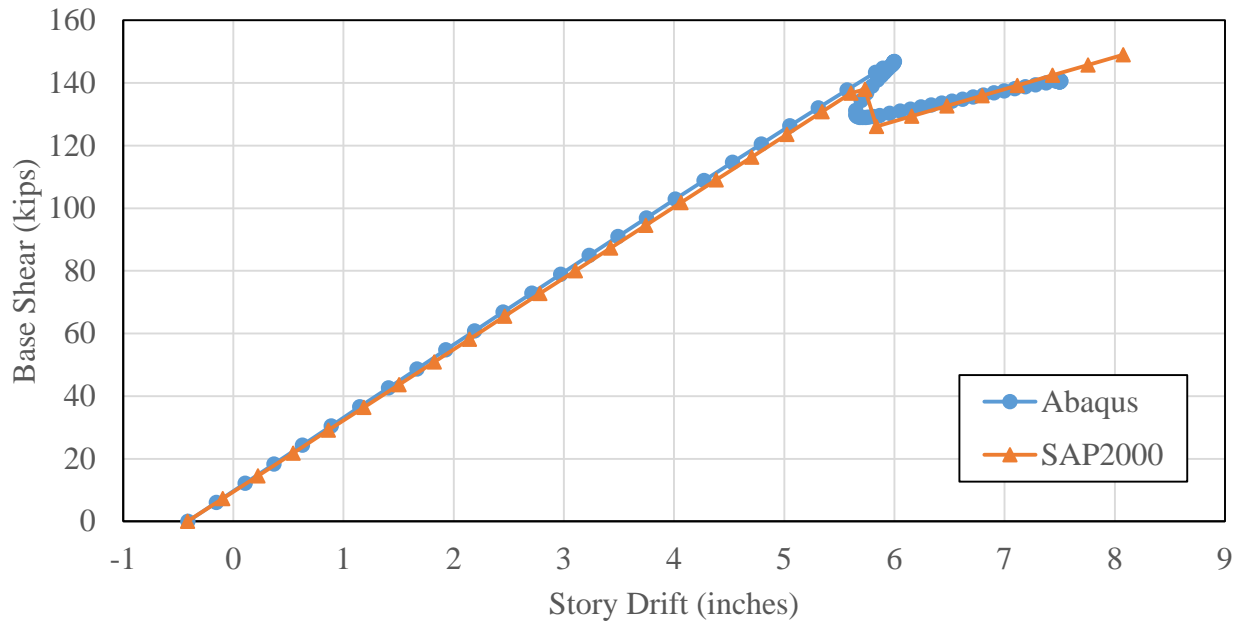
Figure 4.42. Comparison of Pushover Curves for Frame 42

Frame 85

Frame 85 exhibits a significant drop in strength after LTB of all the frames (Figure 4.41). It was challenging to match the Abaqus and the SAP2000 curves. The Abaqus analysis showed that the post-buckling path never achieved a positive stiffness. A SAP2000 hinge backbone curve would not allow for such a post-buckling curve. Instead, the post-buckling path for the SAP2000 model assumes a significant drop in strength with a positive post-buckling stiffness. From the Abaqus results, the second inelastic mechanism was flange local buckling in the top flange near the ridgeline. The SAP2000 model does not consider the second inelastic event due to previously stated reasons concerning the MBIMF.

Figure 4.43. Backbone Curve for LTB Hinge in Frame 85

Figure 4.44. Comparison of Pushover Curves for Frame 85

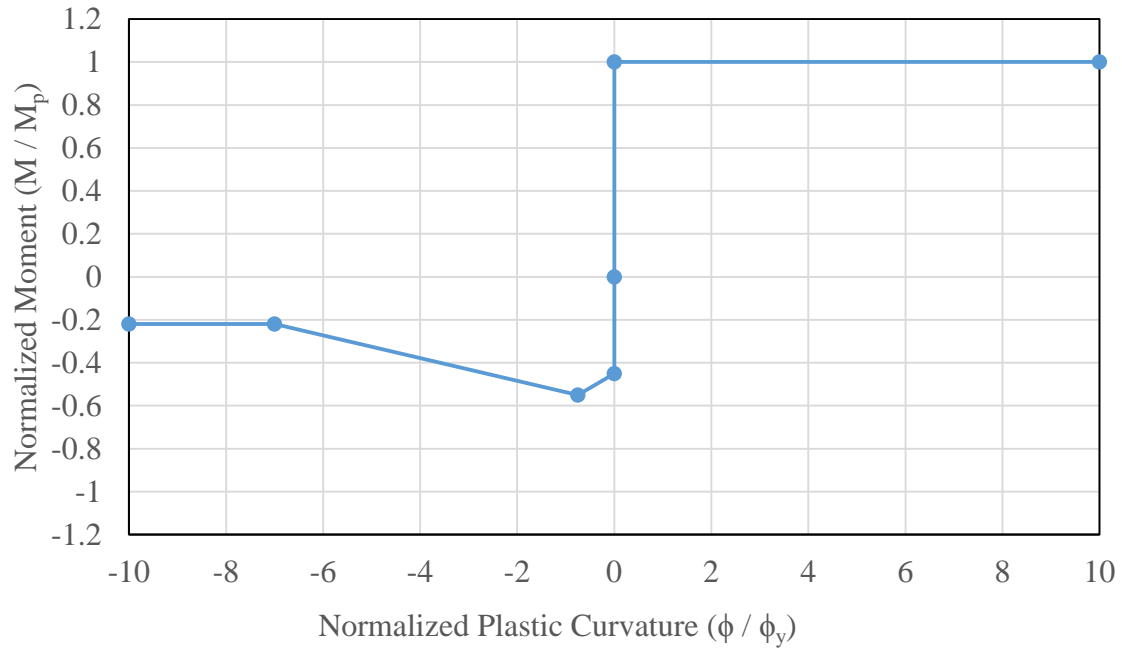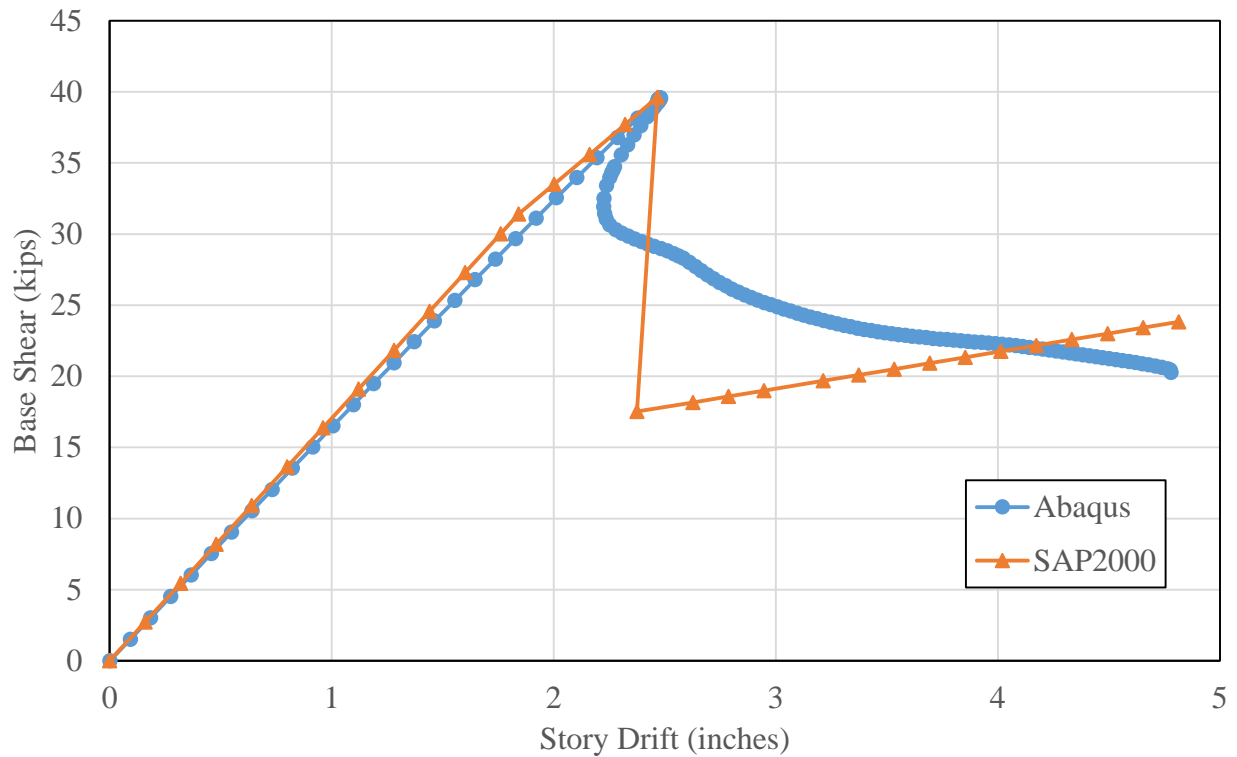### 4.4.2. Dynamic and Hysteretic Behavior for LTB Hinge

To this point, the static behavior of the LTB hinge has been examined and defined. It was then necessary define how cyclic behavior can be modeled with the custom hinge.

One major characteristic of cyclic behavior as noted by Smith was that the compression flange in the buckled segment straightens out and gains stiffness until the flange carries tension again (Smith 2013d). This behavior was the primary consideration in the selection of an appropriate hysteresis method for the LTB hinge.

The available hysteresis behaviors available for SAP2000 frame hinges are multi-linear isotropic plasticity, multi-linear kinematic plasticity, multi-linear Takeda Plasticity, and multi-linear pivot hysteretic plasticity. Isotropic plasticity and Kinematic plasticity have been used successfully to model metallic yielding for traditional plastic hinges. The Takeda method was developed for reinforced concrete members and exhibits a degraded hysteresis loop. This method dissipates less energy than the Kinematic hysteresis method. The Pivot method is similar to the Takeda method, but additional parameters are available for controlling the shape of the degrading hysteresis loop. This method was developed for reinforced concrete members after noticing that unloading and reloading tends to be directed towards specific points, also called pivot points.

The hysteresis method chosen for the LTB buckling hinge was the pivot method. The pivot points can be chosen by modifying the α_1, α_2, β_1, and β_2 scaling parameters, as shown in Figure 4.42. The α_1 value identifies the scaling pivot point for unloading to zero from positive force. α_2 locates the point for unloading to zero from a negative force. β_1 locates the pivot point for unloading to zero from positive force. β_2 locates the pivot point for reverse loading from zero towards negative force (Dowell 1998). The following values were assigned in order to minimize the energy dissipation the hinge would provide for a given cycle. All alpha values selected were

3.0. A β_2 value of 0.5 was assigned. The most important value was the β_1 term as it represents the rate at which the compression flange straightens out after buckling and begins to carry tension upon load reversal. The initial β_1 values assigned correspond to one-half the peak LTB capacity. If convergence was difficult, the β_1 value was increased to allow for more energy dissipation. The final values selected for β_1 are shown in Table 4.1.
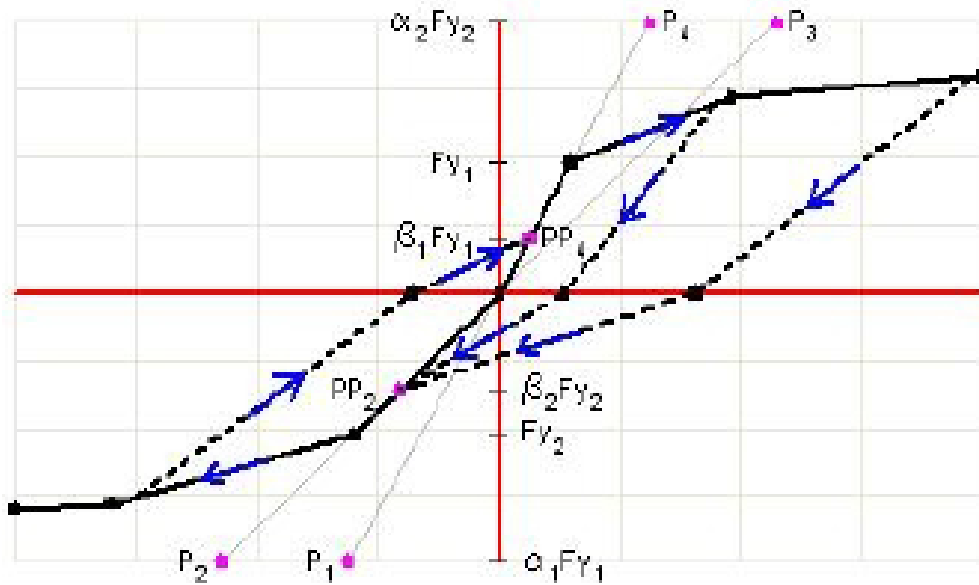

Figure 4.45. Pivot Hysteresis Method (CSI 2015)

Table 4.1. Assigned β_1 Values

Model Number	β_1
16	0.4
41	0.2
42 LTB	0.38
42 FLB	0.25
85	0.275

4.4.3 The Resulting LTB Hinge

The results from the Abaqus nonlinear static pushover analyses were used to generate a backbone curve for the LTB hinge to approximate the post-buckling behavior in SAP2000. The goal for this hinge was to match the reduction in strength and stiffness of the frame. Fundamental characteristics of the LTB cyclic behavior were modeled using the pivot hysteresis method. By matching the Abaqus results to the simplified SAP2000 model, post-buckling behavior was captured in a dynamic analysis using SAP2000. As a result, the time required to run dynamic analyses is reduced by orders of magnitude when comparing a dynamic frame element model versus a dynamic shell element model. It was then necessary to examine the newly developed LTB hinge to determine if this modeling technique successfully captures appropriate post-buckling behavior during a dynamic analysis.

Chapter 5   SAP2000 Dynamic Analysis Results

In order to assess the 3-D model developed in SAP2000, a modal analysis was performed on the five models. In addition, a single model will be used as a case study to examine the LTB hinge behavior and slotted-bolted friction-slip connections during the nonlinear response-history analyses. Frame 85 was selected for this assessment because the pushover curve for this frame was more complete than the other frames. From the Abaqus pushover analysis, the collapse mechanism for this frame was determined. Though the collapse mechanism is not included in the SAP2000 models, the peak frame drifts from the dynamic analyses can be used to determine if the collapse mechanism would have formed.

5.1.   Modal Analysis Results

The fundamental periods of vibration provide insight into the dynamic characteristics of a structure. A modal analysis was performed for each model and some unusual results emerged and are shown in the table below.

Table 5.1. Periods of Vibration and Mass Participation Ratios

Frame Number	Mode Number	Period (Seconds)	Ux	Uy	Uz	Sum Ux	Sum Uy	Sum Uz
16	1	0.6252	0.4961	0	0	0.4961	0	0
	3	0.3683	0.0684	0	0	0.5646	0	0
	7	0.3391	0	0.2793	0	0.5646	0.2794	1.46E-06
41	1	0.7610	0.4636	0	0	0.4636	0	0
	3	0.4358	0	0.412	0	0.4636	0.412	0
	4	0.3786	0	0	0.000467	0.4636	0.412	0.000467
	5	0.3768	0	0.000427	0	0.4636	0.4124	0.000467
	6	0.3767	0.0235	0	0	0.4871	0.4124	0.000467
42	1	0.8572	0.4867	0	0	0.4867	5.08E-06	0.0013
	3	0.751	0.0147	0	4.22E-05	0.5014	6.43E-06	0.0013
	4	0.6310	2.7E-05	0.4483	0.000211	0.5014	0.4483	0.0015
	6	0.5372	0.0077	0	0	0.5092	0.4483	0.0015
	8	0.5365	0.0042	0	0	0.5134	0.4484	0.0015
	9	0.5134	0.0014	0	3.31E-05	0.5148	0.4484	0.0016
85	1	0.4174	0.4689	0	0	0.4689	0	0
	2	0.2179	0	0.3071	0	0.4689	0.3071	0
	5	0.1858	0	0.0017	0	0.4689	0.3088	0.0011
	6	0.1849	0.0527	0	0	0.5215	0.3088	0.0011
	10	0.1268	0.0231	0	5.45E-05	0.5446	0.3088	0.0012
138	1	0.7421	0.4219	7.5E-06	0	0.4219	7.5E-06	0
	3	0.5660	3.74E-06	0.3697	1.75E-05	0.422	0.3697	1.75E-05
	4	0.3798	0.000304	1.28E-05	0	0.4223	0.3697	1.76E-05
	5	0.3696	0.0025	0	0	0.4248	0.3697	1.76E-05
	7	0.3646	0.0061	2.61E-06	0	0.431	0.3697	1.76E-05
	8	0.3634	0.0199	4.72E-05	0	0.4509	0.3698	1.76E-05
	9	0.3628	0.0089	0.000254	0	0.4598	0.37	1.76E-05

As illustrated in Table 5.1, there exists very low mass participation ratios for each structure. In Smith's (2013d) fundamental period study, metal building frames with a low aspect ratio exhibited lower mass participation ratios. The results suggest that there may have been an error in the model itself. However, this was not the case. Although these results appear highly unusual, there may be a logical explanation. When looking at the first longitudinal mode of vibration, it

makes sense that the only mass that participates in that mode of vibration is mass that is attached to the flexible steel frame. The rest of the mass is locked away in the stiff side wall panels. Shear wall vibration can only be excited at very high frequency vibrations due to its high stiffness. This demonstrates that metal building systems with hard walls are essentially two different systems tied together, each with very different stiffness and dynamic characteristics. This further emphasizes the importance of the connections between these two elements.

The fact that the mass participation ratios in this research are so low for metal building systems with hard walls, the applicability of the Equivalent Lateral Force (ELF) method to design these structures comes into question. The ELF method is used to determine the seismic load for design. It assumes that the first mode of vibration has a mass participation of 100%. Another finding of this research was that hundreds of modes were required to reach 90% mass participation. The ASCE 7 procedures for a modal response spectrum analysis must have sufficient modes such that the mass participation is at least 90%. This method appears impractical. For these reasons, a linear time-history analysis procedure may need to be used for determining seismic demands for these structures.

5.2.   Case Study of Model 85 for Nonlinear Time-History Analysis Results

5.2.1.   2-D Model LTB Hinge Results and Frame Behavior

Dynamic analyses of the 11 earthquakes were performed using the same 2-D model from the SAP2000 pushover analyses. The inclusion of an element with negative stiffness and significant strength loss can be numerically challenging for a solution algorithm to converge. Despite this, SAP2000 converged to a solution for all 11 earthquake cases (Table 5.2). However,
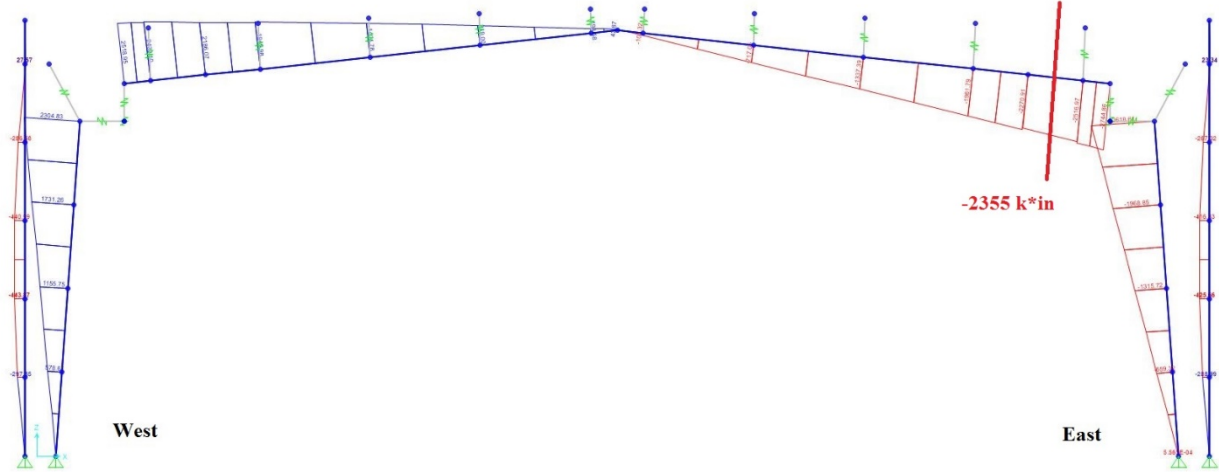
a numerical error in the LTB hinge did occur for a few of the dynamic analyses and will be discussed in the next section.

Table 5.2. LTB Hinge Activation with Peak Frame Demands for Frame 85

Earthquake Case	LTB Hinges Activated	Peak Displacement at Ridgeline (inches)	Peak Absolute Acceleration at Ridgeline (in/sec^2)
San Fernando	Hinge Error	2.83	1162
		-3.11	-2303
Friuli, Italy	2	7.25	530
		-4.60	-456
Gazli, USSR	0	2.35	401
		-2.37	-436
Imperial Valley	1	1.36	420
		-4.07	-281
Superstition Hills	2	3.07	549
		-3.85	-419
Loma Prieta	2	6.02	495
		-3.39	-427
Northridge Canyon	1	2.31	411
		-4.70	-374
Northridge Sylmar	1	4.02	284
		-1.86	-373
Kobe	1	2.25	406
		-3.47	-366
Kocaeli, Turkey	Hinge Error	2.40	15893
		-4.46	-3168
Chi-Chi, Taiwan	1	1.91	464
		-4.69	-347

The results from the Friuli, Italy earthquake will be used to further investigate the response history of the LTB hinge. This dynamic load case was selected because LTB occurred in both sides of the frame during the earthquake. At time t = 3.925 seconds, the buckling load of -2355 kip-inches at the east LTB hinge (Figure 5.1) is about to be reached. It should be noted that the

moment diagram is drawn on the compression side. At this instance, the lateral displacement at the ridgeline is 2.58 inches. At time t = 4.08 seconds, the LTB hinge on the east side has activated and the flexural capacity of the hinge has drop to -929 kip-inches (Figure 5.2). The moments in the frame have redistributed and the inflection point has moved from the center of the frame towards the activate LTB hinge. This is expected behavior and the LTB hinge appears to be dropping load as it should and moment redistribution is occurring.

Figure 5.1. Moment Diagram at t = 3.925 seconds of Friuli, Italy Earthquake

Figure 5.2. Redistributed Moment Diagram at t = 4.08 seconds of Friuli, Italy Earthquake

The cyclic behavior of the LTB hinge will now be assessed. At time t = 5.41 seconds, both LTB hinges have already reached their peak moment. As shown in Figure 5.3, the moment at the east LTB hinge is -599 kip-inches with a plastic rotation of -37.2e-3 radians. The moment at the west LTB hinge is 943 kip-inches with a plastic rotation of 6.33e-4 radians. When t = 5.79 seconds, the frame is now displaced to the west (Figure 5.4). The flexural moment in the west LTB hinge has reversed to -852 kip-inches with a plastic rotation of -57.3e-3 radians, which means that the buckling segment is active at this instant in the analysis. The flexural moment in the east hinge is now 1099 kip-inches and a plastic rotation of zero radians, which means that what was previously a buckled segment has straightened out. This alternating of the buckling segment was present in all the dynamic load cases in which LTB hinges formed on both sides of the frame. For dynamic load cases in which one LTB hinge, the straightening effect of the buckled segment was present. From these results, it can be concluded that the LTB hinge with the pivot hysteresis method is capturing the behavior identified by the shake table tests and the cyclic LTB tests performed by Smith (2013d).

The hysteresis loops for the 2-D dynamic analysis for Frames 16, 41, 42, and 85 are located in the Appendix. The results indicate that the LTB hinge developed in this research successfully approximates post-buckled frame behavior for every frame tested.

96
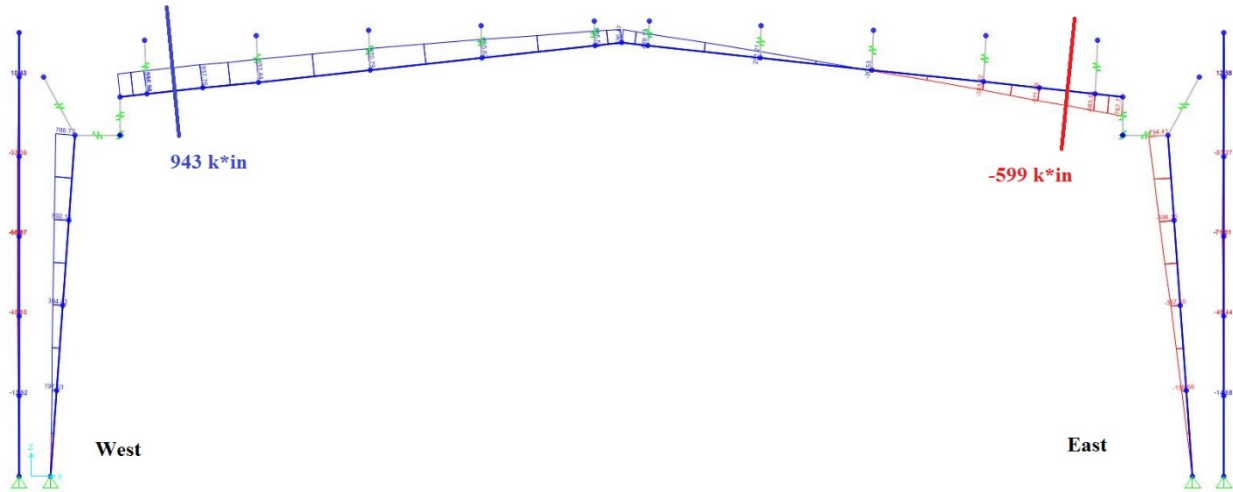
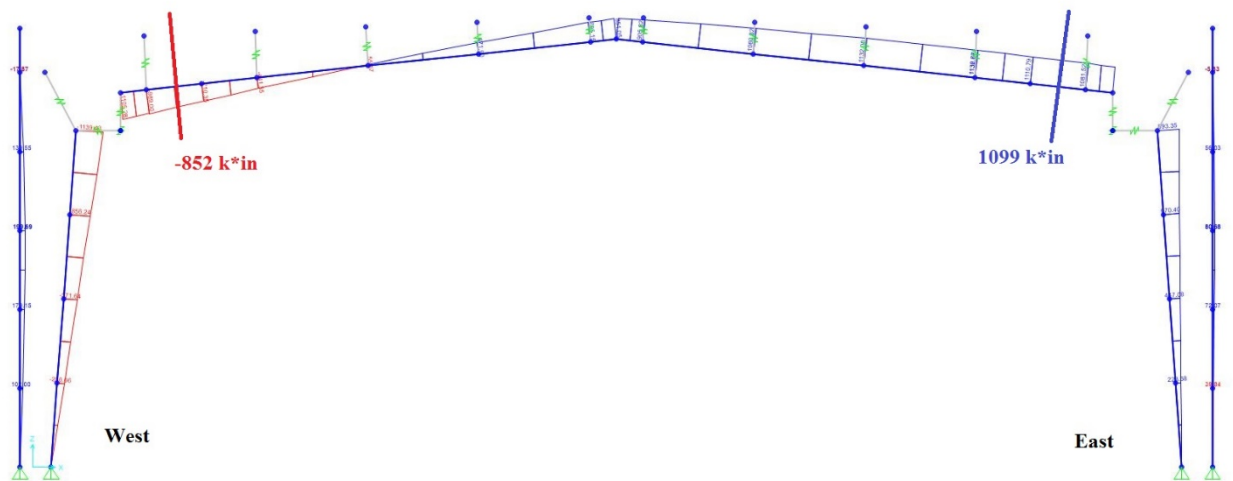**Figure 5.3. Moment diagram at t = 5.41 seconds of Friuli, Italy Earthquake**

Figure 5.4. Moment diagram at t = 5.79 seconds of Friuli, Italy Earthquake

The response history of the LTB hinges during the Friuli, Italy Earthquake are shown in Figures 5.5 and 5.6 below. The maximum plastic rotation achieved in the LTB hinges were -0.069 radians and -0.098 radians, which are quite large. However, this is not a traditional plastic hinge. The large rotations and corresponding large strains that develop in the LTB hinge certainly exceeds the ductility limits of the steel material. It should be noted that this custom hinge does not simulate

97

the true kinematics of a segment undergoing lateral-torsional buckling as the frame element does

not buckle out-of-plane or twist. The increase in major axis rotations due to LTB is captured in

the custom hinge by remaining in-plane with the frame line and undergoing large plastic rotations.

Therefore, these rotation values have been deemed acceptable.
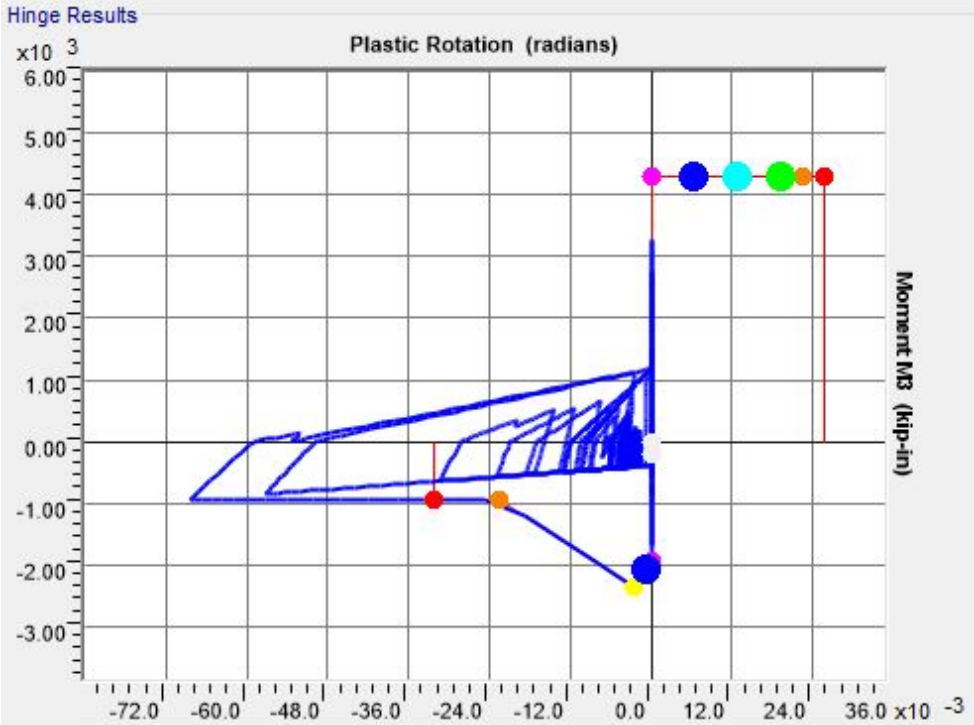
Figure 5.5. Plastic Hysteresis of the West LTB Hinge

98
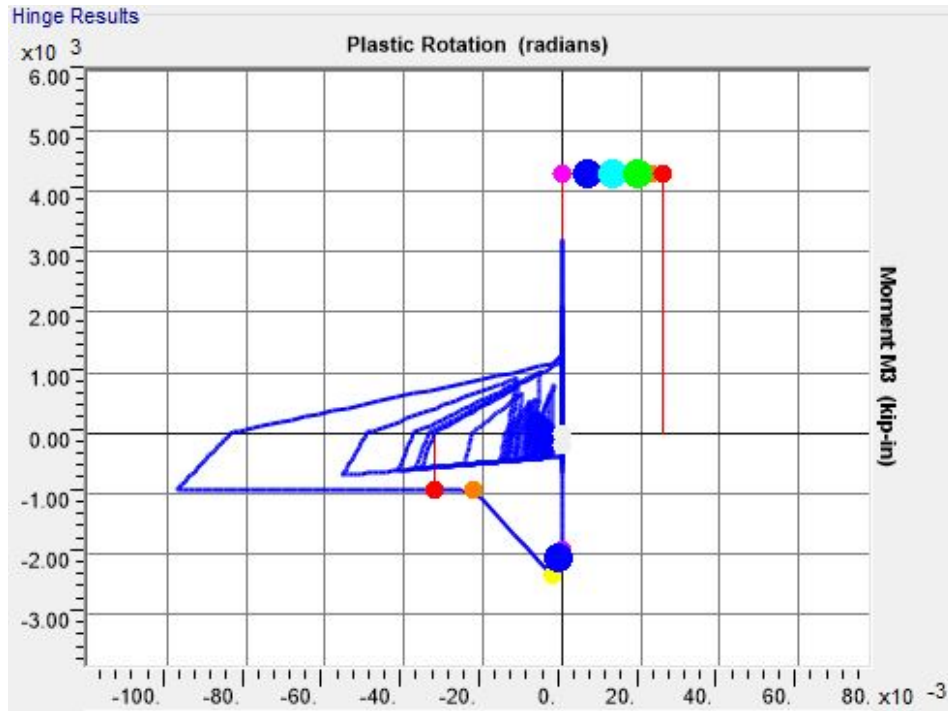
Figure 5.6. Plastic Hysteresis of the East LTB Hinge

5.2.2. Potential Numerical Instability of LTB Hinge

The Kocaeli, Turkey earthquake case will be used here to illustrate the nature of the numerical problem encountered. After the peak flexural capacity of the LTB hinge was reached, the equilibrium path started down the negative stiffness portion beyond the yellow point (Figure 5.7). The hysteresis loop that resulted appears to violate the pivot hysteresis rules assigned. As a result, when the hinge was trying to remove the load, an elastic snapback occurred and sent a shockwave throughout the structure. This was a numerical convergence error as the state of equilibrium of the hinge violently changed over a short period of time, as illustrated in Figures 5.8 and 5.9. All convergence issues arise in the hinge when the load is attempting to reverse direction while within the negative stiffness portion of the backbone curve. The use of a more robust solution algorithm may potentially reduce the likelihood of this issue.

99
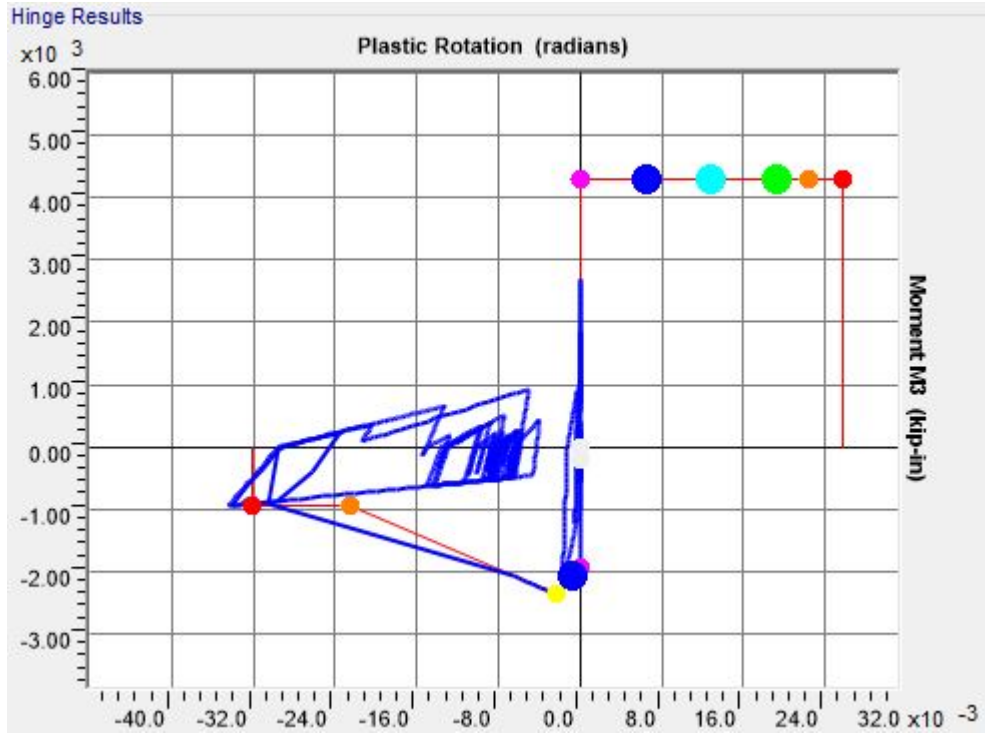
Figure 5.7. Error in Plastic Hysteresis in the East Hinge
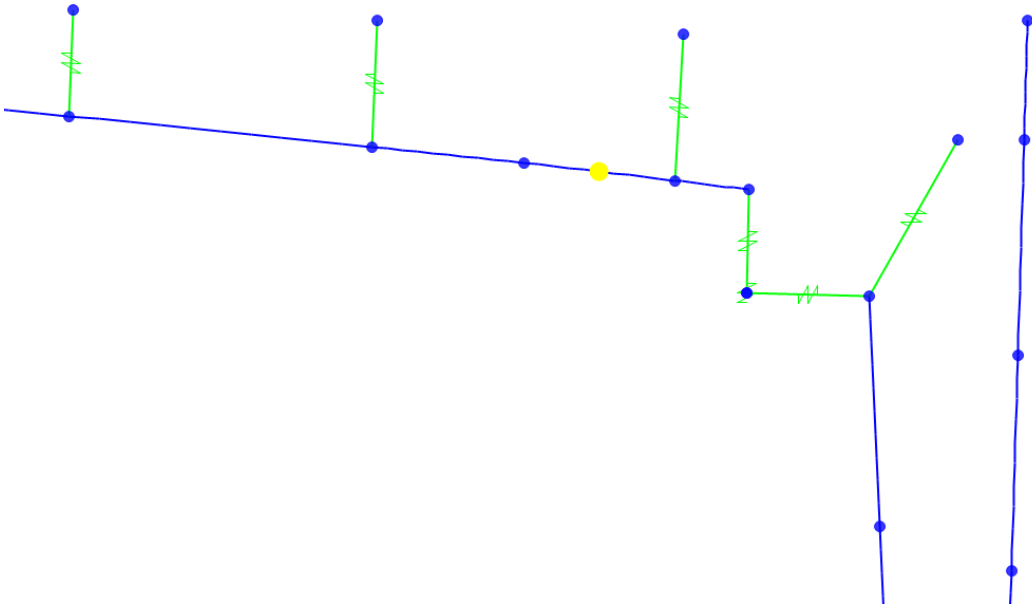
Figure 5.8. Deflected Shape of LTB hinge at t = 8.69 seconds
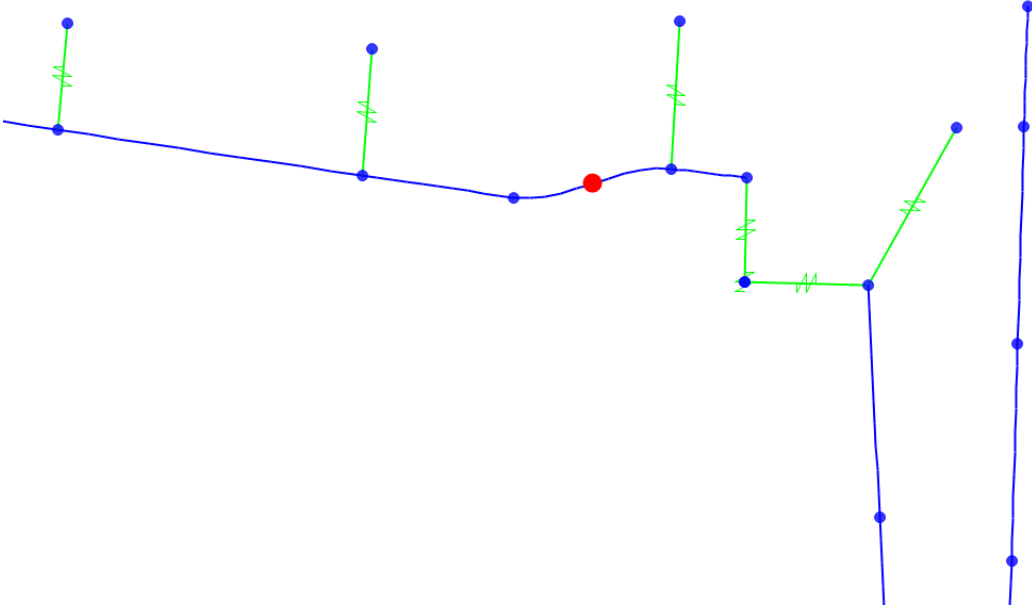
Figure 5.9. Deflected Shape of LTB hinge at t = 8.71 seconds

101

5.2.3. 3-D Model LTB Hinge Results and Frame Behavior

After the development of the LTB hinge for a planar frame model, the next step was to evaluate the behavior for use in a 3-D model. Because the model is now 3-D, three additional degrees of freedom, out-of-plane displacement, minor axis rotation, and torsion, are now involved. It is believed that there will be little change in behavior because the stiffness of the frame element in these directions is significantly smaller than the major axis bending stiffness and axial stiffness. Using the ground motions of the 11 earthquakes identified in Chapter 3, the nonlinear-dynamic analyses were performed for Model 85. As stated previously, the inclusion of an element with negative stiffness and significant strength loss can be numerically challenging for a solution algorithm to converge. SAP2000 converged to a solution for all 11 earthquake cases, as seen in Table 5.3. At least one LTB hinge formed during 9 of the 11 analysis. The LTB hinge can be utilized for 3-D dynamic analyses.

Table 5.3. Convergence and LTB Hinge Activation for 3-D Model

Earthquake Case	LTB Hinges Activated
San Fernando	2
Friuli, Italy	4
Gazli, USSR	2
Imperial Valley	4
Superstition Hills	4
Loma Prieta	4
Northridge Canyon	2
Northridge Sylmar	0
Kobe	0
Kocaeli, Turkey	3
Chi-Chi, Taiwan	3

The peak transverse displacements and accelerations are shown in Table 5.4. The values in Table 5.4 are reasonable as the LTB hinge worked properly in these models. Numerical convergence errors occurred in several of the earthquake analyses. Those earthquake cases were rerun with a slightly higher numerical damping value and the analyses were successful.

Table 5.4. Peak Transverse Displacements and Accelerations for 3-D Model

	Joint at Ridgeline	Imperial Valley	Friuli, Italy	Kobe	Kocaeli, Turkey	Loma Prieta	Northridge Canyon	Northridge Sylmar	San Fernando	Superstition Hills	Chi-Chi, Taiwan	Gazli, USSR
Peak Transverse Displacement at the Ridgeline (inches)	211	2.95	6.46	1.67	3.94	3.69	2.00	1.99	3.20	3.89	2.52	2.30
		-3.74	-6.20	-1.94	-2.72	-2.55	-3.43	-2.00	-2.31	-4.48	-3.30	-2.52
	311	2.75	5.81	1.75	3.71	3.87	2.02	2.08	3.24	4.16	2.40	2.51
		-3.31	-6.14	-1.74	-2.35	-2.62	-3.41	-1.96	-2.36	-4.38	-3.42	-2.37
Peak Absolute Acceleration (in/sec^2)	211	787	1124	501	687	597	638	431	582	584	560	548
		-791	-983	-476	-590	-733	-569	-431	-616	-743	-1001	-599
	311	832	1008	422	520	845	547	458	629	673	590	698
		-561	-895	-535	-624	-695	-484	-575	-565	-639	-583	-782

The final state of the 3-D model after Imperial Valley excitation is shown in Figure 5.10 with the LTB hinges identified. The response-history of the four hinges are displayed in Figures 5.11-5.14. The hysteresis loop shows that the LTB hinge qualitatively exhibited the cyclic behavior described by Smith (2013d). After the critical load was reached, the strength dropped substantially. When load reversal began, the hinge was able to recover from the large plastic rotations and dissipate some energy in the process. The hinge appeared to be successfully representing the straightening of the compression flange during the reloading cycle. Upon subsequent cycles, the negative moment never achieved the peak moment again, which is another of the characteristics described by Smith (2013c). Though all four LTB hinges activated during the analysis, only two hinges were buckling simultaneously while the other two segments were straightening out. This behavior is in accordance with the shake table findings.
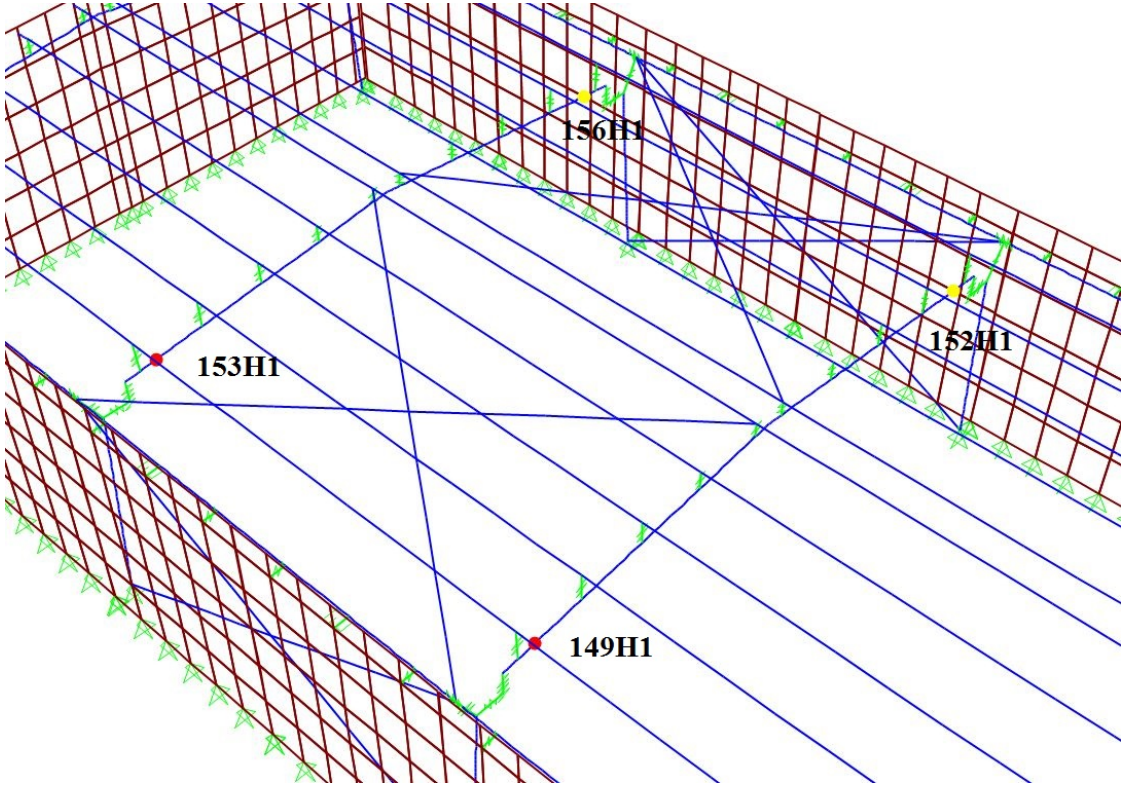
Figure 5.10. Frame 85 with Hinge Labels at the End of Imperial Valley Excitation.
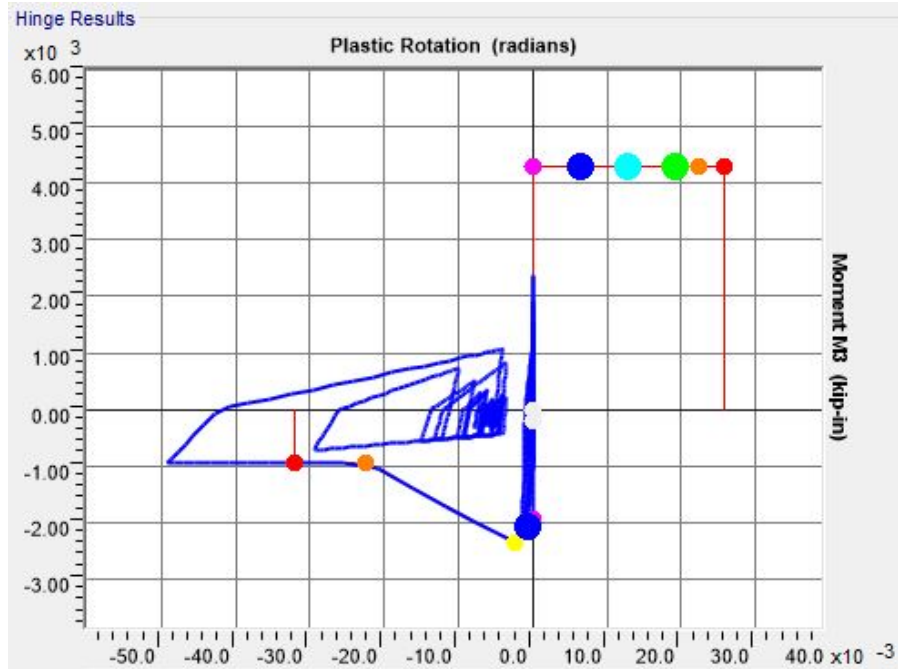
Figure 5.11. Plastic Hysteresis of Frame Hinge 149H1
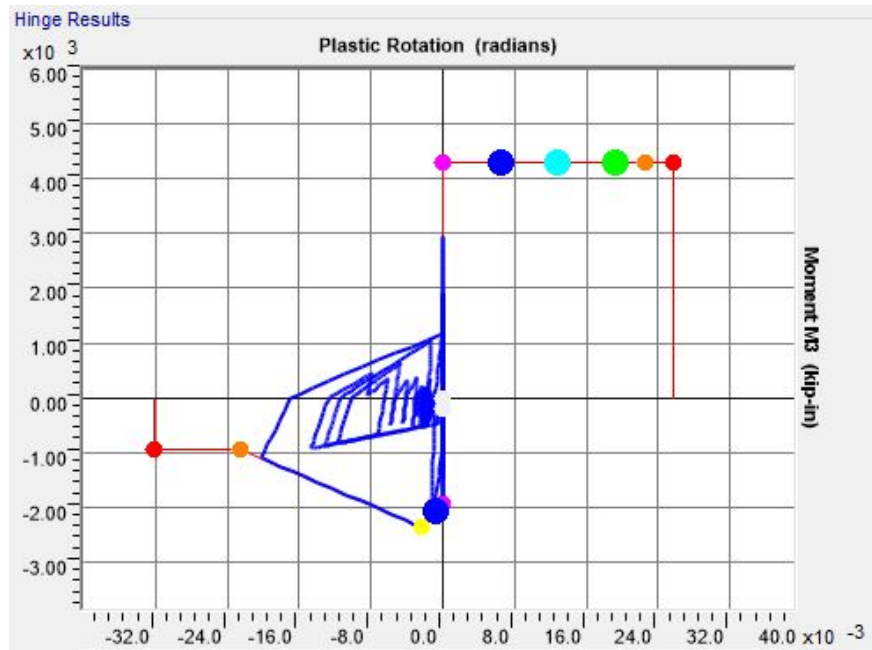
Figure 5.12. Plastic Hysteresis of Frame Hinge 152H1

106
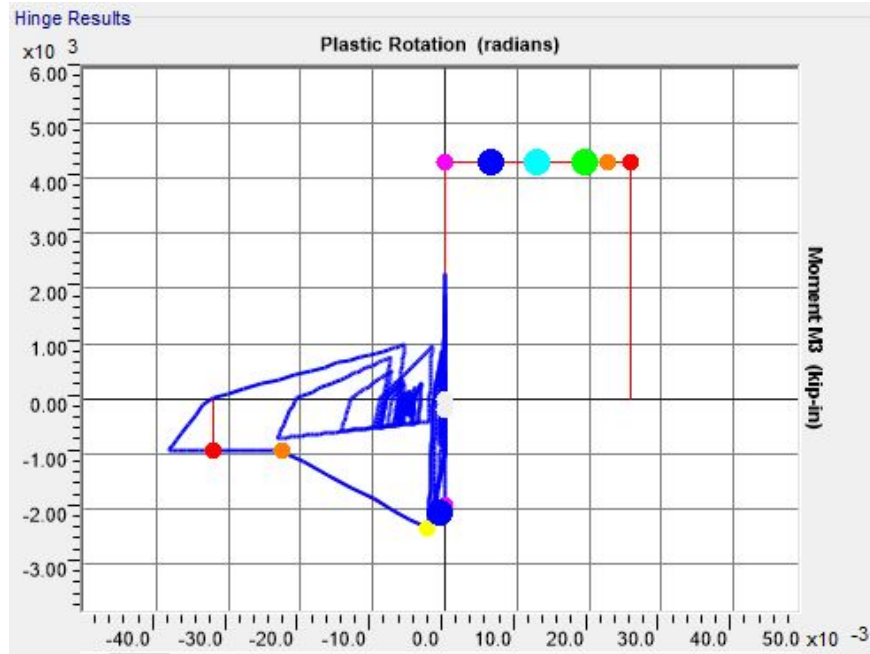
Figure 5.13. Plastic Hysteresis of Frame Hinge 153H1
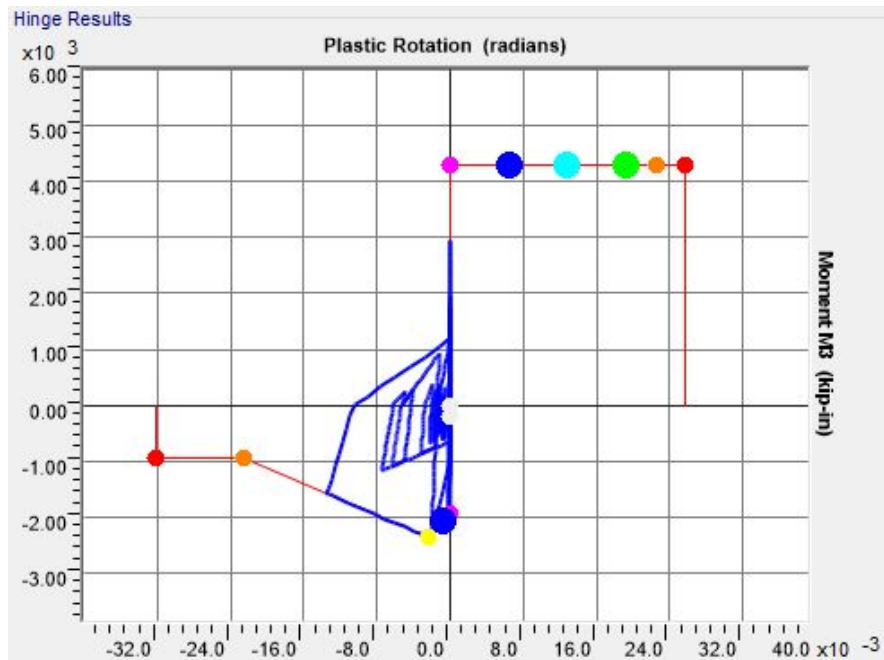
Figure 5.14. Plastic Hysteresis of Frame Hinge 156H1

107

One successful aspect of this research was that the custom hinge exhibited the same LTB behavior for both 2-D and 3-D analyses. However, a similar numerical issue in the LTB hinge occurred during several of the converged dynamic analyses for the 3-D model. Modifying the alpha value for numerical damping helped eliminate the hinge error. Again, this seems to be SAP2000 related, and with the use of a more advanced solution algorithm, this problem would likely be eliminated.

5.2.4. Slotted-Bolted Friction Connection Behavior

The 3-D model utilized 2-node link elements to model a friction connection between the side wall panels and the spandrel beam. As discussed in Chapter 3, the slip force assigned to the link element was 3 kips with an elastic stiffness of 300 kips per inch in out-of-plane direction, and 30 kips per inch in the in-plane direction. One slotted-bolted friction connection was placed in each side wall panel. For each bay, there were a total of 6 wall connections with two being slotted-bolted friction connections.

The response history of the two tension-only side wall braces and one of the friction connections during the Imperial Valley excitation is shown in Figure 5.15. The axial force of the braces is plotted along with the horizontal shear force of the friction connection. The results show that the friction device reached its prescribed slip force and successfully relieved the large stresses that would have developed in the wall panel. The cyclic response of the friction device demonstrates favorable behavior in regard to energy dissipation. Figure 5.16 displays the hysteresis loop of one of the friction connections. The maximum positive displacement was 1.34 inches and the maximum negative displacement was -1.46 inches. The tension-only braces provide

self-centering characteristics to the friction connection throughout the earthquake. The fact that this new connection can activate several times and self-center is a promising means of adding energy dissipation and improving the global performance of the system.
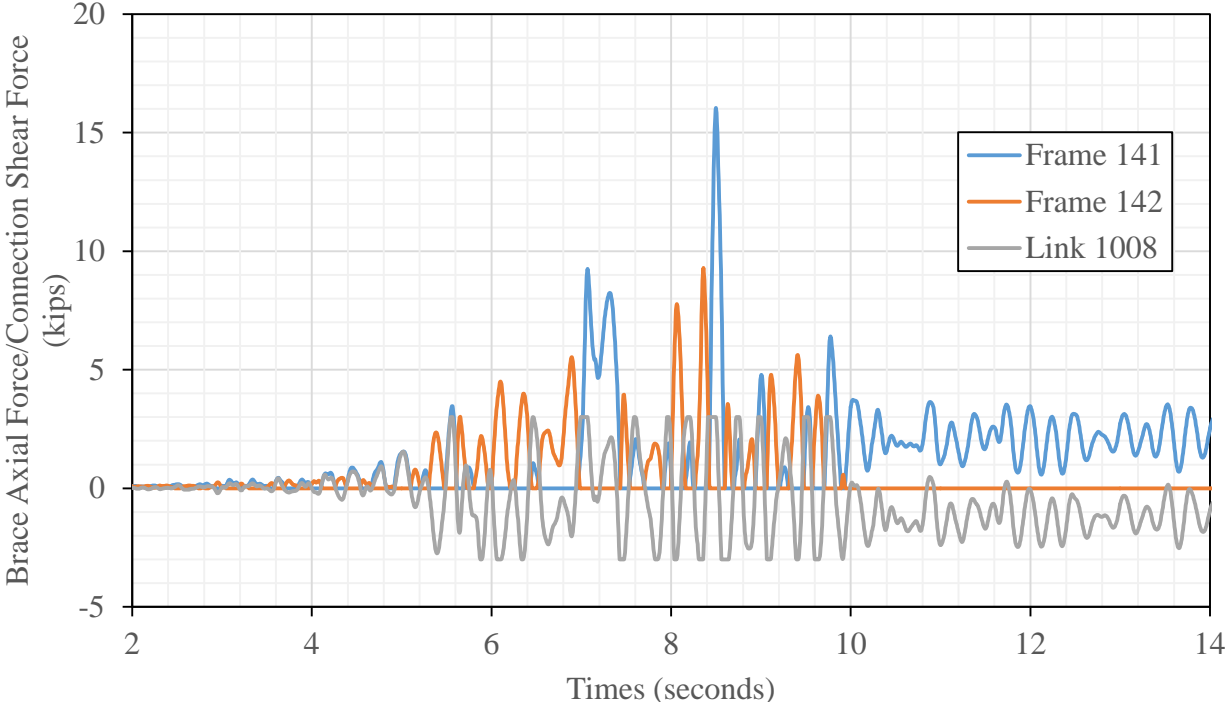

Figure 5.15. Response History of Tension-Only Side Wall Braces and Friction Connection
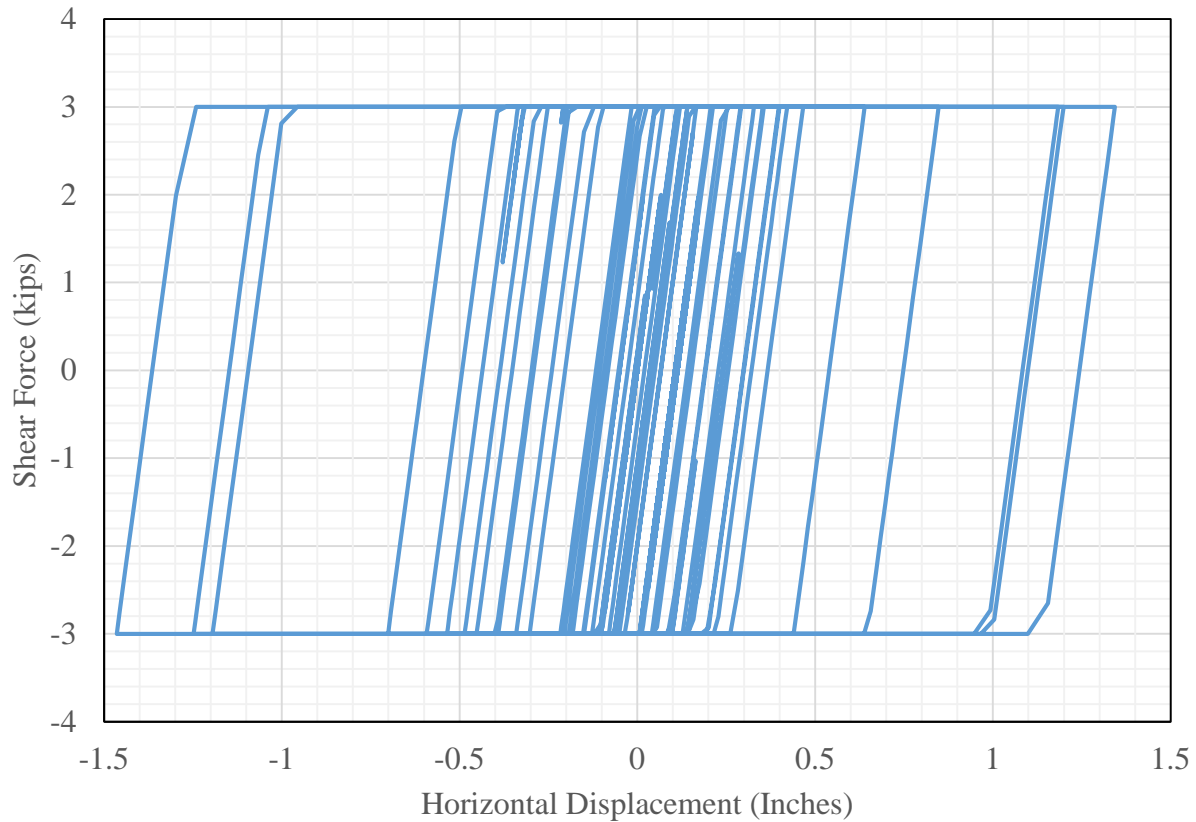
Figure 5.16. Hysteresis Loop of Friction Connection 1008 during Loma Prieta Excitation

5.3.   3-D Model Development Results

The objective was to develop a successful 3-D structural model of a metal building system with hard walls for use in nonlinear-dynamic analyses. A modeling procedure for lateral-torsional buckling of a metal building frame was developed using a custom plastic hinge. The behavior of the hinge was verified in both the 2-D and 3-D model. The strength loss and cyclic behavior of LTB was successfully captured. With this new modeling procedure for post-buckling behavior, the connection demands will be more realistic than if the frame were allowed to remain elastic.

These models have shown that the displacement incompatibility between the hard walls and steel frame can be resolved through the use of slotted-bolted friction connections. A multi-linear plastic link element successfully simulates these types of friction connections. Preliminary results show the energy dissipating characteristics, multiple activation, and self-centering behavior to be promising in enhancing the performance of these structures.

Chapter 6   Summary, Conclusions, and Future Work

6.1.   Summary

Metal building systems provide an economical alternative to conventional construction for non-residential low-rise buildings, accounting for the high demand of these systems. Recent trends have been to include precast concrete or masonry walls with the metal buildings. In previous research, Hong (2007) showed that light weight metal building specimens have a high level of overstrength and were likely to remain elastic even during a MCE event. For metal building systems with hard walls, the overstrength was lower. Smith's (2013a) shake table findings were in agreement with Hong's case study. The shake table findings and cyclic LTB tests led to a conceptual development of a new seismic force resisting system for metal building frames that relies on a LTB fuse element. These developments will impact a positive change in the seismic performance of these structures.

All previous research has focused on the seismic performance in the transverse direction (moment frame direction). Post-earthquake reconnaissance (Marshall and Gould 2012) revealed that seismic performance of metal building systems in the longitudinal direction is unacceptable. Poorly designed connections between the hard walls and steel frame can fail in a brittle manner and the wall can fall away from the structure. A new seismic force resisting system that relies on resilient connections can relieve the stiffness incompatibility that exists between the hard wall and steel frame and dissipate energy. Before work could proceed, a 3-D computer model for metal building systems with hard walls needed to be developed. The interaction between the steel frame

and hard wall is a 3-D problem as the connections experience both in-plane and out-of-plane behavior. A modeling procedure that captures the metal building frame post-buckling behavior during an earthquake event had yet to be successfully modeled using frame elements.

The research presented in this thesis lays out a modeling procedure for metal building systems with hard walls in SAP2000 that can be used for nonlinear dynamic analyses. The first step toward the development of the 3-D model was to determine the metal building frame capacities, as well as the demarcation between elastic and inelastic frame behavior, through finite element analyses using Abaqus. Post-buckled frame behavior was modeled in SAP2000 using a lateral-torsional buckling hinge. A 2-D planar frame analysis was used to calibrate the custom backbone curve such that the SAP2000 pushover curve matched, as closely as possible, the Abaqus pushover curve. Cyclic behavior of the LTB hinge was approximated using the pivot hysteresis method. A case study was performed for one of the metal building systems in 3-D to assess the performance of the LTB hinge and other component behavior. Based on the success of preliminary results, this 3-D model can effectively be used to quantify connection strength, post-yield deformation, and energy dissipation capacities required to achieve enhanced performance of metal building systems with hard walls.

6.2. Conclusions

The major findings from this research regarding the 3-D modeling procedure are:

1) Lateral torsional buckling component hinge backbone curves can be defined using nonlinear static pushover analyses.

2) The pivot hysteresis method successfully captures many aspects of cyclic LTB described in previous shake table experiments and cyclic LTB tests.

113

3) The LTB hinge developed is highly convergence sensitive in the SAP2000 analysis software. Small adjustments to the α value in the Hibler-Hughes-Taylor time integration method can have a significant impact on convergence.

4) The LTB hinge can be used in models for metal building frames for both 2-D and 3-D nonlinear dynamic analyses.

5) The 3-D model developed for metal building systems with hard walls can be successfully used to quantify seismic performance of the frame and wall connections.

6) A two-node multilinear plastic link element is appropriate for modeling the friction connection between the hard walls and steel frame.

7) Tension-only x-bracing provides self-centering characteristics to the friction connections.

8) Friction connections successfully relieve the stiffness incompatibility between the stiff hard walls and flexible steel frames during earthquake excitation.

9) Energy dissipation capacities of the friction connections show promising behavior due to self-centering characteristics and potential for multiple activation cycles.

10) 3-D models of metal building systems that have explicitly modeled hard walls exhibit very low mass participation ratios in both horizontal directions. It is likely that the mass within the hard walls is not participating in the fundamental modes of vibration.

6.3. Future Work

It is anticipated that the new longitudinal seismic force resisting system will be validated using this newly developed 3-D model in a FEMA P695 study for incorporation into the building codes. Research tasks needed to accomplish this goal include:

1) A parametric study on the wall connections to determine the energy dissipation capacities required to enhance global system seismic performance. Deformation demands and out-of-plane strength demands should also be ascertained.

2) The possibility of using a yielding device or viscous device for the connections between the hard wall and steel frame.

3) A comparative evaluation of new resilient connections using 3-D finite element models to assess strength, stiffness, energy dissipation reliability, deformation capacity, constructability, reparability, and economy. Experimental tests for the connections will be used to validate the computer models.

References

AISC (2010a), ANSI/AISC 360-10, *Specification for Structural Steel Buildings*, American Institute of Steel Construction, Inc., Chicago, IL.

AISC (2010b), ANSI/AISC 341-10, *Seismic Provisions for Structural Steel Buildings,* American Institute of Steel Construction, Chicago, IL.

AISC (2011), *Steel Construction Manual,* 14th Edition, American Institute of Steel Construction, Chicago, IL.

ASCE/SEI (2010), *Minimum Design Loads for Buildings and Other Structures,* ASCE/SEI 7-10, American Society of Civil Engineers, New York, NY.

ATC (2009), "Quantification of building seismic performance factors," *Report No. FEMA-P695*, Applied Technology Council, Redwood City, CA.

Bajwa, M.S., Charney, F.A., and Moen, C.D. (2010), "Assessment of Analytical Procedures for Designing Metal Buildings for Wind Drift Serviceability," *Report No. CE/VPI-ST 10/05,* The Charles E. Via, Jr. Department of Civil and Environmental Engineering, Virginia Polytechnic Institute and State University, Blacksburg, VA.

Charney, F.A. and Marshall, J. (2006), "A Comparison of the Krawinkler and Scissors Models for Including Beam-Column Joint Deformations in the Analysis of Moment-Resisting Steel Frames," *Engineering Journal*, AISC, 1st Quarter, pp 31-48.

Chopra, A.K. (2009), *Dynamics of Structures,* 4th Edition.*,* Pearson Prentice Hall, Upper Saddle River, NJ.

CSI (2015), SAP2000, Version 17.3.0, Computers and Structures, Inc., Berkeley, CA.

CSI (2011), Perform-3D, Version 5, Computers and Structures, Inc., Berkeley, CA.

Dowell, R.K., Seible, F.S., and Wilson, E.L. (1998), "Pivot Hysteretic Model for Reinforced Concrete Members," *ACI Structural Journal*, Vol. 95, pp. 607–617.

FEMA (2000), *Prestandard and Commentary for Seismic Rehabilitation of Buildings*, Prepared by the American Society of Civil Engineers for the Federal Emergency Management Agency (Report No. FEMA-356), Washington, D.C.

Hilber, H.M., Hughes, T.J.R., and Taylor, R.L. (1977), "Improved Numerical Dissipation for Time Integration Algorithms in Structural Dynamics" *Earthquake Engineering and Structural Dynamics*, 5:282-292.

Hong, Y.D. (2007), "Development of A Seismic Design Procedure for Metal Building Systems," *Doctoral Dissertation*, Department of Structural Engineering, University of California, San Diego, La Jolla, CA.

Kaehler, R.C., White., D.W., and Kim, Y.D. (2011), "Frame Design Using Web-Tapered Members," Steel Design Guide 25, AISC/MBMA, Chicago, IL.

Kim, Y.D. (2010), "Behavior and Design of Metal Building Frames with General Prismatic and Web-Tapered Steel I-Section Members," *Doctoral Dissertation*, School of Civil and Environmental Engineering, Georgia Institute of Technology, Atlanta, GA.

Marshall, J.D. and Gould, N.C. (2012). The Performance of Low-Rise Industrial Facilities in the 2010 Haiti and 2011 Christchurch, New Zealand Earthquakes. 15th World Conference on Earthquake Engineering, Lisbon, Portugal, September 24-28, 2012.

Mazzoni, S., McKenna, F., Scott, M.H., Fenves, G.L., et al. (2007). *Open System for Earthquake Engineering Simulation (OpenSEES) Command Language Manual.* Pacific Earthquake Engineering Research Center, University of California, Berkeley.

NCMA (2011). *Concrete Masonry Walls for Metal Buildings Systems*, National Concrete Masonry Association, Herndon, VA.

Newman, A. (2004), Metal Building Systems: Design and Specifications, 2nd Edition, McGraw-Hill, New York, NY.

Nucor (2009), *Products and Engineering Manual*, 4.10.3, http://www.nucorbuildingsystems.com/nbsproductandengineeringmanual/.

PEER (2015), *PEER NGA Database,* Pacific Earthquake Engineering Research Center, University of California, Berkeley, California, http://peer.berkeley.edu/nga/.

Simulia (2015), Abaqus, Standard Version 6.14-1. Dassault Systemes Simulia Corp. Providence, RI

Smith, M.D. and Uang, C.M. (2013a), "Earthquake Simulator Testing of a Metal Building with Metal Panel Sidewalls*," Report No. SSRP-12/03*, Department of Structural Engineering, University of California, San Diego, La Jolla, CA

Smith, M.D. and Uang, C.M. (2013b), "Earthquake Simulator Testing of a Metal Building with Concrete Sidewalls," *Report No. SSRP-12/04*, Department of Structural Engineering, University of California, San Diego, La Jolla, CA

Smith, M.D., Turner, K.T., and Uang, C.M. (2013c), "Experimental Investigation of Cyclic Lateral Buckling of Web-Tapered I-Beams," *Report No. SSRP-12/06*, Department of Structural Engineering, University of California, San Diego, La Jolla, CA

Smith, M.D., and Uang, C.M. (2013d), "Seismic Testing and Analytical Studies for the Development of New Seismic Force Resisting Systems for Metal Buildings," *Doctoral Dissertation*, Department of Structural Engineering, University of California, San Diego, La Jolla, CA.

Appendix   LTB Hinge Results for 2-D Frames

Numerous 2-D nonlinear dynamic analyses were performed to assess the behavior of the newly developed lateral-torsional buckling (LTB) hinge. The hysteresis loops repeatedly show that the hinge is successfully capturing post-buckled frame behavior during an earthquake excitation. The full lateral-torsional buckling hinge results for Frames 16, 41, 42, and 85 are presented in this section.

As seen in Table A.1., the LTB hinge was considered activated if the equilibrium state of reached the negative slope portion of the backbone curve. Hinges that did not exceed the LTB capacity, or remained elastic, were not included in the Appendix.

Table A.1. LTB Hinge Activation and Peak Frame Displacement for Frame 16

Earthquake Case	LTB Hinges Activated	Peak Displacement at Ridgeline (inches)	Peak Absolute Acceleration at Ridgeline (in/sec^2)
San Fernando	2	6.11	388
		-2.36	-396
Friuli, Italy	2, Collapse Possible	12.87	1271
		-2.93	-545
Gazli, USSR	2	5.99	458
		-8.98	-359
Imperial Valley	2	4.85	400
		-6.41	-365
Superstition Hills	2	6.47	398
		-6.24	-393
Loma Prieta	2, with Hinge Error	3.62	7275
		-6.06	-9864
Northridge Canyon	1	2.62	279
		-7.55	-272
Northridge Sylmar	2, Collapsed Possible	13.66	316
		-12.49	-297
Kobe	1	3.72	295
		-2.74	-889
Kocaeli	2, Collapse Possible	13.01	417
		-11.19	-466
Chi-Chi, Taiwan	2	6.94	419
		-7.63	-450
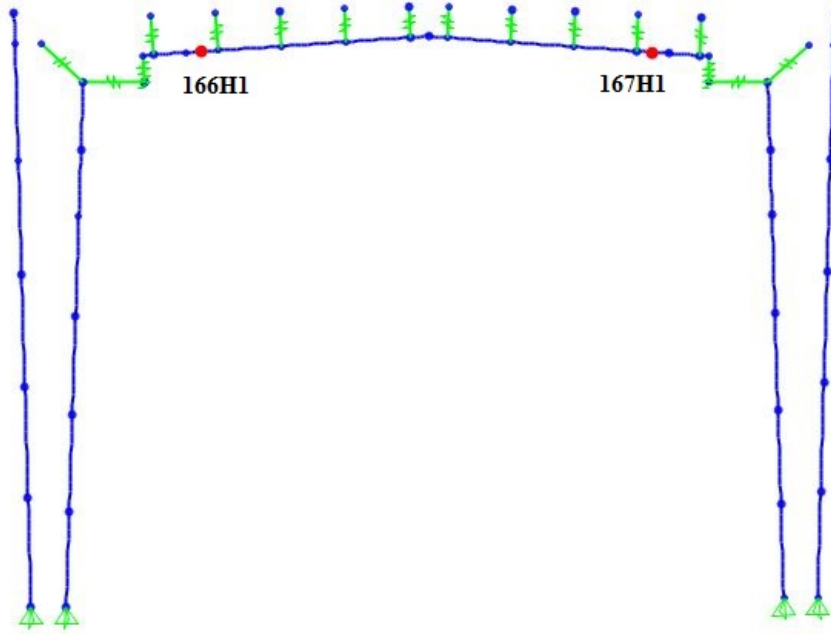
Figure A.1. LTB Hinge Identification for Frame 16
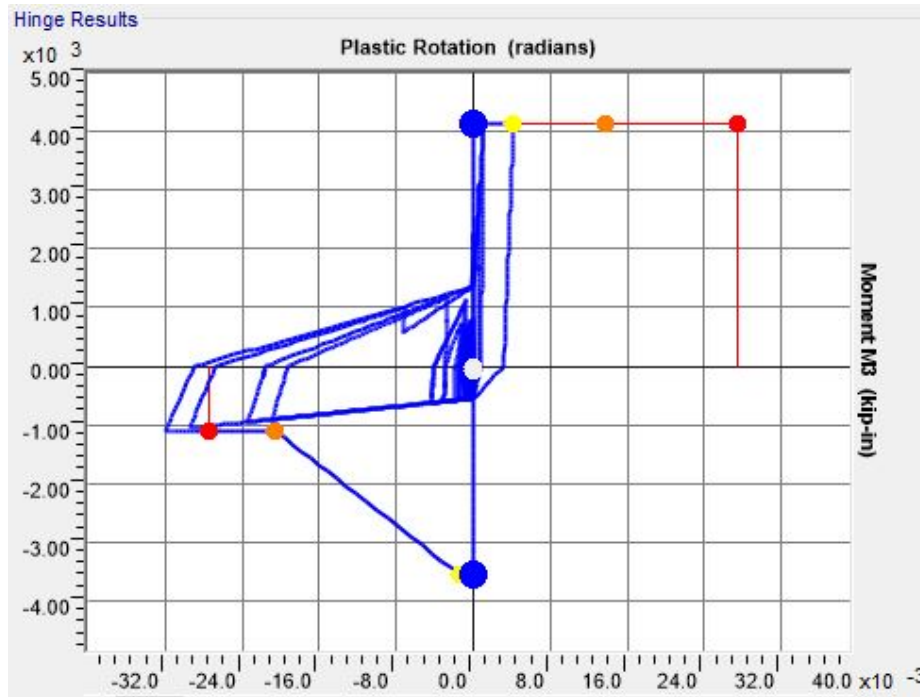
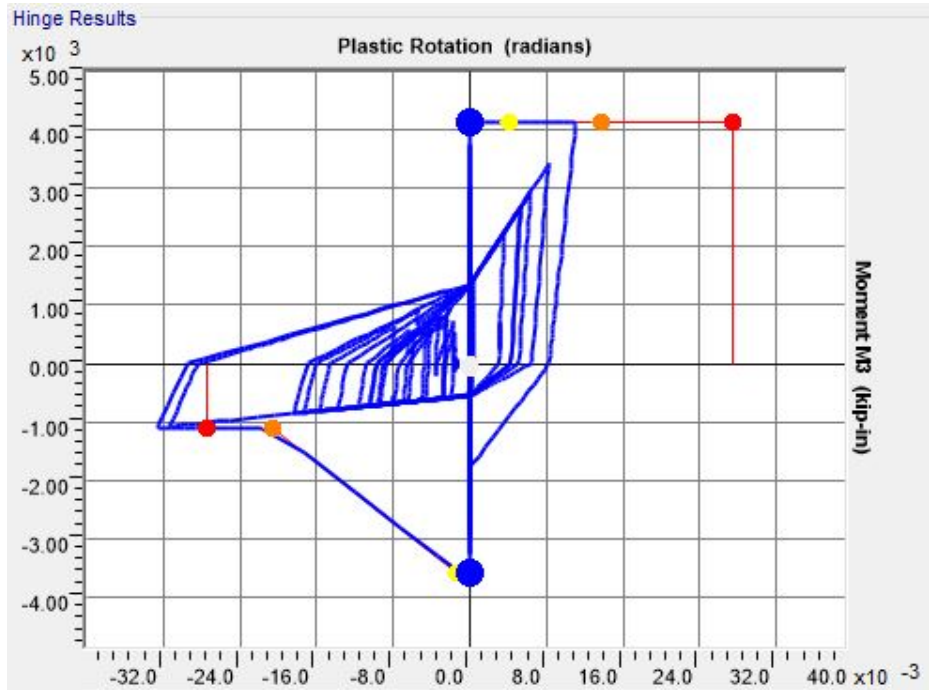**Figure A.2. Plastic Hysteresis of 166H1 during Imperial Valley Excitation (2D-16)**
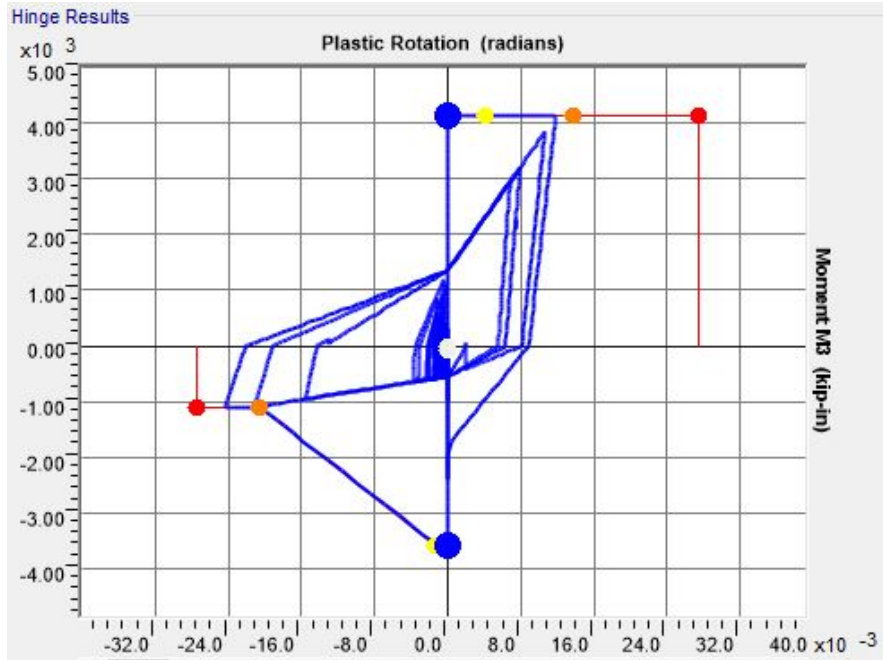
Figure A.3. Plastic Hysteresis of 167H1 during Imperial Valley Excitation (2D-16)
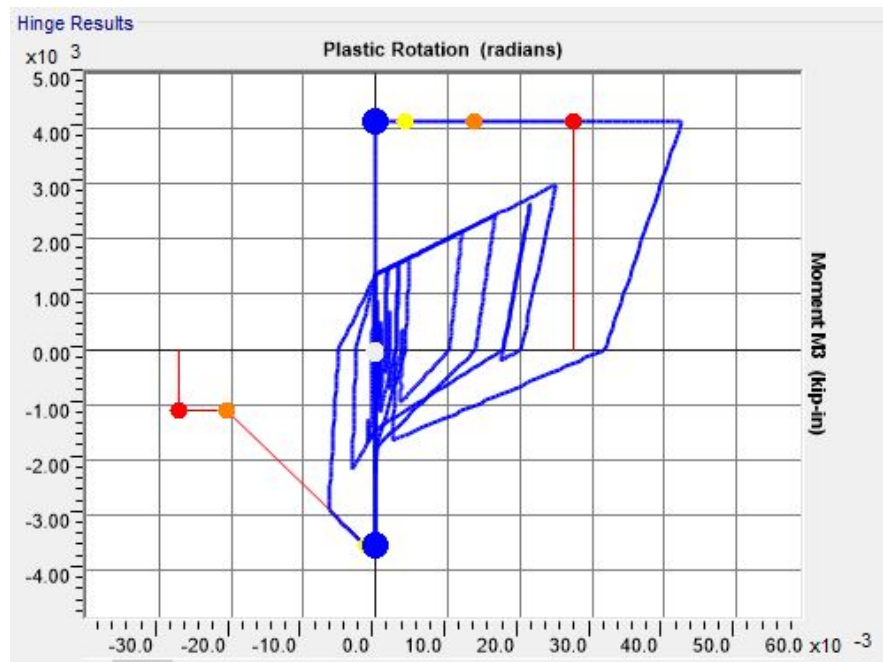
Figure A.4. Plastic Hysteresis of 166H1 during Friuli, Italy Excitation (2D-16)

A4
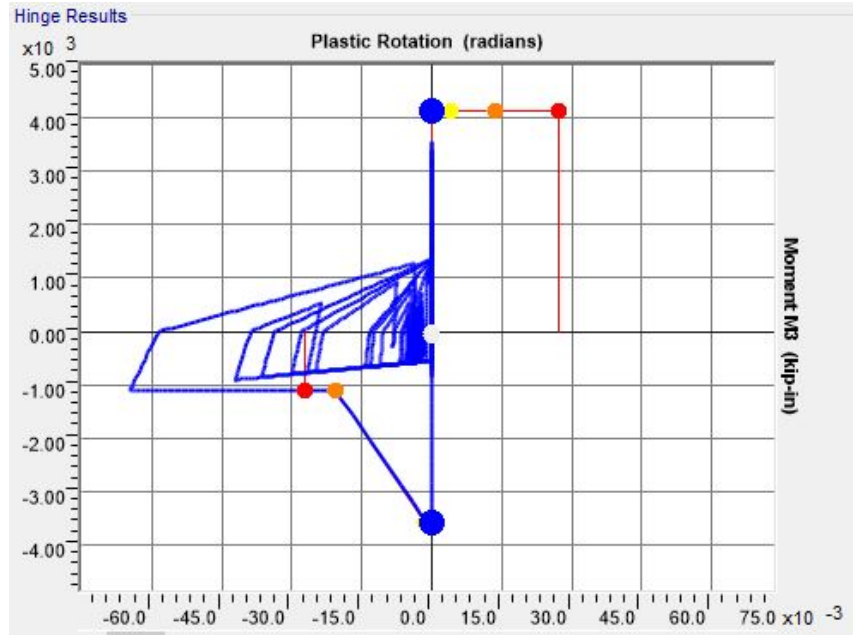
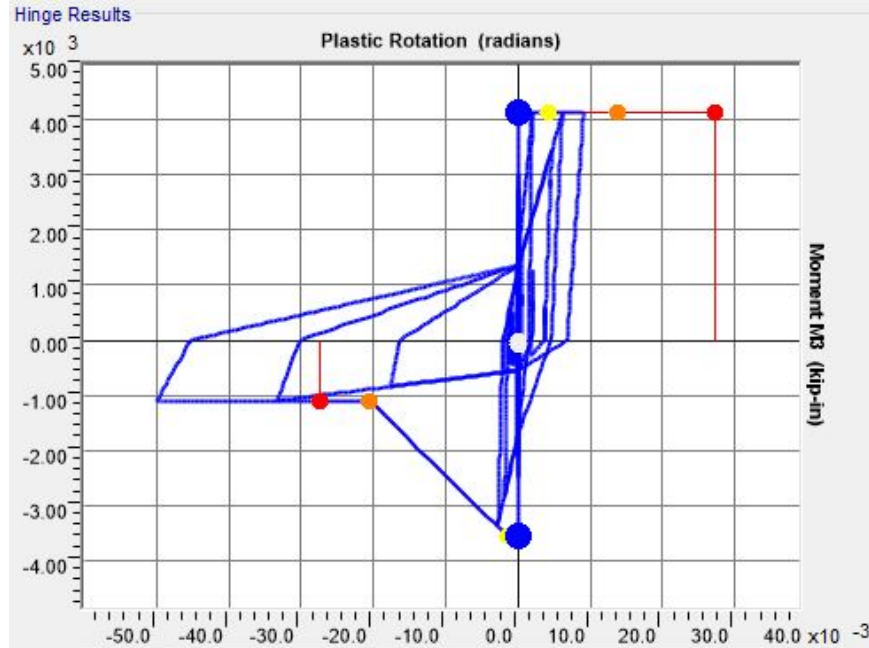**Figure A.5. Plastic Hysteresis of 167H1 during Friuli, Italy Excitation (2D-16)**
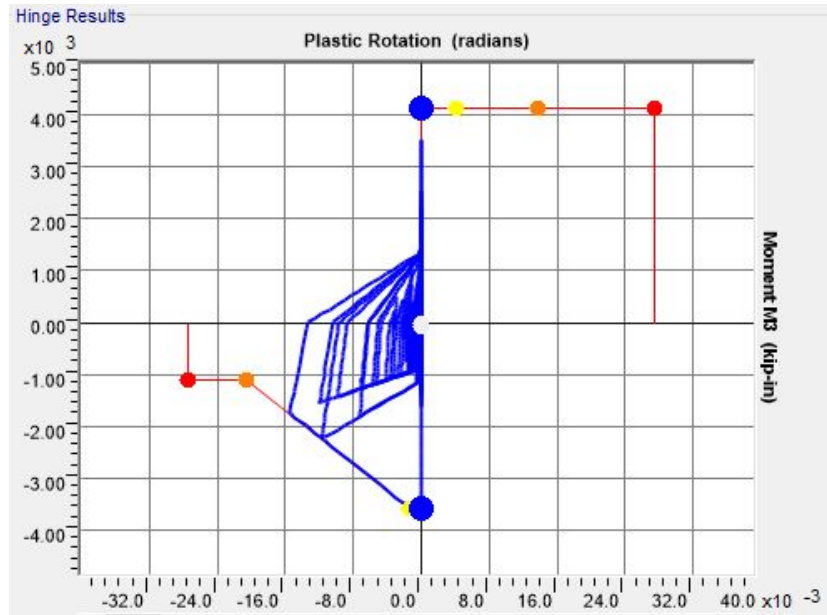
Figure A.6. Plastic Hysteresis of 167H1 during Kobe Excitation (2D-16)

A5
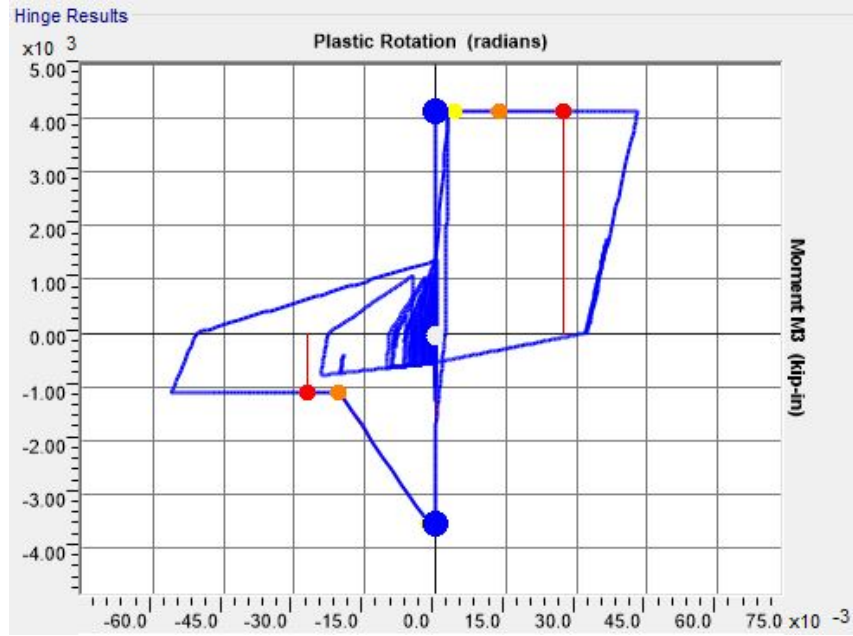
Figure A.7. Plastic Response History of 166H1 during Kocaeli Excitation (2D-16)
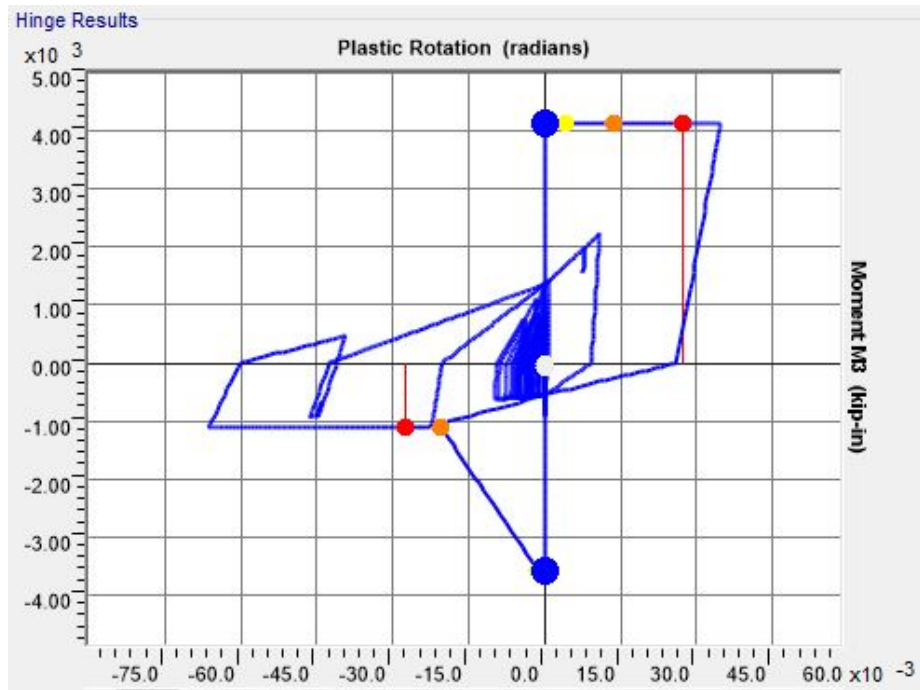
Figure A.8. Plastic Hysteresis of 167H1 during Kocaeli Excitation (2D-16)

A6
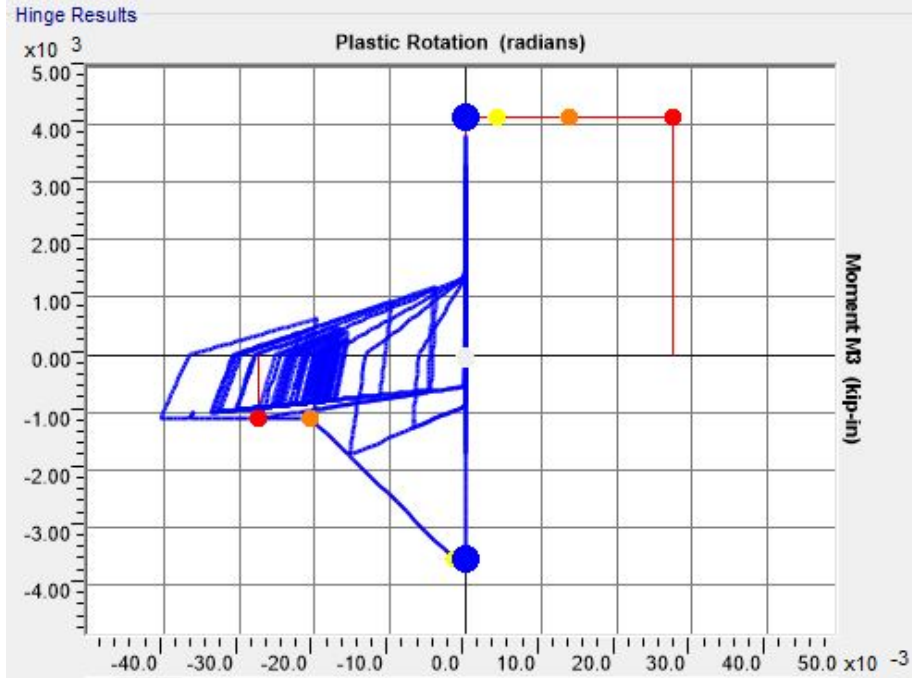
Figure A.9. Plastic Hysteresis of 166H1 during Loma Prieta Excitation (2D-16)
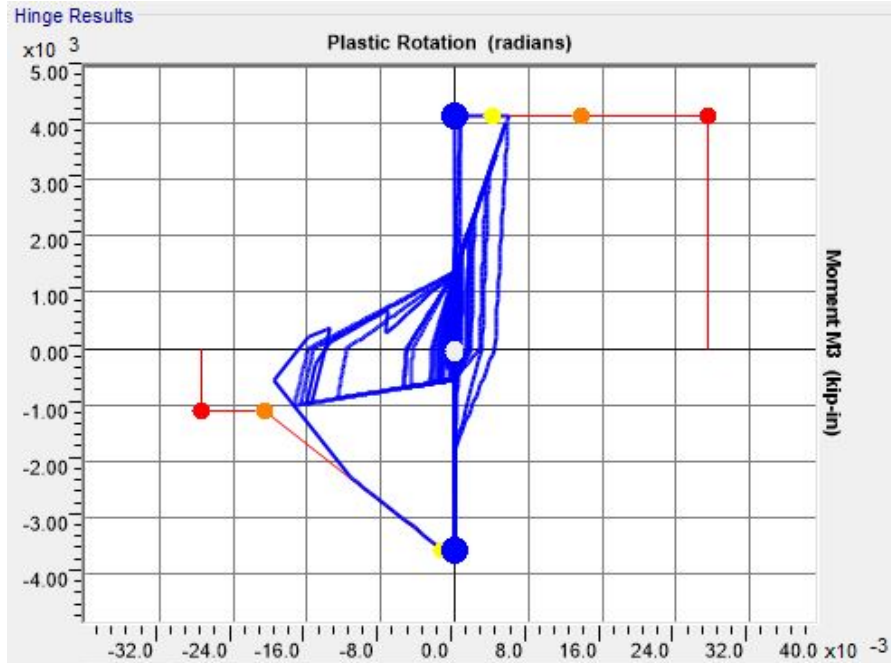
Figure A.10. Plastic Hysteresis of 167H1 during Loma Prieta Excitation (2D-16)

A7
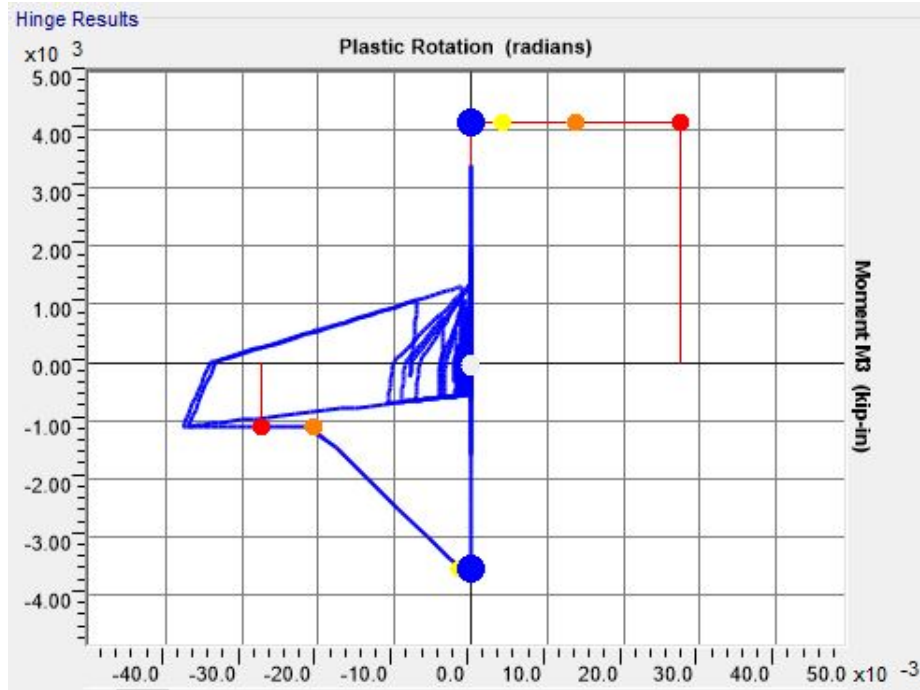
Figure A.11. Plastic Hysteresis of 166H1 during Northridge Canyon Excitation (2D-16)
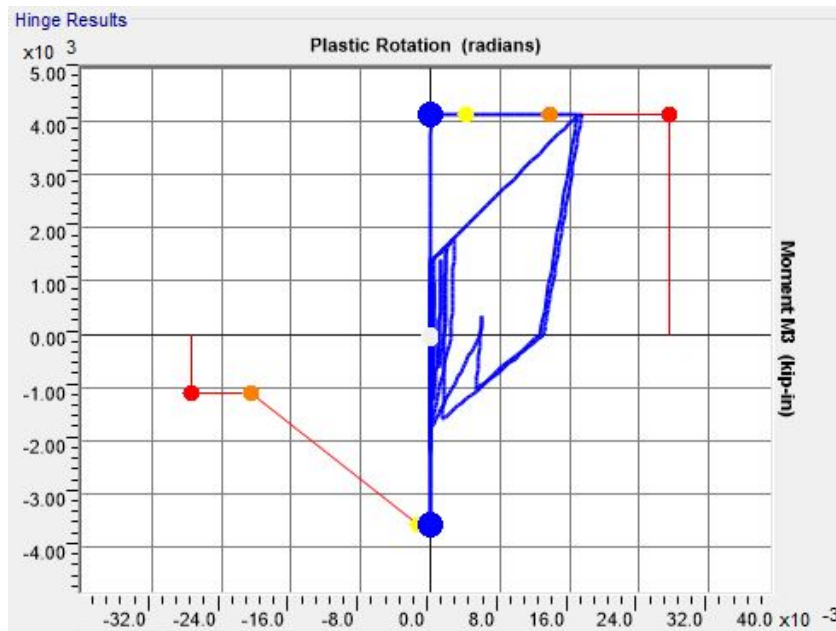
Figure A.12. Plastic Hysteresis of 167H1 during Northridge Canyon Excitation (2D-16)

A8
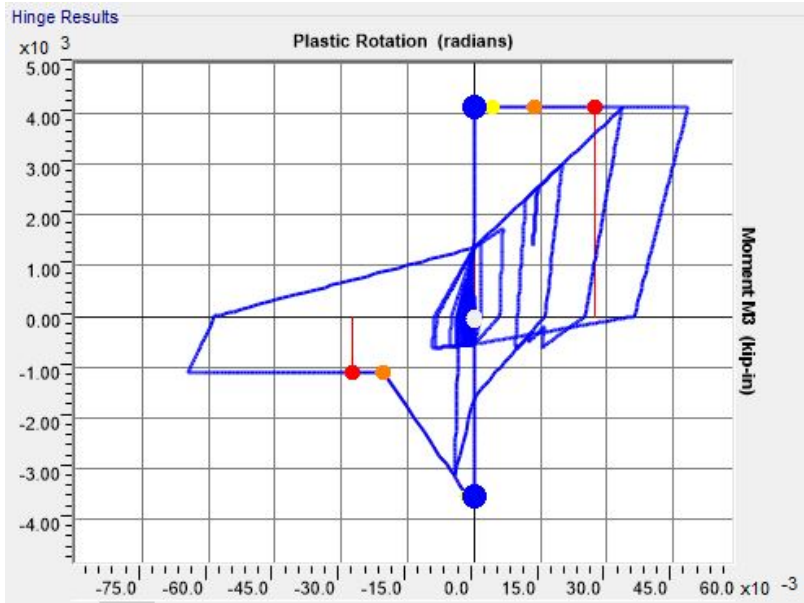
Figure A.13. Plastic Hysteresis of 166H1 during Northridge Sylmar Station Excitation (2D-16)
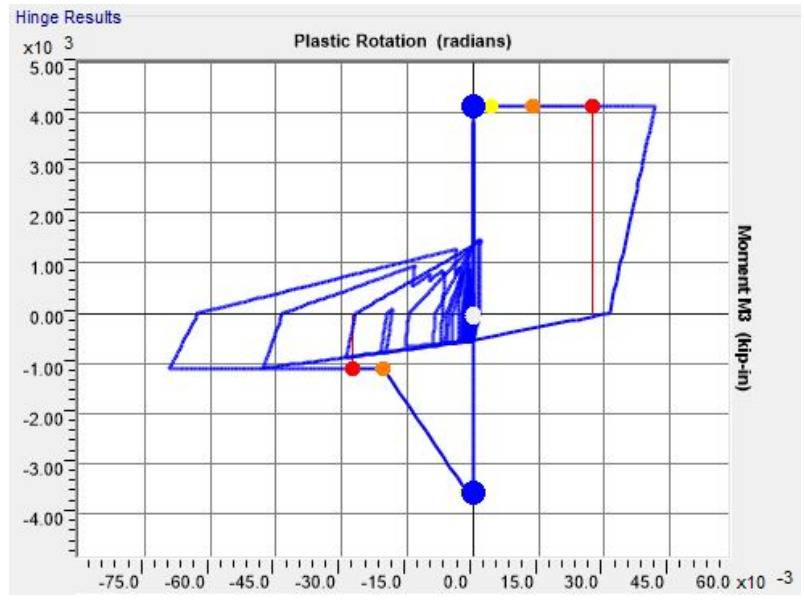
Figure A.14. Plastic Hysteresis of 167H1 during Northridge Sylmar Station Excitation (2D-16)
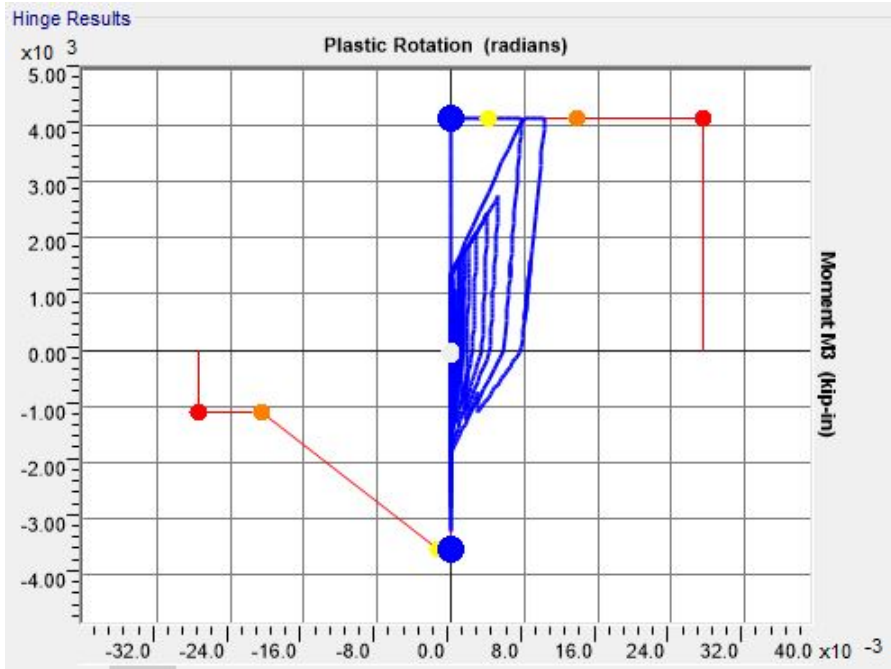
Figure A.15. Plastic Hysteresis of 166H1 during San Fernando Excitation (2D-16)
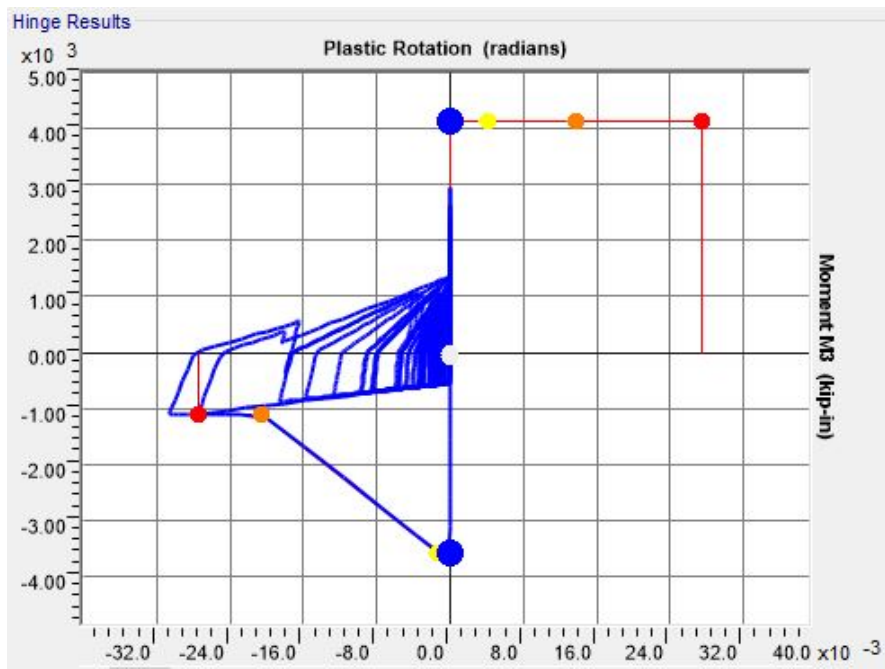
Figure A.16. Plastic Hysteresis of 167H1 during San Fernando Excitation (2D-16)

A10
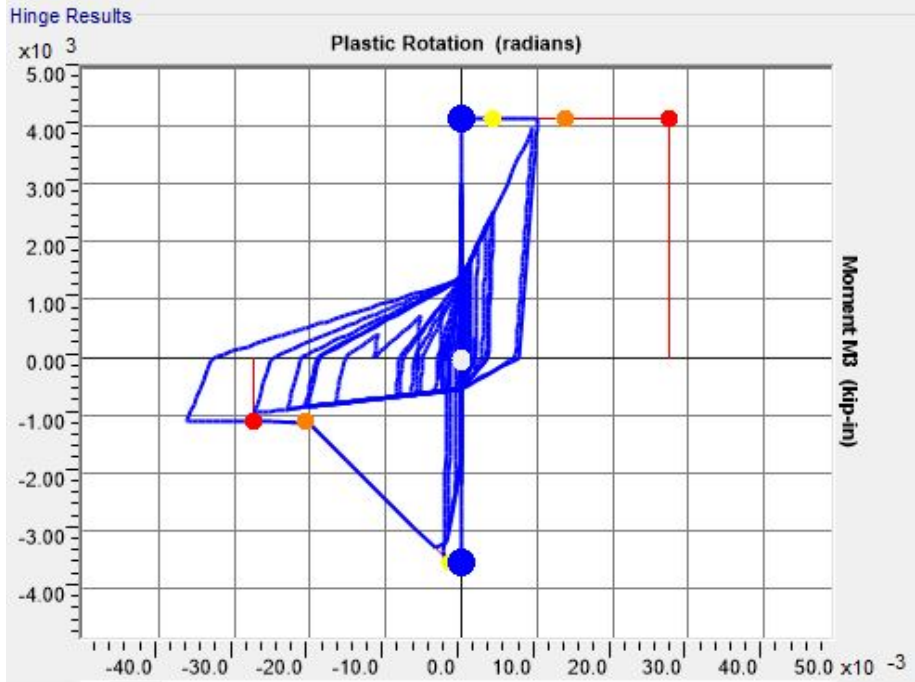
Figure A.17. Plastic Hysteresis of 166H1 during Superstition Hills Excitation (2D-16)

Figure A.18. Plastic Hysteresis of 167H1 during Superstition Hills Excitation (2D-16)

A11
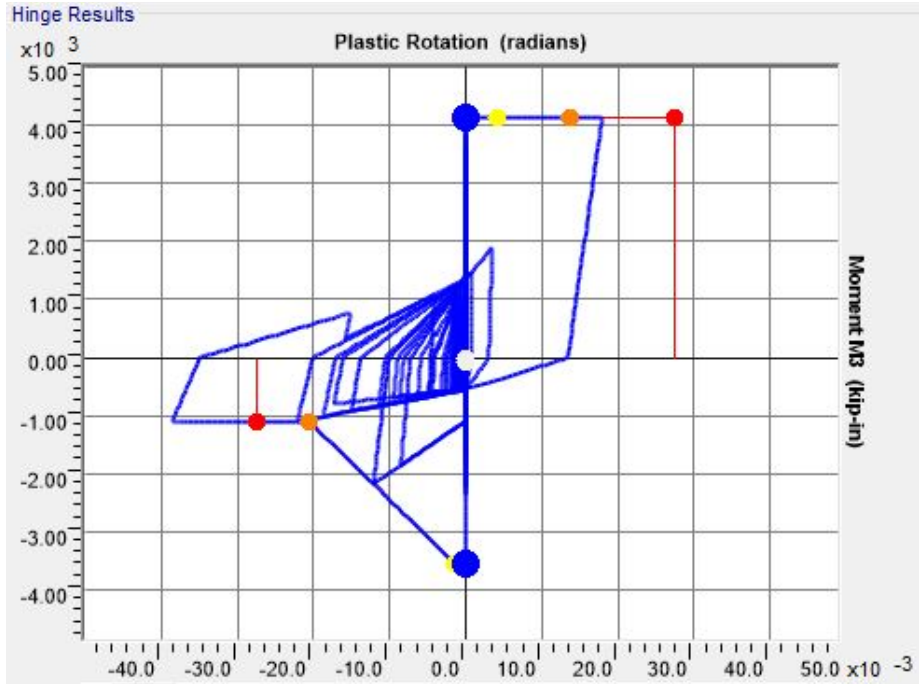
Figure A.19. Plastic Hysteresis of 166H1 during Chi-Chi, Taiwan Excitation (2D-16)
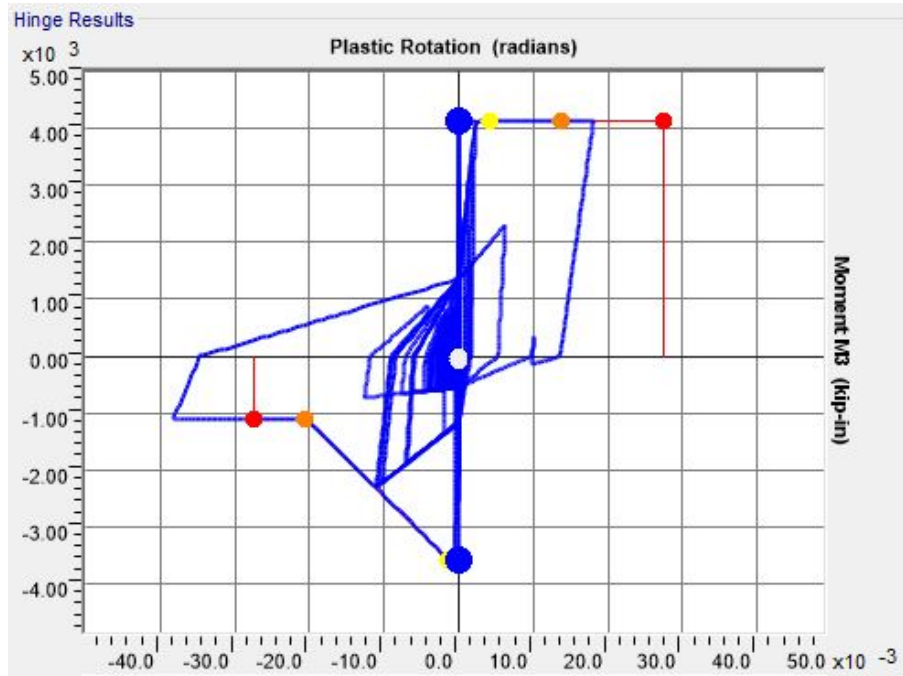
Figure A.20. Plastic Hysteresis of 167H1 during Chi-Chi, Taiwan Excitation (2D-16)

A12

Figure A.21. Plastic Hysteresis of 166H1 during Gazli, USSR Excitation (2D-16)
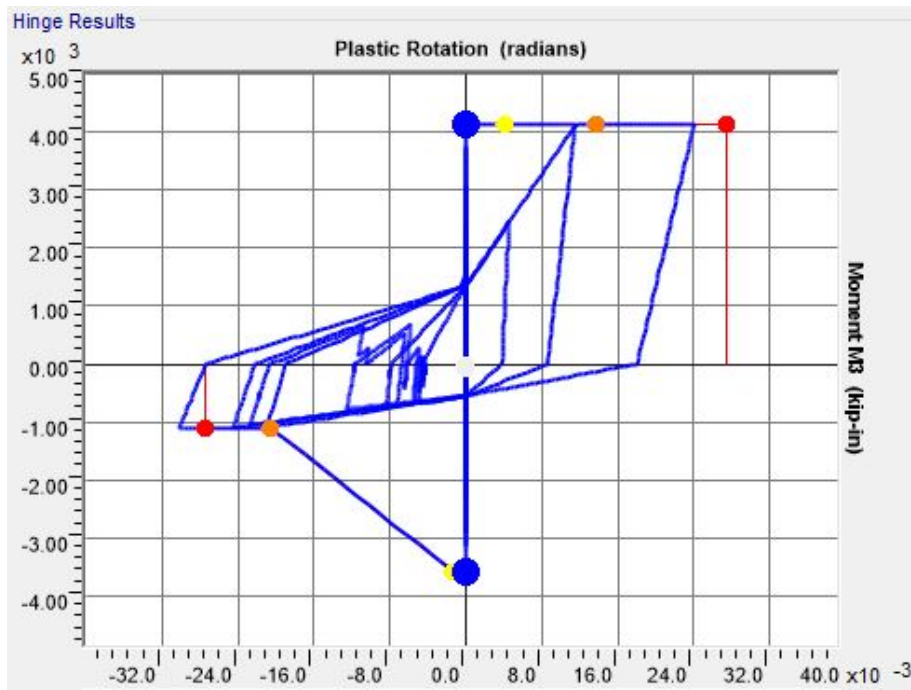
Figure A.22. Plastic Hysteresis of 167H1 during Gazli, USSR Excitation (2D-16)

A13

Table A.2. LTB Hinge Activation and Peak Frame Displacement for Frame 41

Earthquake Case	Hinges where LTB Capacity Exceeded	Peak Displacement at Ridgeline (inches)	Peak Absolute Acceleration at Ridgeline (in/sec^2)
San Fernando	1	5.98	408
		-4.58	-435
Friuli, Italy	2	12.85	657
		-11.53	-814
Gazli, USSR	2	8.66	598
		-9.19	-661
Imperial Valley	2	6.73	357
		-5.36	-418
Superstition Hills	2	8.40	615
		-7.48	-535
Loma Prieta	2	10.44	641
		-10.47	-642
Northridge Canyon	1	4.92	250
		-4.45	-348
Northridge Sylmar	2	13.40	733
		-14.04	-701
Kobe	0	4.19	281
		-4.29	-324
Kocaeli	2	7.61	555
		-8.21	-604
Chi-Chi, Taiwan	2	9.83	659
		-9.75	-679

Table A.3. LTB Hinge Activation and Peak Frame Demands for Frame 42

Earthquake Case	LTB Hinges Activated	Maximum Ridgeline Displacement (inches)	Peak Absolute Acceleration at Ridgeline (in/sec^2)
San Fernando	0	6.53	309
		-3.77	-396
Friuli, Italy	1	8.19	415
		-10.02	-477
Gazli, USSR	1	7.90	359
		-5.62	-408
Imperial Valley	1	7.09	329
		-5.56	-401
Superstition Hills	1	6.68	391
		-7.39	-509
Loma Prieta	1	6.31	322
		-5.47	-332
Northridge Canyon	0	4.44	278
		-4.60	-240
Northridge Sylmar	Hinge Error	9.18	4050
		-20.65	-10631
Kobe	0	4.29	207
		-3.17	-247
Kocaeli	1	8.15	313
		-8.45	-425
Chi-Chi, Taiwan	2	8.72	386
		-10.81	-492
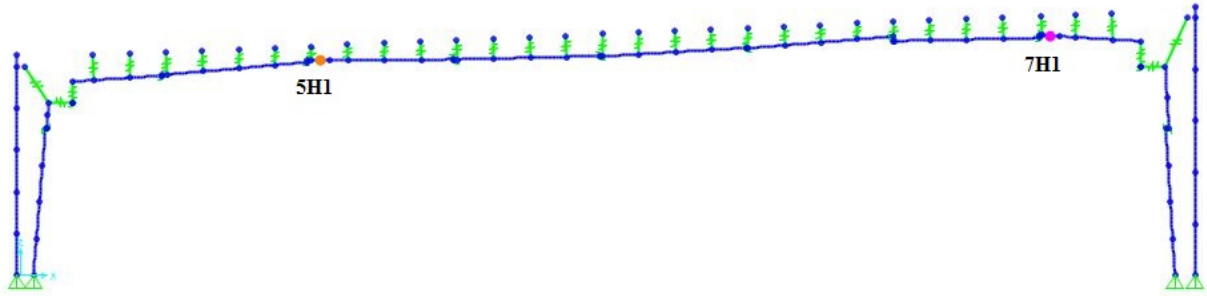
Figure A.23. Hinge Identification for Frame 42
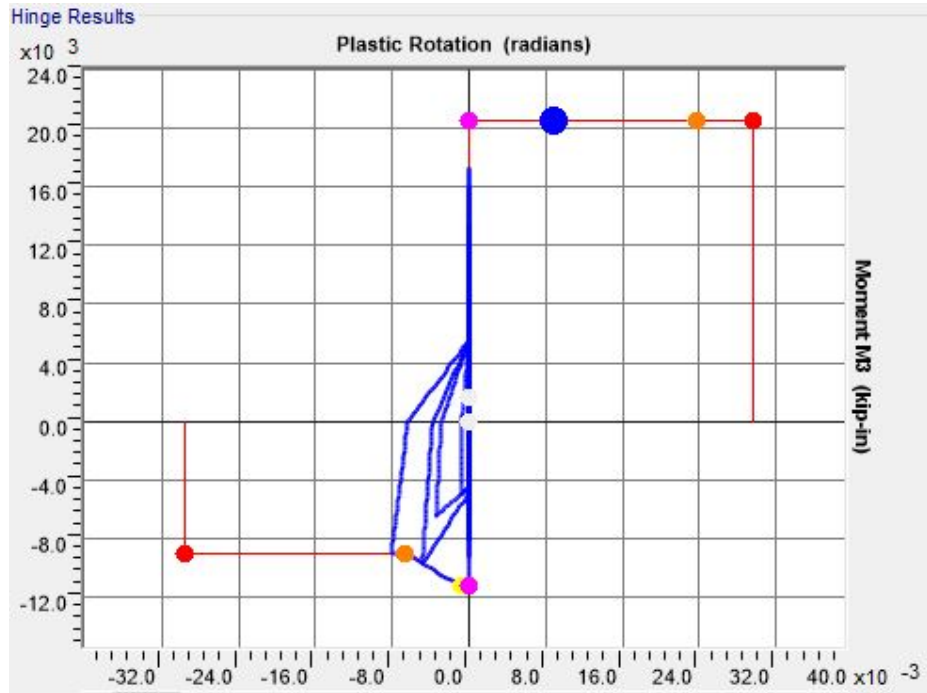
Figure A.24. Plastic Hysteresis of Hinge 5H1 Imperial Valley Excitation (2D-42)

A16
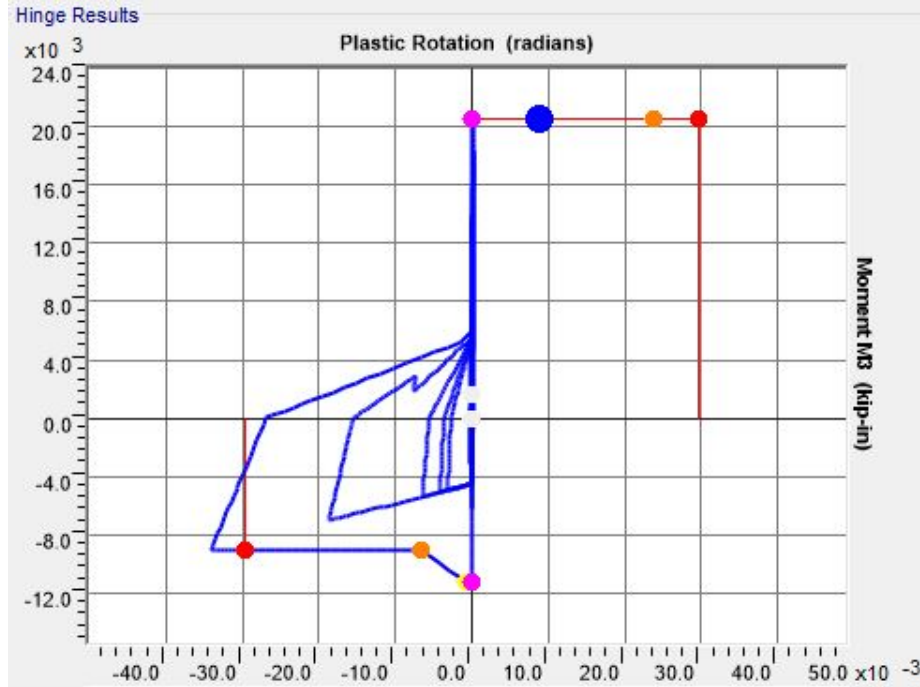
Figure A.25. Plastic Hysteresis of Hinge 5H1 Friuli, Italy Excitation (2D-42)
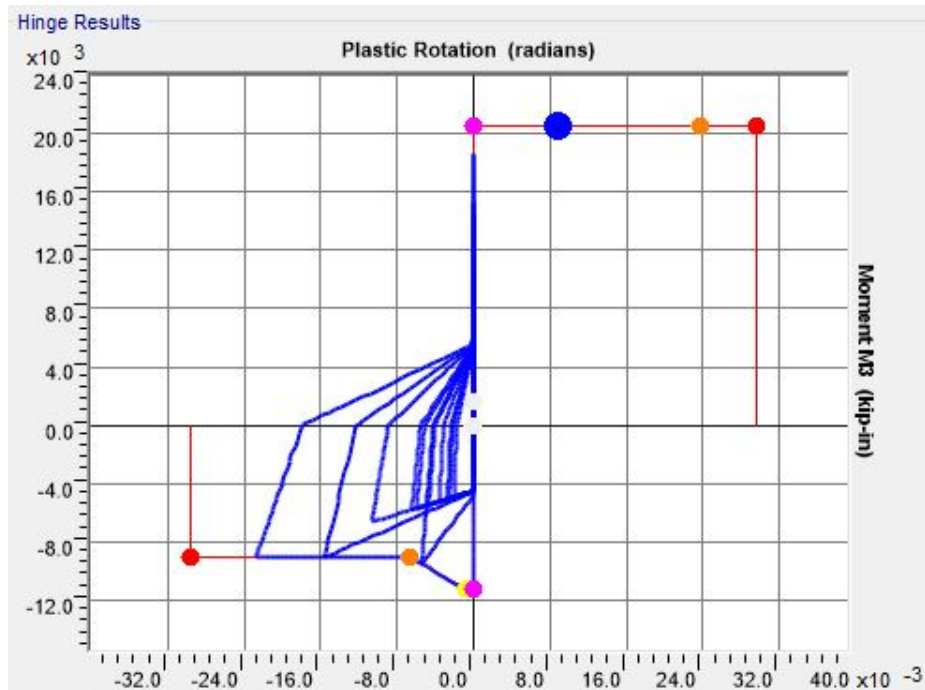
Figure A.26. Plastic Hysteresis of Hinge 5H1 Kocaeli, Turkey Excitation (2D-42)

A17
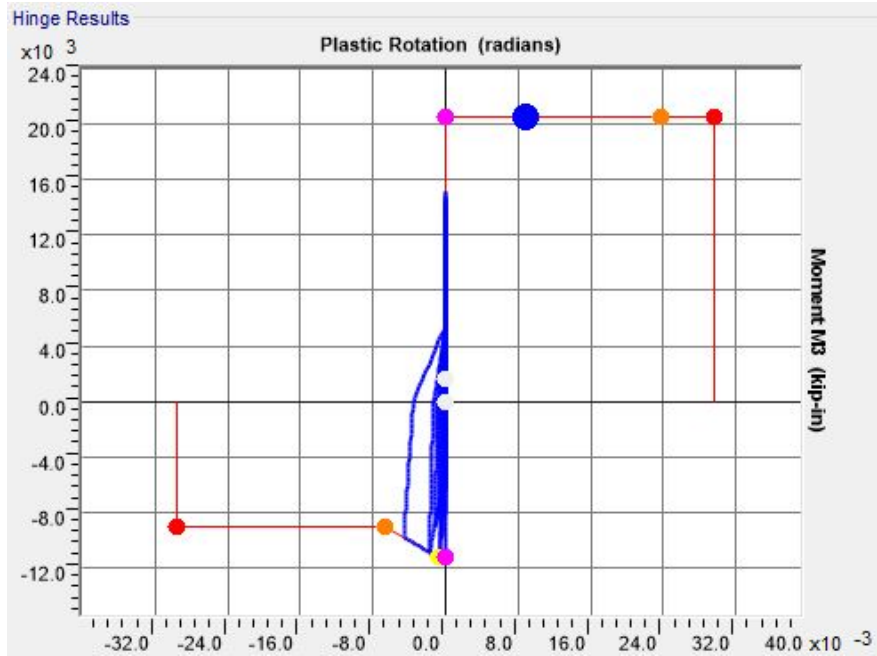
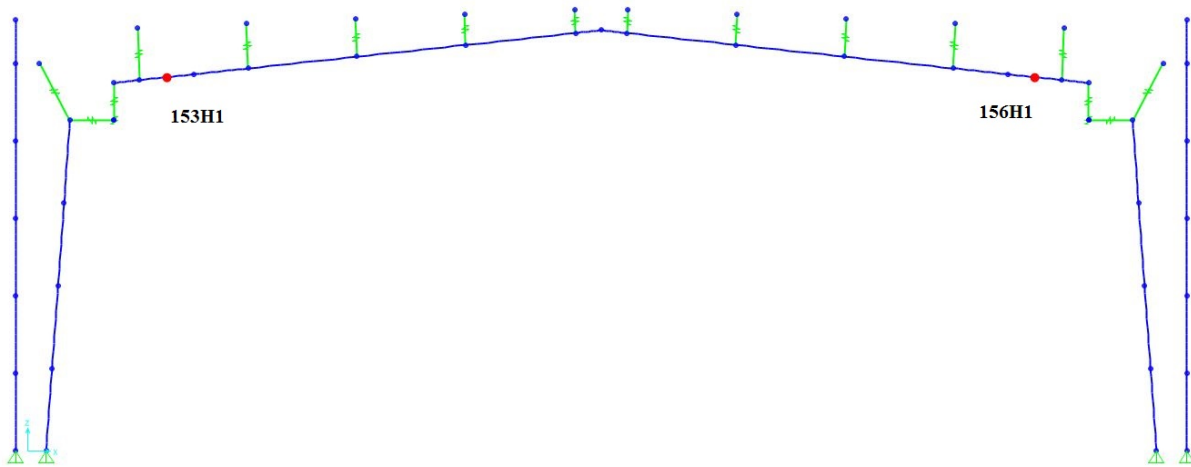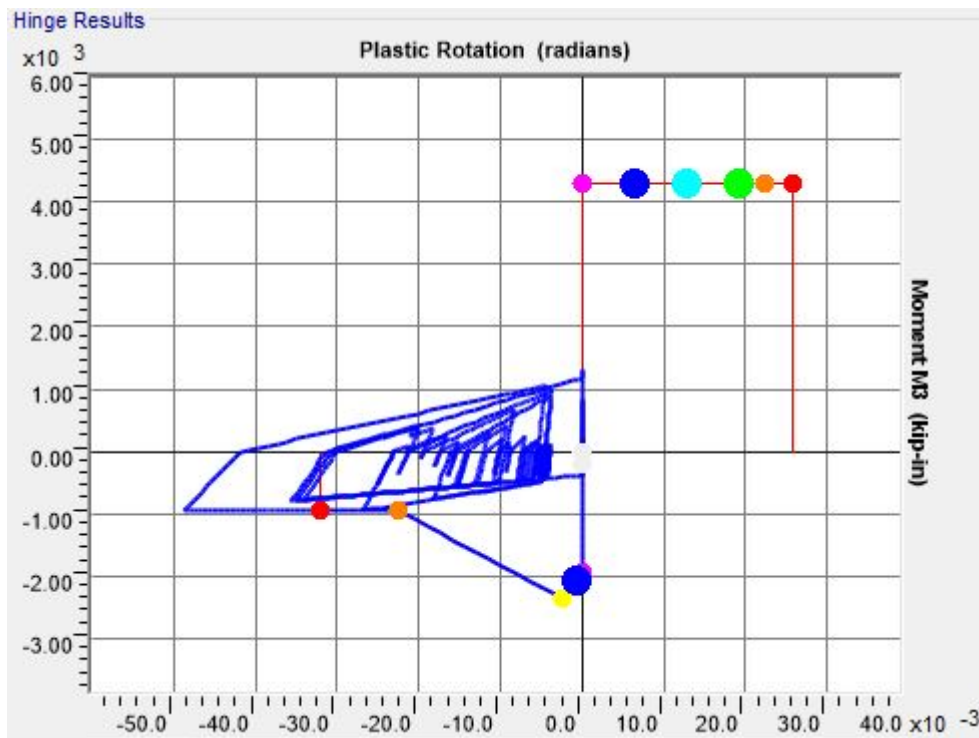**Figure A.27. Plastic Hysteresis of Hinge 5H1 during Loma Prieta Excitation (2-D 42)**
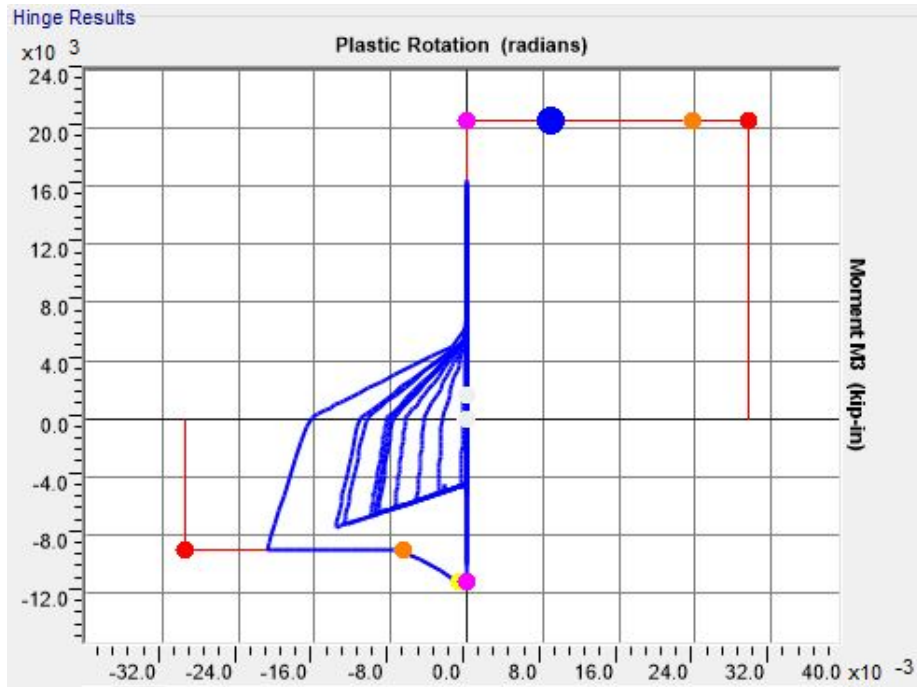
Figure A.28. Plastic Hysteresis of Hinge 5H1 during Superstition Hills Excitation (2-D 42)

A18
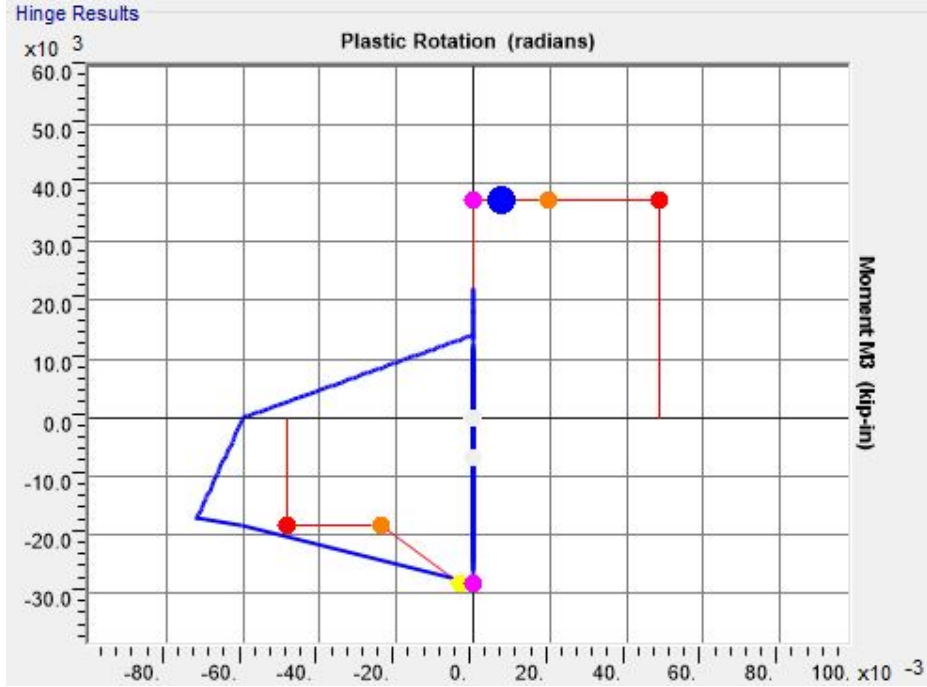
Figure A.29. Error in Plastic Hysteresis of Hinge 7H1 during Northridge Sylmar Station Excitation (2-D 42)
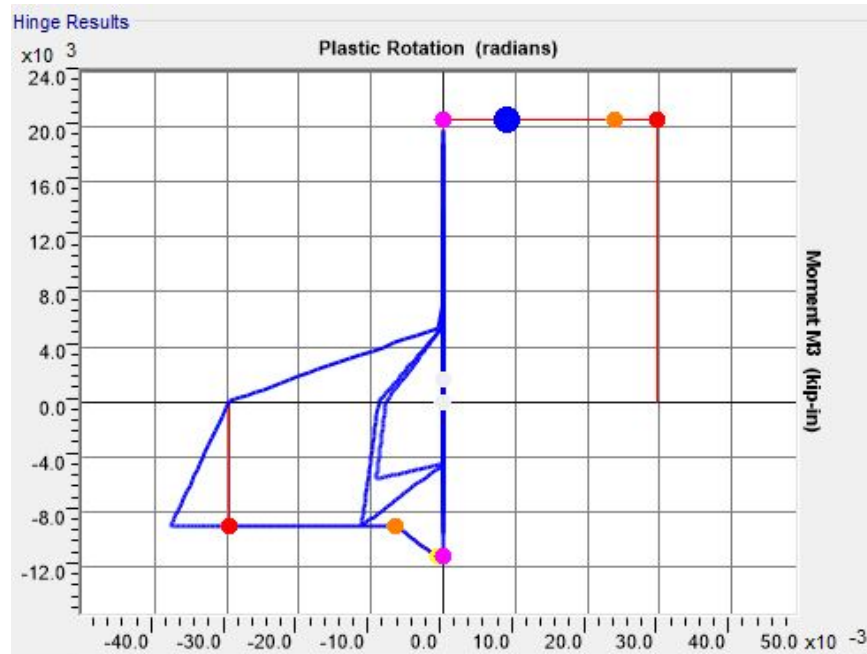
Figure A.30. Plastic Hysteresis of Hinge 5H1 during Chi-Chi, Taiwan Excitation (2-D 42)

A19
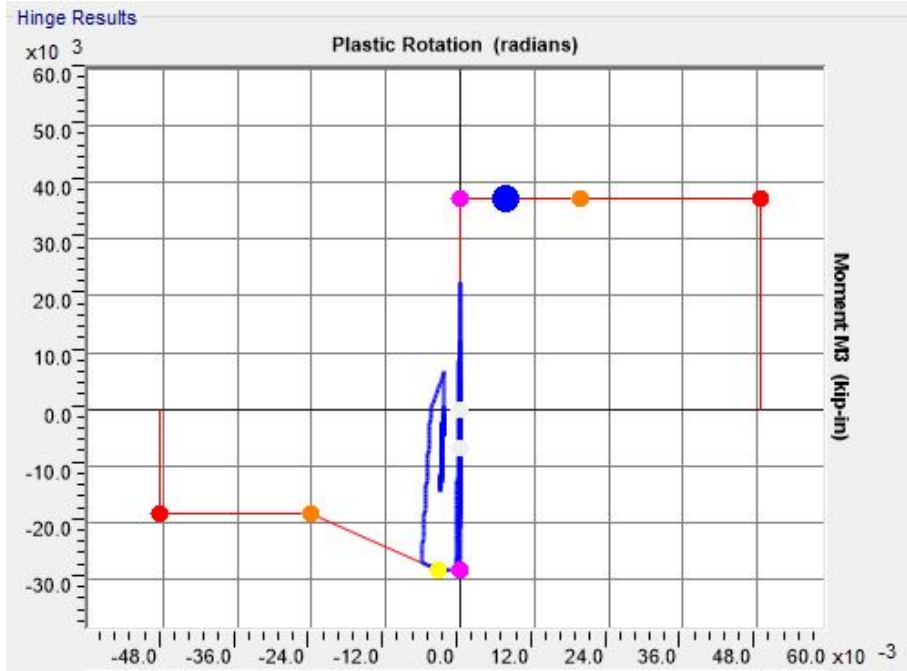
Figure A.31. Plastic Hysteresis of Hinge 7H1 during Chi-Chi, Taiwan Excitation (2-D 42)
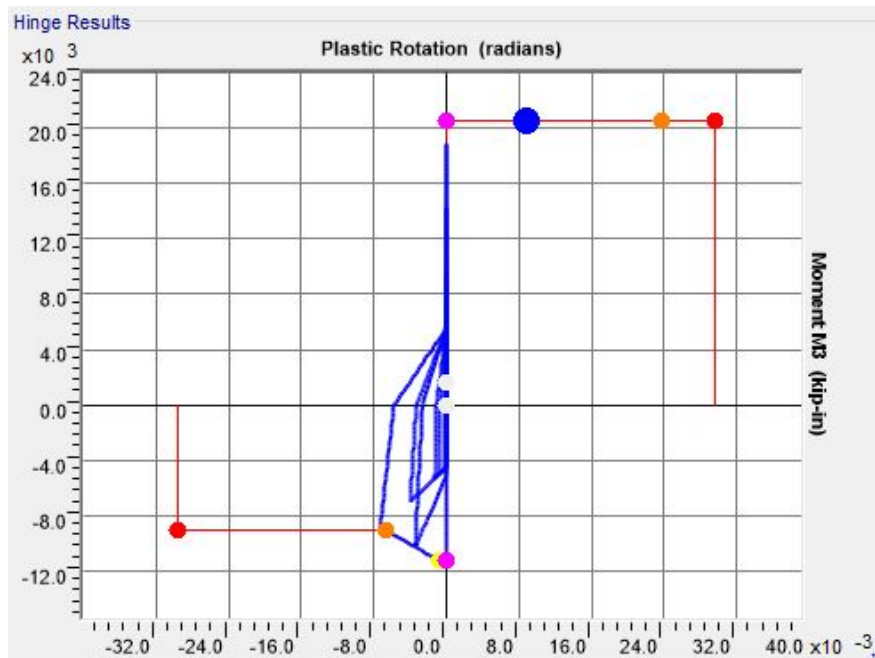
Figure A.32. Plastic Hysteresis of Hinge 5H1 during Gazli, USSR Excitation (2-D 42)

A20

Table A.4. LTB Hinge Activation and Peak Frame Demands for Frame 85

Earthquake Case	LTB Hinges Activated	Maximum Ridgeline Displacement (inches)	Maximum Ridgeline Absolute Acceleration (in/sec^2)
San Fernando	Hinge Error	2.83	1162
		-3.11	-2303
Friuli, Italy	2	7.25	530
		-4.60	-456
Gazli, USSR	0	2.35	401
		-2.37	-436
Imperial Valley	1	1.36	420
		-4.07	-281
Superstition Hills	2	3.07	549
		-3.85	-419
Loma Prieta	2	6.02	495
		-3.39	-427
Northridge Canyon	1	2.31	411
		-4.70	-374
Northridge Sylmar	1	4.02	284
		-1.86	-373
Kobe	1	2.25	406
		-3.47	-366
Kocaeli, Turkey	Hinge Error	2.40	15893
		-4.46	-3168
Chi-Chi, Taiwan	1	1.91	464
		-4.69	-347

Figure A.33. Hinge Identification for Frame 85

Figure A.34. Plastic Hysteresis of Hinge 153H1 during Imperial Valley Excitation (2-D 85)

A22
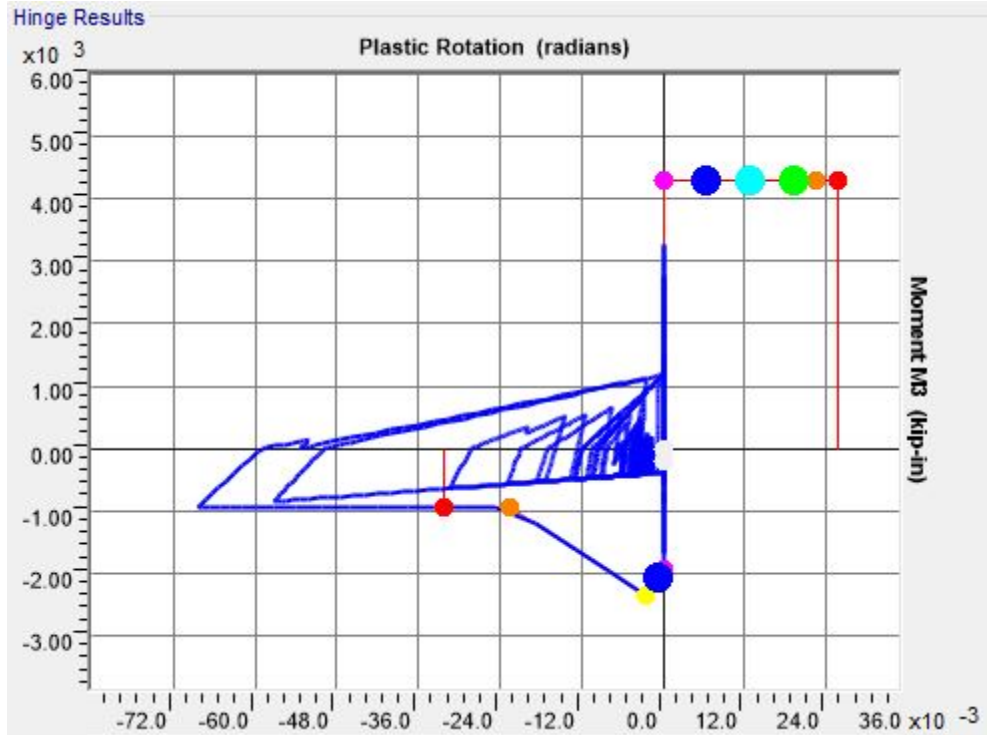
Figure A.35. Plastic Hysteresis of Hinge 153H1 during Friuli, Italy Excitation (2-D 85)
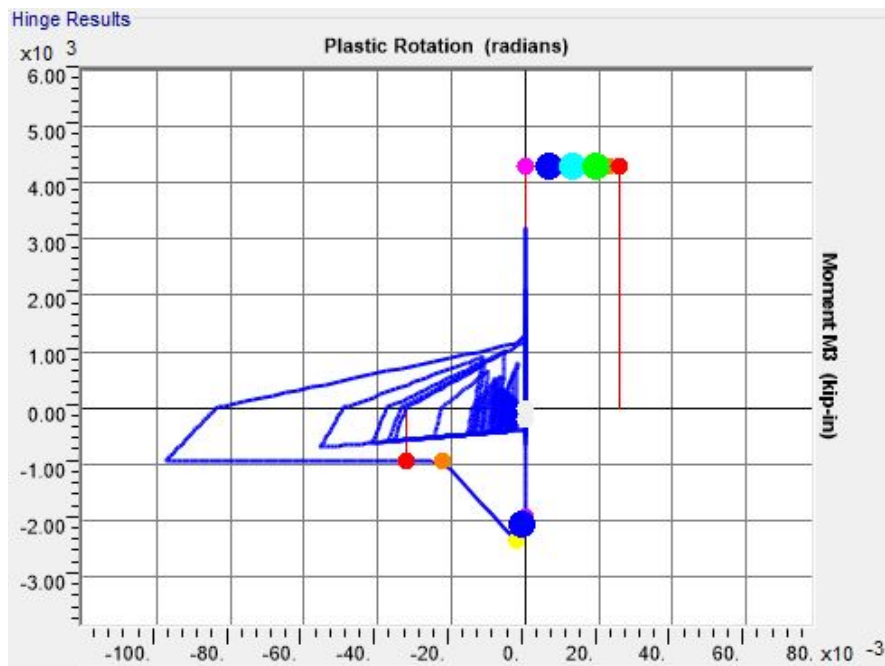
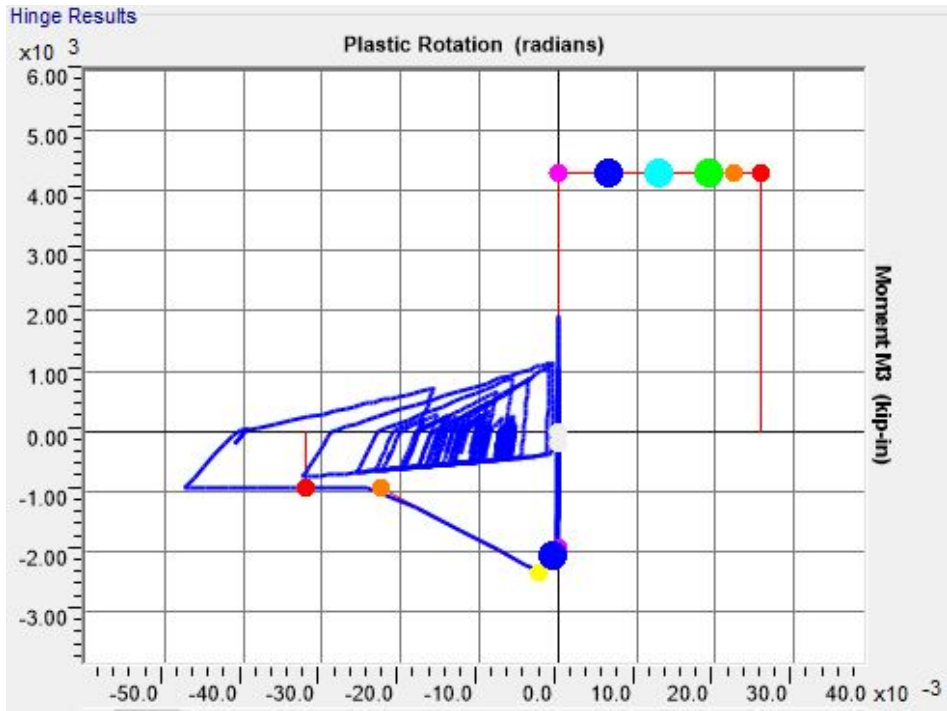**Figure A.36. Plastic Hysteresis of Hinge 156H1 during Friuli, Italy Excitation (2-D 85)**

A23

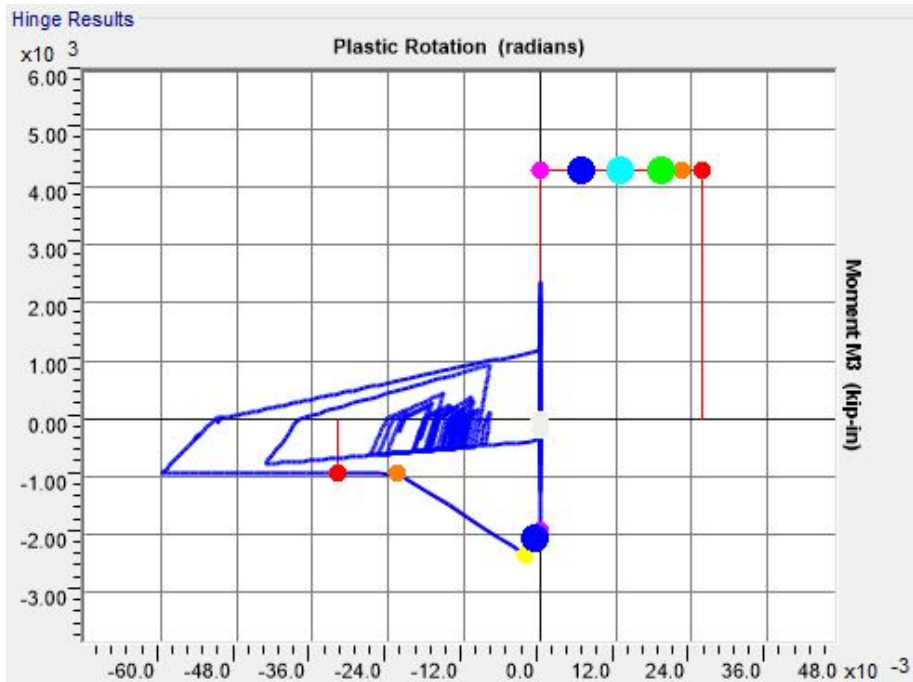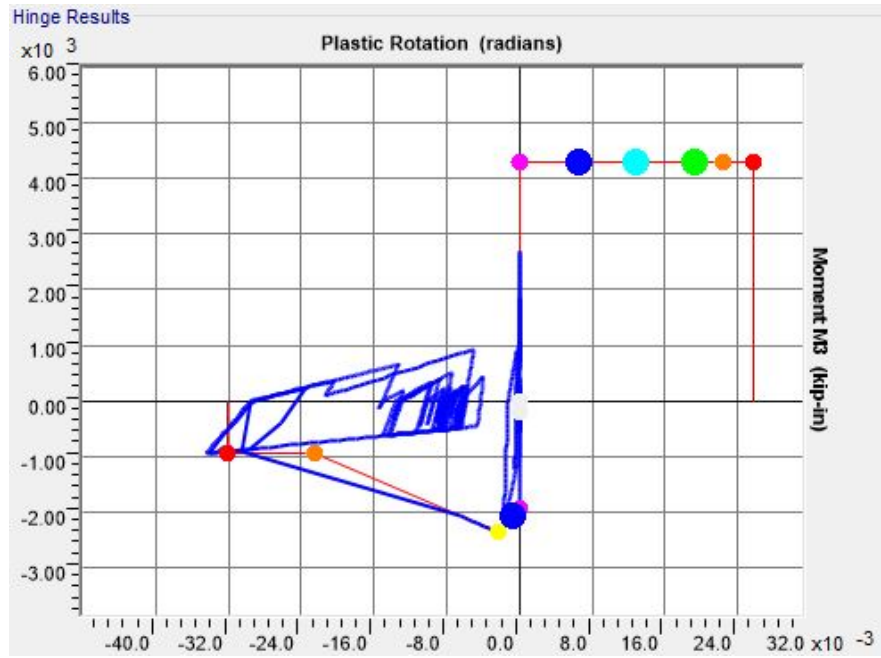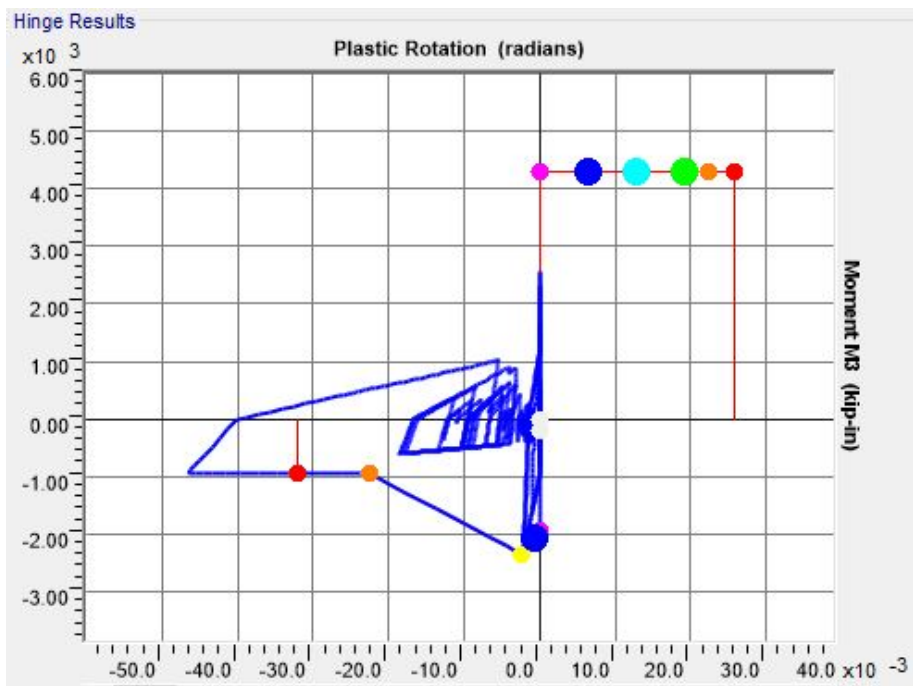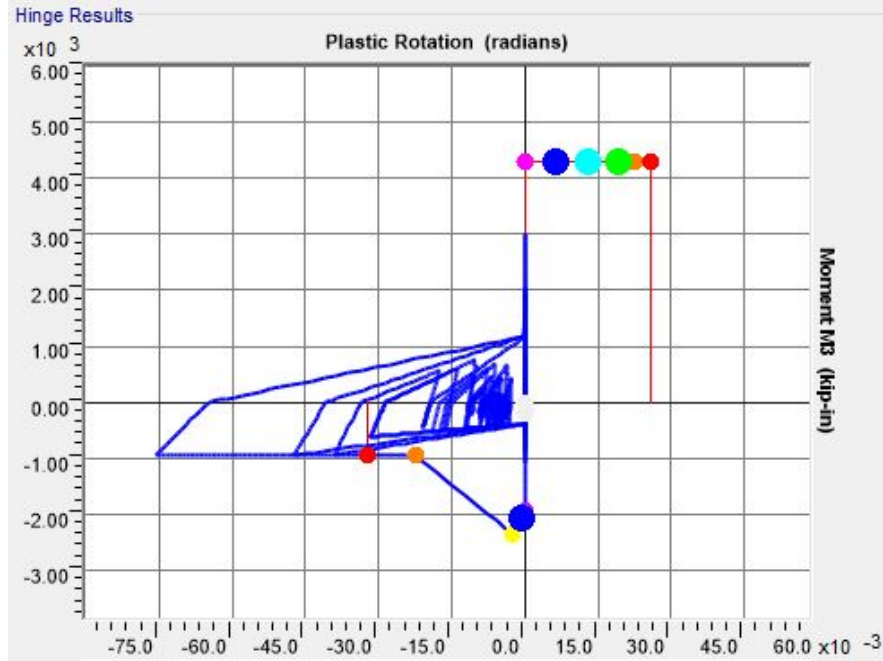**Figure A.37. Plastic Hysteresis of Hinge 153H1 during Kobe Excitation (2-D 85)**

Figure A.38. Plastic Hysteresis of Hinge 153H1 during Kocaeli, Turkey Excitation (2-D 85)

Figure A.39. Error in Plastic Hysteresis of Hinge 156H1 during Kocaeli, Turkey Excitation

(2-D 85)

Figure A.40. Plastic Hysteresis of Hinge 153H1 during Loma Prieta Excitation (2-D 85)

A25

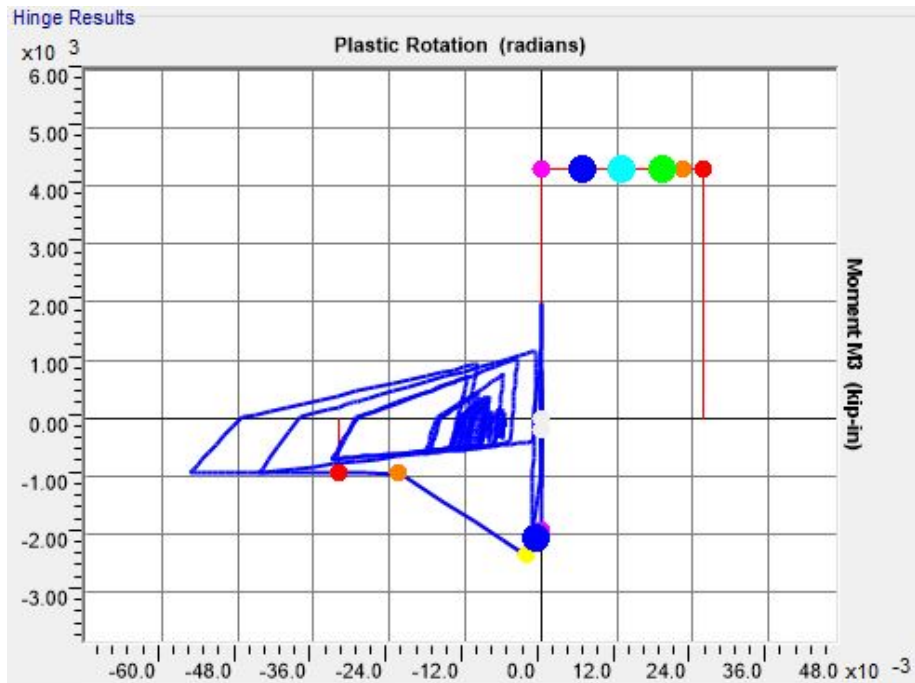**Figure A.41. Plastic Hysteresis of Hinge 156H1 during Loma Prieta Excitation (2-D 85)**

Figure A.42. Plastic Hysteresis of Hinge 153H1 during Northridge Canyon Excitation (2-D
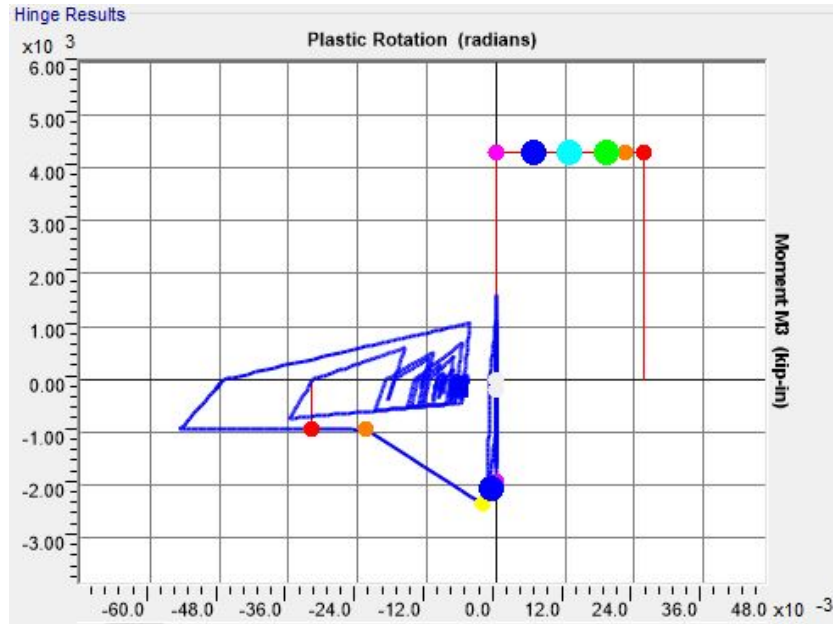
85)

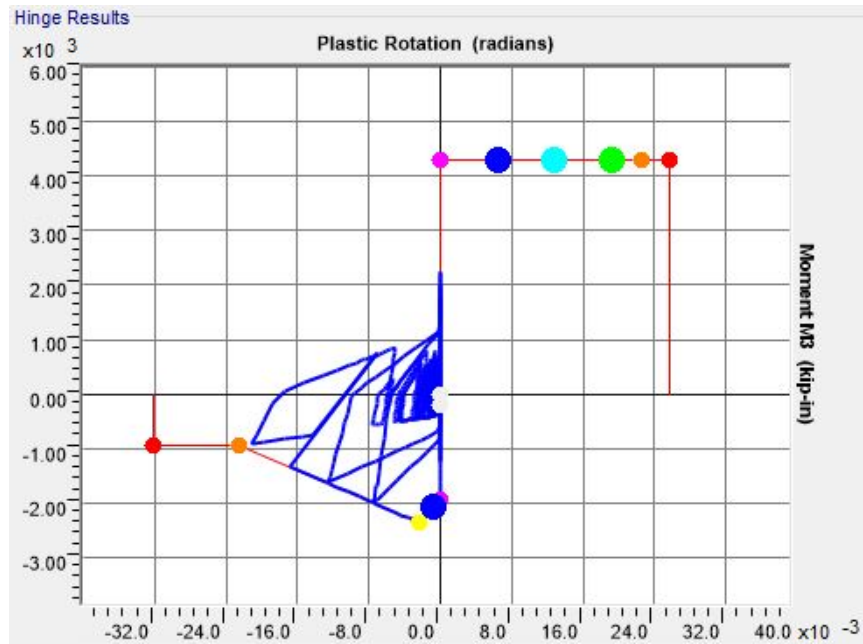**Figure A.43. Plastic Hysteresis of Hinge 156H1 during Northridge Sylmar Excitation (2-D 85)**
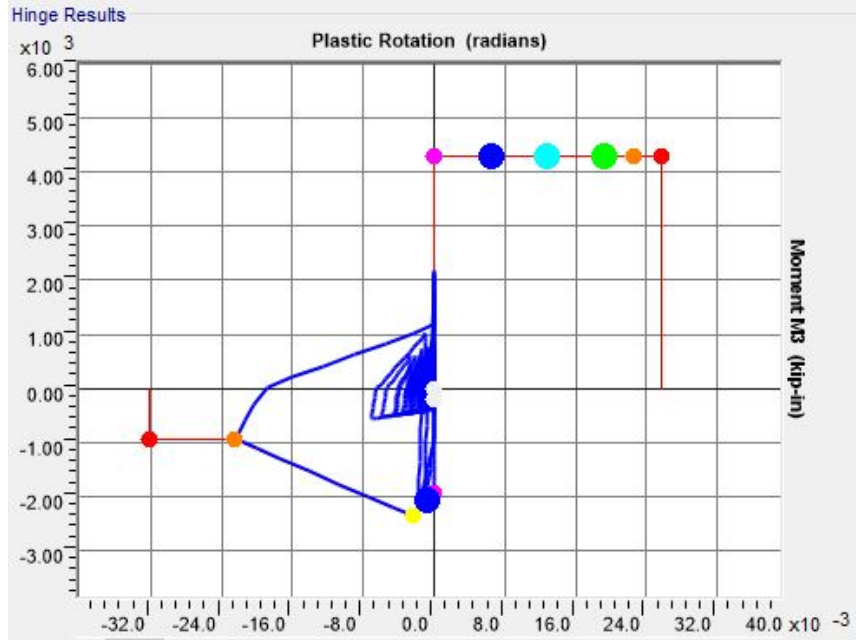

Figure A.44. Error in Plastic Hysteresis of Hinge 153H1 during San Fernando Excitation (2-D 85)

A27

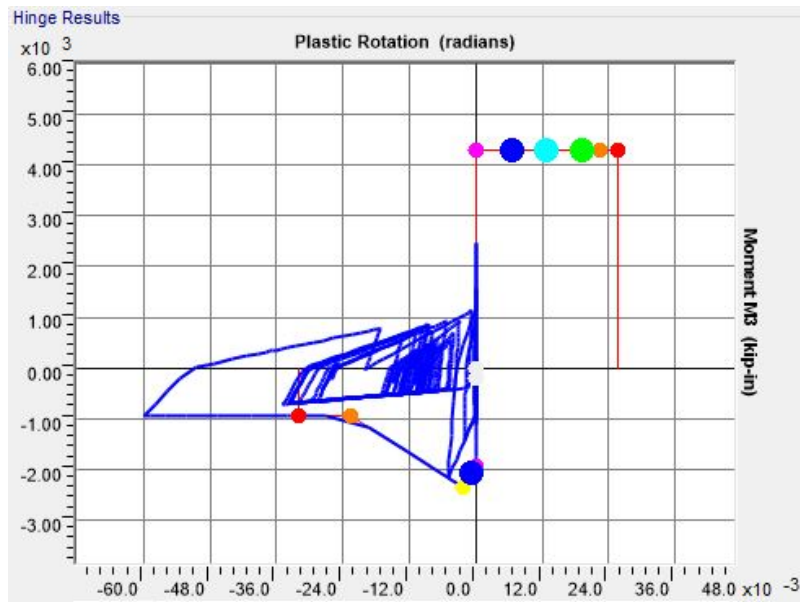**Figure A.45. Error in Plastic Hysteresis of Hinge 156H1 during San Fernando Excitation**

(2-D 85)

Figure A.46. Plastic Hysteresis of Hinge 153H1 during Superstition Hills Excitation (2-D
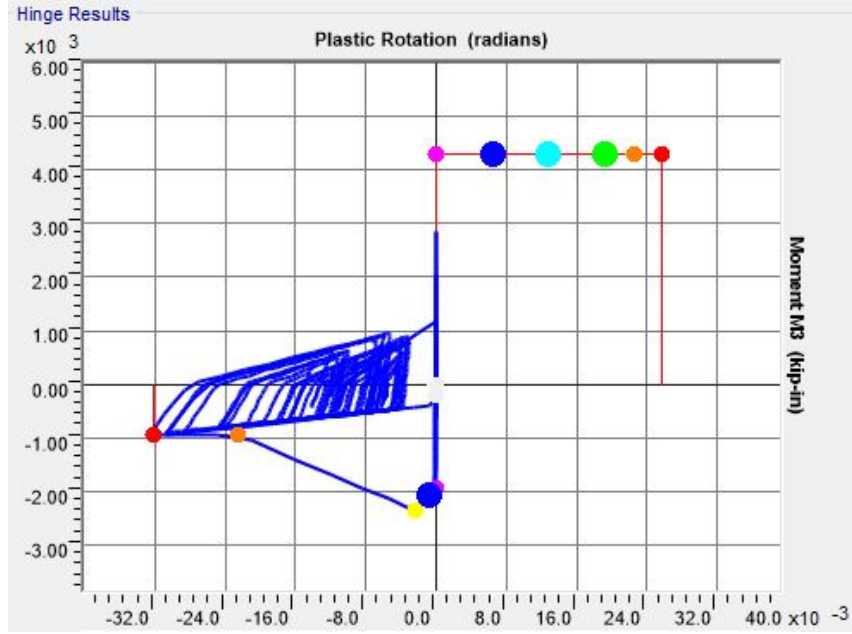
85)

Figure A.47. Plastic Hysteresis of Hinge 156H1 during Superstition Hills Excitation (2-D 85)
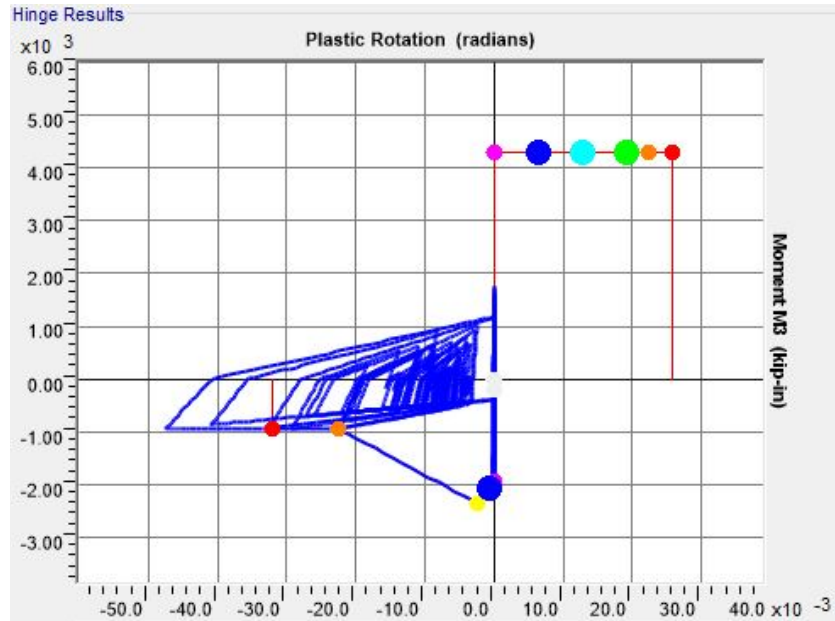

Figure A.48. Plastic Hysteresis of Hinge 153H1 during Chi-Chi, Taiwan Excitation (2-D 85)

A29

Table A.5. Peak Frame Demands for Frame 138

Earthquake Case	Peak Displacement at Ridgeline (inches)	Peak Absolute Acceleration at Ridgeline (in/sec^2)
San Fernando	6.49	388
	-4.23	-479
Friuli, Italy	12.67	638
	-11.58	-822
Gazli, USSR	8.52	499
	-8.36	-582
Imperial Valley	7.09	457
	-6.37	-425
Superstition Hills	8.64	546
	-8.20	-471
Loma Prieta	11.07	589
	-10.61	-627
Northridge Canyon	4.85	314
	-4.47	-342
Northridge Sylmar	14.24	839
	-15.12	-766
Kobe	4.70	264
	-4.63	-277
Kocaeli, Turkey	8.38	558
	-9.25	-529
Chi-Chi, Taiwan	9.43	521
	-9.25	-528